UiT The Arctic University of Norway

Faculty of Health Sciences, Department of Pharmacy

Computational studies on the human GnRH-I and the GnRH-receptor

Molecular modeling

Anton Tran

Master's thesis in Pharmacy FAR-3911 May 2022

Acknowledgements

This thesis would not have been completed without the help and guidance of Ph.D. fellow Clizia Russotto and associate professor Mari Gabrielsen from the research group Molecular Pharmacology and Toxicology at the University of Tromsø. Their feedback and recommendations were invaluable, thought-provoking, and essential for finalizing the work and bringing the thesis to a higher level. I would also like to acknowledge research group leader Ingebrigt Sylte, chief engineer Imin Wushur, and lab engineer Torkild Pettersen for supporting me and making me feel welcome in the research group. A special thanks to my fellow classmates for providing feedback from another perspective, along with much-needed small-talk and breaks from thesis writing. Last but not least, I would like to thank my family and my girlfriend for being pillars of support and always encouraging me.

Anton Tran
Tromsø, May 2022

Abstract

Gonadotropin-releasing hormone receptor (GnRH-R), which is a Class A G-protein coupled receptor (GPCR), has a vital role in the regulation of sex hormones. The receptor also has a prominent role in diseases, with examples being reproductive cancers and non-reproductive cancers like glioblastoma. Gonadotropin-releasing hormone (GnRH) agonists have been proven to combat cell proliferation in cancers.

Therefore, studies on how GnRH binds to GnRH-R using computational methods are valuable for further investigation of the GnRH-R activation. The aim was to study the activation mechanism of GnRH-R, in addition to discover how an active model of GnRH-R in complex with GnRH would conformationally change using the computational methods docking and molecular dynamics (MD).

GnRH was docked into a published X-ray crystal structure of GnRH-R and a GnRH-R homology model using Glide® ligand docking and induced fit docking (IFD), this was to study ligand poses and the ligand binding mode. Homology modeling through Prime® was done in order to generate an active structure that was different from the crystal structure, which was inactive. MD-simulations were executed in Desmond® to study the ligand binding mode further along with conformational changes.

The results from the docking indicated that GnRH made some known interactions with protein residues in the binding pocket of GnRH-R. However, the ligand did not fully occupy the orthosteric site, and specific residues were sticking out of the binding pocket. MD-simulations highlighted differences between the X-ray crystal structure (inactive) and the homology model (active). At the end of the MD-simulation, the homology model attained a conformation where transmembrane helices were reminiscent of an active GPCR structure. The crystal structure did not undergo any great conformational change during the MD-simulation.

Table of Contents

List of Tables

List of Figures

Abbreviations

cAMP: cyclic adenosine monophosphate

DAG: Diacylglycerol

ECL: Extracellular loop

EM: Electron Microscopy

EMA: European Medicines Agency

ERK: Extracellular signal-regulated kinases

FDA: U.S Food and Drug Administration

FSH: Follicle- stimulating hormone

GBM: Glioblastoma multiforme

GDP: Guanosine diphosphate

GnRH: Gonadotropin-releasing hormone

GnRH-R: Gonadotropin-releasing hormone receptor

GPCR: G-protein coupled receptor

GTP: Guanosine triphosphate

H-bond: Hydrogen bond

HPG axis: Hypothalamic- pituitary- gonadal axis

ICL: Intracellular loop

IFD: Induced Fit Docking

IP_3: Inositol 1,4,5-triphosphate

LH: Luteinizing hormone

LID: Ligand Interaction Diagram

MAPK: Mitogen activated protein kinases

MD: Molecular dynamics

MSA: Multiple sequence alignment

OPM: Orientations of Proteins in Membrane

PDB: Protein Data Bank

PIP_2: Phosphatidylinositol 4,5-bisphosphate

PKC: Protein kinase C

PLC: Phospholipase C

POPC: palmitoyl-oleoyl-phosphatidylcholine

RMSF: Root Mean Square Fluctuation

RMSD: Root Mean Square Deviation

SID: simulation Interaction Diagram

SPC: simple point charge

TM: transmembrane

TSH: thyroid-stimulating hormone

VFT: Venus fly trap

1 Introduction

The first crystal structure of a G-protein coupled receptor (GPCR) was published in the year 2000 (1). Since then, about 70 unique GPCR structures and over 370 GPCR structures bound to different ligands have been discovered (2). A study from 2018 estimated that 25-35% of approved drugs target GPCRs, this was based on lists from the European Medicines Agency (EMA) and the U.S Food and Drug Administration (FDA), signifying the importance of GPCRs as drug targets (3). Pharmaceuticals identified through computational structure-based drug design on GPCRs are rapidly increasing (2). A GPCR, where the structure-activity relationship is still being studied, is the gonadotropin-releasing hormone receptor (GnRH-R). GnRH-R is a target for diseases affecting the reproductive system and has been expressed on non-reproductive cancer cells as well (4). Recently, a GnRH-R X-ray crystal structure was identified and published in the Protein Data Bank (PDB). The crystal structure discovered was bound to the GnRH-antagonist Elagolix (5). The published X-ray crystal of GnRH-R, in addition to 3D structures of gonadotropin-releasing hormone (GnRH), form the basis for further research using computational methods for both GnRH-R and GnRH.

2 Background

2.1 The endocrine system and the feedback mechanism

The basis of the endocrine system is how stimuli affect endogenous glands, which in turn release hormones in the bloodstream (6). The endocrine system covers every gland which releases hormones and its belonging signaling system. Hormones lead to biological activity as a result of receptor binding, and their activity consists mostly of regulation, in fact, many hormonal receptors are GPCRs (6, 7). Hormones regulate factors connected to reproduction, electrolyte balance in body fluids, and metabolism (6). Along with the executive control organ hypothalamus, major glands which make up the endocrine system are the pituitary gland, parathyroid- and thyroid glands, the thymus, the adrenal gland, the pancreas, the ovary, and the testis (6). The location of the hypothalamus and primary glands can be seen in Figure 1.

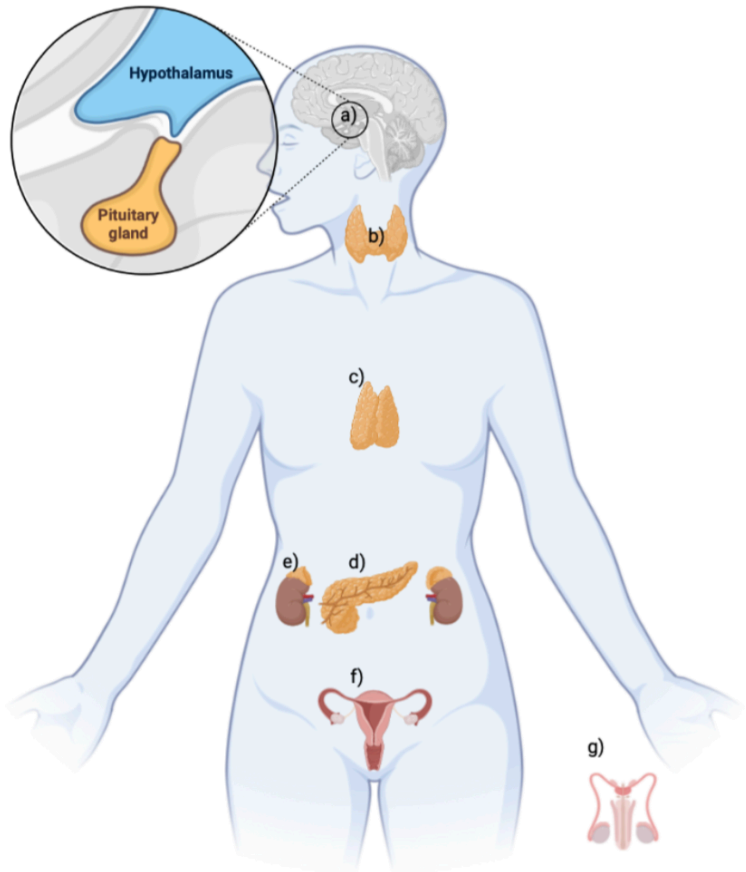

Figure 1: The human body and the organs and glands making up the endocrine system: a) the hypothalamus and pituitary gland, b) the thyroid gland, c) the thymus, d) the pancreas, e) the adrenal gland, f) the ovary (females), and g) the testis (males), the testis is located roughly the same place as the ovaries. Inspiration taken from Figure 1-1 in Endocrine Physiology by Molina P.E. (8). Created with BioRender.com.

Different endocrine glands secrete different hormones (9). The hypothalamus produces the following releasing hormones: GnRH, corticotropin-releasing hormone, thyrotropin-releasing hormone, and growth hormone-releasing hormone. Inhibitory hormones released by the hypothalamus are somatostatin, dopamine, vasopressin, and oxytocin (10). The anterior pituitary gland produces thyroid-stimulating hormone (TSH), adrenocorticotropic hormone, growth hormone, luteinizing hormone (LH), follicle-stimulating hormone (FSH), and prolactin (11). The posterior pituitary gland secretes oxytocin and arginine vasopressin (10). The thyroid gland produces triiodothyronine and thyroxine, which are involved in cell differentiation, energy balance, and growth (12). The pancreas secretes insulin (13). The adrenal gland produces principal hormones such as aldosterone, dehydroepiandrosterone, and cortisol, as well as epinephrine and norepinephrine, which relate to stress response (14). The testes produce testosterone (15), and the ovaries produce estrogen (16), both essential for sex differentiation and reproduction.

To uphold a correct regulatory function, the gland in the endocrine system requires feedback on the current state of hormone activity. The feedback mechanism can be separated into negative and positive feedback (17). Negative feedback regulation works on the hypothalamus and the anterior pituitary gland. It is a mechanism that results in the secretion of stimulating hormones getting reduced(18). An example is how an increase in the release of thyroid hormone from the thyroid gland into the bloodstream, which is secreted by the thyroid gland, inhibits the secretion of TSH. In this case, the anterior pituitary is the target for TSH. Positive feedback regulation, however, happens under specific conditions, and an example is how LH is affected by positive feedback during ovulation when estradiol is released. During positive feedback the hormones in circulation feed forward and trigger the release of the initial hormone (18). Negative feedback is more common than positive feedback and is important for the regulation of hormone secretion, for example, a well-functioning feedback regulation prevents hormonal disorders (18).

2.1.1 Hypothalamus and the pituitary gland

The hypothalamus is a nuclei-dense area with vital bodily functions (19). It is part of the interbrain, also called the diencephalon, which is located between the endbrain and the midbrain (20). Hypothalamus has connections to the following structures: the amygdala, hippocampal region, olfactory bulb, retina, and the cerebral cortex (21). These connections allow it to affect regulatory processes in the body. It is mainly considered the link between the nervous system and the endocrine system. The hypothalamus is deeply involved in convoluted systems, but in short, it has a key function in upholding homeostasis, which is connected to the endocrine system (21).

The hypothalamus consists of parvocellular and magnocellular neurons, and these two types express neurohormonal activity (10). Parvocellular neurons are smaller in size than the magnocellular neurons and release releasing hormones such as GnRH or inhibiting hormones such as somatostatin. These peptides are transported through portal veins, where they eventually affect the anterior pituitary. Magnocellular neurons are both larger than parvocellular neurons and produce more hormones. Magnocellular neurons produce oxytocin and vasopressin, which through axonal transport, affect the posterior pituitary (10).

The pituitary gland, which is a pea-sized endocrine gland attached underneath the brain and has a wide array of essential functions (22). These functions are guiding the homeostasis, preserving the reproductive cycle, and conducting the activity of other glands in the endocrine system (22). The pituitary gland consists of the anterior- and posterior pituitary gland. The posterior pituitary gland is smaller than the anterior pituitary and is essentially an extension of the hypothalamus, it stores oxytocin and vasopressin, which are later released (10). The anterior pituitary is larger and is responsible for the release of tropic hormones, which target organs and result in the release of the target hormone (11). The hypothalamus, the anterior pituitary gland, together with the gonadal glands, make up the hypothalamic-pituitary-gonadal axis (HPG axis), a single system important for developing and maintaining the reproductive- and the immune system (23).

The HPG axis is displayed in Figure 2, and it begins with the hypothalamus secreting GnRH. GnRH binds to the GnRH-R, which is present on pituitary gonadotropic cells in the anterior pituitary (23). This, in turn, triggers the gonadotropic cells to produce and release LH and FSH, both a part of the gonadotropin family of glycoproteins (24, 25). At the end of the axis for males, LH will bind to receptors expressed on Leydig-cells situated in the testis, this starts the production of testosterone (26). For females, a rise in the concentration of LH, especially acute, will bring about ovulation (27). FSH binds to Sertoli-cells in males which are connected to testis growth (15). In females, FSH brings about follicular growth amid the follicular phase (16). The HPG-axis is regulated by the hypothalamus, but the system itself is susceptible to both positive and negative feedback (10). This means that testosterone or estrogen can suppress the release of gonadotropins. One mechanism is inhibiting the release of GnRH from the hypothalamus and another mechanism affecting GnRHs binding to the GnRH-R on the anterior pituitary (28).

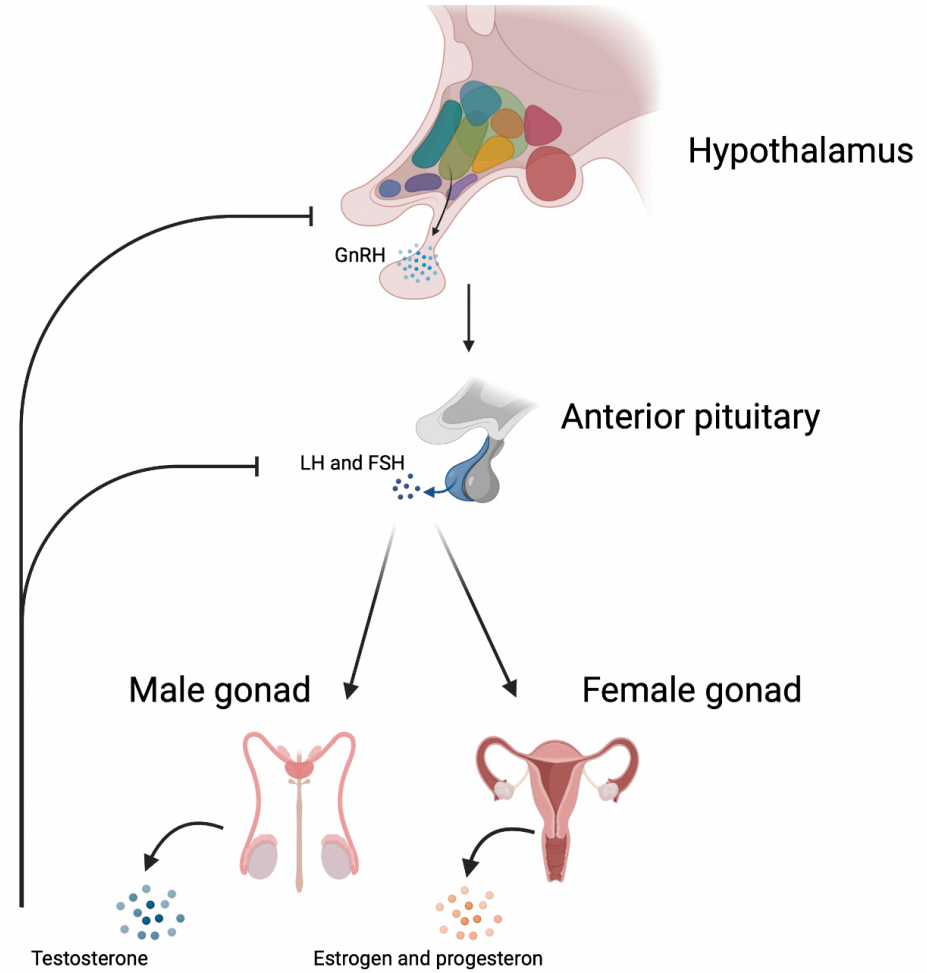

Figure 2: The HPG-axis. The sex hormones at the end of the axis can inhibit both the hypothalamus and anterior pituitary. Inspiration taken from Geoffrey Harris´ 1955 monograph model(29). Created with BioRender.com

2.2 G-protein coupled receptors

GPCRs are a group of transmembrane (TM) proteins that can detect extracellular signaling in form of small molecules/ligands and translate it to intracellular signaling (30). Examples of ligands are adrenaline and salbutamol, both agonists which activate the β_2-adrenergic receptor, a GPCR (31). There are over 800 human GPCRs in the GPCR-superfamily, and these can be classified and sorted into five dominant families: Rhodopsin-like (Class A), Frizzled/TAS2 (Class F), Glutamate (Class C), Adhesion (Class B2) and Secretin(Class B) (32, 33). Regarding the structure, GPCRs have a TM domain consisting of 7 TM helices which are bound by intracellular loops (ICL) and extracellular loops (ECL) (34). Three-dimensionally, the helices are bundled together and embedded in a cell membrane, with the C-terminus on the intracellular side and the N-terminus on the extracellular side of the membrane (34).

Besides having low sequence identity and different N-terminals, the different classes of GPCR have different ligand binding sites (35). GPCRs belonging to class A have their orthosteric ligand-binding site located in the 7TM-domain. Class B GPCRs differ by having their orthosteric ligand recognizing site both in the 7TM-domain and the Venus fly trap (VFT) domain of the protein. Class C GPCRs have their orthosteric ligand-binding pocket exclusively in the VFT domain. For Class F GPCRs, ligands are recognized based on their orthosteric extracellular cysteine-rich domain. GPCRs also have allosteric binding sites, which are another site than the active site/orthosteric site, except for class A GPCRs, where the allosteric site overlaps with the orthosteric site (35).

The G-protein coupled with all human GCPRs are assumed to be heterotrimeric, meaning the protein consists of three different subunits: Gα, Gβ, and Gγ (36). The G-protein itself can be divided into different families based on the α-subunit. The different families are $G\alpha_s$, $G\alpha_i$, $G\alpha_{q/11}$, and $G\alpha_{12/13}$. These distinctive subunits lead to specific signaling pathways: Both $G\alpha_s$ and $G\alpha_i$ are connected to the adenylyl cyclase signaling pathway, $G\alpha_{q/11}$ stimulates phospholipase C (PLC), and $G\alpha_{12/13}$ are involved in GTPase activation (37). The ability to bind nucleotides guanosine triphosphate (GTP) and guanosine diphosphate (GDP) is shared among all known GCPRs and plays a leading role in its intracellular signaling(36). Some GPCRs, such as GnRH-

R, can couple with multiple G-proteins, depending on a context and specific cells, therefore leading to different signaling cascades (38).

2.2.1 Class A G-protein coupled receptors, structure and activation

Class A GPCRs, also defined as ´Rhodopsin-like´, are the most significant and well-studied family within the superfamily of GPCRs (39). A simplified class A GPCR structure is displayed in Figure 3. A distinct molecular signature class A GPCRs possess is the ECL2 (40). ECL2 in GPCR class A is relatively longer than ECL1 and ECL2, and has a unique β-hairpin motif (40). It has been proven that ECL2 forms a ´lid´-like purpose which is responsible for both restricting and guiding ligands to the ligand-binding site within the 7TM domain facing the extracellular site (40). Class A GPCRs have also been proven to undergo conformational changes when activated, where both TM6 and TM7 have shown movement on the intracellular side upon activation, with TM7 also showing movement on the extracellular side (41). TM3 has been shown to have cystolic rotation (41). In comparison, TM6 has shown outward movement (34). A study on the β_2-adrenergic receptor, a class A GPCR, shows that the movements of helices on the cytoplasmic side ultimately open up space for the Gα-subunit (42). In the same study, helices TM5, TM6, and TM7 moved relative to TM3 on the cytoplasmic side, making G-protein coupling possible and attaining an active conformation(42).

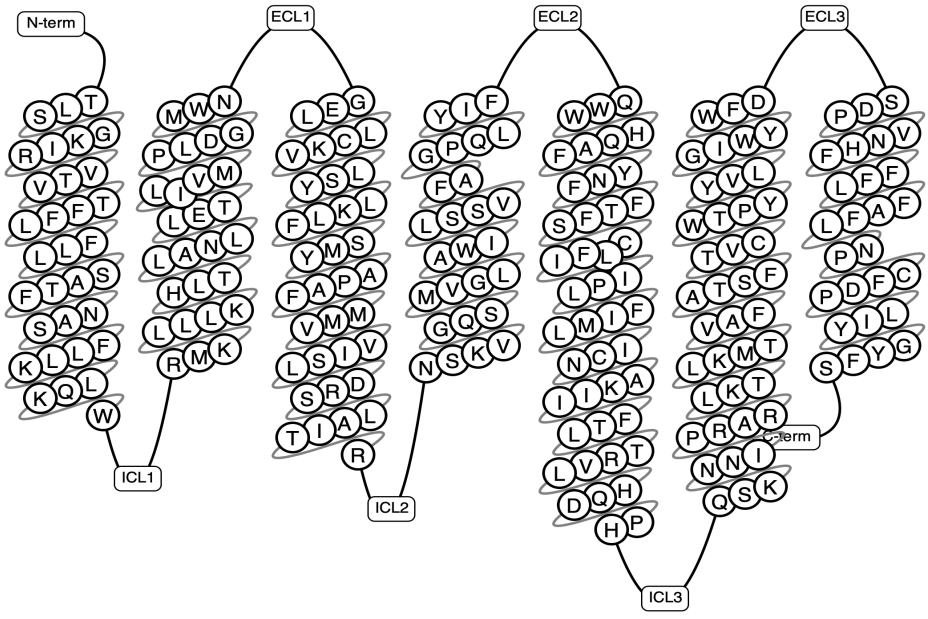

Figure 3: A simplified two-dimensional representation of the primary structure of the GnRH-R, a class A GPCR. Acquired from gpcrdb.org (43).

2.2.1.1 GnRH-R structure

GnRH-R is a class A GPCR. While the termini and loops are different from other GPCRs, the TM domains in GnRH-R are conserved (44). Flanagan et al. reported the following highly conserved GnRH-R residues/motifs in 2017 based on site-directed mutagenesis studies: Asn53, Asn87, Asp138-Arg139-Ser140 (DRS), Trp164, Pro223, Cys279-Trp280-Thr281-Pro282-Tyr283 (CWxPY), and Asp319-Pro320-Leu321-Ile322-Tyr323 (DPxxY) (44). GnRH-R does not have a free C-terminus, this is common for GnRH-R in both human and mammalian cells(45). Like other class A GPCRs GnRH-R have a distinct ECL2 which connects TM4 and TM5 (46). ECL2 in GnRH-R consists of 25 amino acids (46). It should be noted that the length of ECL2 for class A GPCRs depends on the receptor (47). A 3D structure for GnRH-R in a complex with the GnRH antagonist Elagolix has been acquired through X-ray crystallography and published with accession code 7BR3 in PDB (5).

In a review article, Tzoupis et. al. propose that the following protein residues in GnRH-R are important for ligand-receptor binding: Asn212, Asp98, Lys121, Tyr290, Asp302, and Asn102 (46). These protein residues have been highlighted in Figure 4 and helps visualize where the binding pocket of GnRH-R is located. It should be noted that the residues Tzoupis et. al. propose are gathered from site-directed mutagenesis data as well as data on ligand binding assays connected to GnRH (46).

The protein residues mentioned are specifically for the β-hairpin conformation of GnRH, and the ligand-receptor interactions are as follows: pGlu1 from the peptide with Asn212 from the protein, His2 with Asp98 along with His2 with Lys121, Tyr5 with Tyr290, Arg8 with Asp302, lastly Gly10 with Asn102 (46). Flanagan et. al. have concluded that there is a consensus ligand binding pocket in addition to interactions made outside of this ligand binding pocket (44). For the consensus ligand binding pocket, suggested protein residues are Lys121, Trp280, Tyr283, and Phe309 (44). For the interactions made outside the ligand binding pocket suggested by Flanagan et. al. the protein residues Asp98, Tyr290 and Asp302 holds significant importance (44).

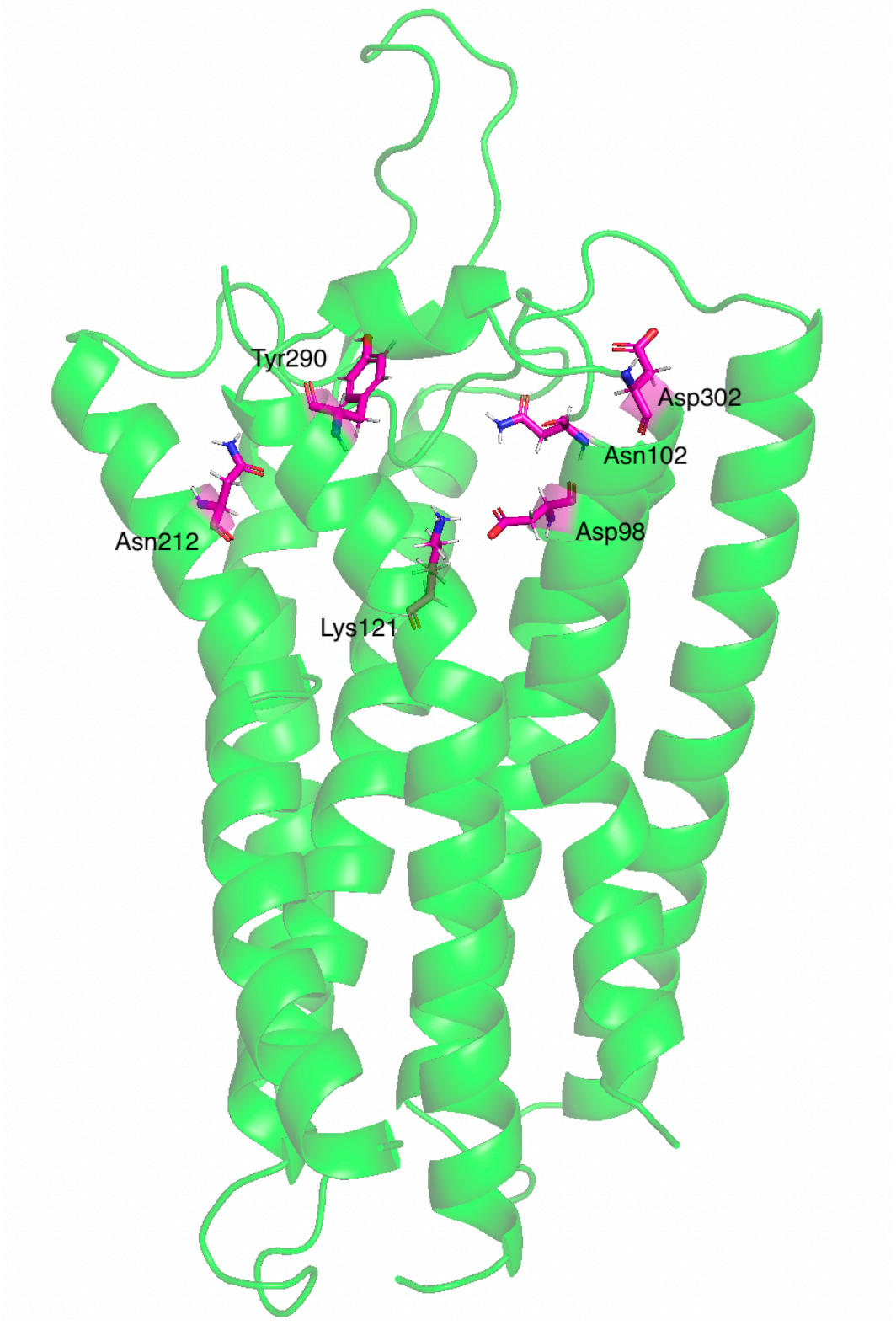

Figure 4: GnRH-R (PDB: 7BR3(5)) in green. The bound Pyrococcus abysi glycogen synthase domain has been removed. Transparency of the 3D structure has been set to 0.5 in PyMol. Amino acids responsible for ligand binding have been highlighted and colored magenta.

2.3 The gonadotropin-releasing hormone

GnRH is an endogenous decapeptide, which is related to human development and reproduction (48). Two different isoforms of GnRH have been discovered in humans, GnRH-I and GnRH-II (46). The difference between the GnRH-isoforms is the four residues between the conserved N-terminus amino acids: pGlu1, His2, Trp,3 Ser4, and C-terminus amino acids: Pro9, Gly10 (46). GnRH 1 is the most well-known and studied (46). GnRH 1 consists of the following amino acids: pGlu1-His2-Trp3-Ser4-Tyr5-Gly6-Leu7-Arg8-Pro9-Gly10 (49). GnRH-I will hereby be termed GnRH.

The N-terminal of GnRH has a pyroglutamate. Pyroglutamate is an amino acid derivate which is a lactam of glutamic acid (50). While the origins and exact function of pyroglutamate as an amino acid derivate is unclear, its presence has been confirmed in living cells (50). At the C-terminal there is an amine, which makes the last amino acid in the decapeptide chain a carboxamide (49). Amino acids near the N-terminal and C-terminal in GnRH, are involved in receptor binding (44, 46). Their respective domains are pGlu1-His2-Trp3-Ser4 and Pro9-Gly10, which are both conserved and necessary for binding and activation of the GnRH-R (51). The non-conserved domain which consists of Tyr5-Gly6-Leu7-Arg8 has shown to be the basis of other isoforms of GnRH while also increasing ligand specificity for the GnRH-R (46, 52).

GnRH is considered fundamental for altering the release of FSH and LH. The release of GnRH is done in a pulsatile manner from the hypothalamus, and this pulsatile secretion is different for FSH and LH (53). FSH secretion seems to be more irregular than LH. In addition, over 90% of GnRH pulses are related to FSH release (54, 55). GnRH also plays a pivotal role in LH release, a GnRH surge is interlinked with pre-ovulatory LH- release, and this specific occurrence and interaction is dose-dependent (56). The biological relevance of GnRH is associated with both puberty and reproduction; this is indirectly through the secretion of FSH and LH (57, 58). Drastic changes in GnRH pulses do lead to certain endocrine disorders such as chronic anovulation or luteal insufficiency (59). Changes in GnRH release can result in GnRH deficiency in males, with symptoms being infertility, decreased muscle mass as well as other symptoms of incomplete sexual maturation (60).

2.3.1 Gonadotropin-releasing hormone receptor function

When GnRH binds to the GnRH-R located in the anterior pituitary, it triggers the activation of the receptor, the receptor then recruits the Gα subunit of the G-protein on the cytoplasmic side (61). The general consensus among researchers is that the coupled G-protein is of the $G_{q/11}$ family for the pituitary cells and it is coupled with GnRH-R(61). As shown in Figure 5, the active receptor induces the exchange of a GDP for GTP, and this releases the α-subunit from the G-protein. The α-subunit, now released and activated, continues to activate the PLC β-signaling pathway(62). The PLC β-signaling pathway involves the endogenous molecules: Phosphatidylinositol 4,5-bisphosphate (PIP_2), Diacylglycerol (DAG), and Inositol 1,4,5-triphosphate (IP_3). (63). An activated PLC will cleave PIP_2. PIP_2 together with other phospholipids make up the cell membrane and have the inositol head group facing towards the intracellular environment. PIP_2 is cleaved into IP_3 and DAG, which works as second messengers (64).

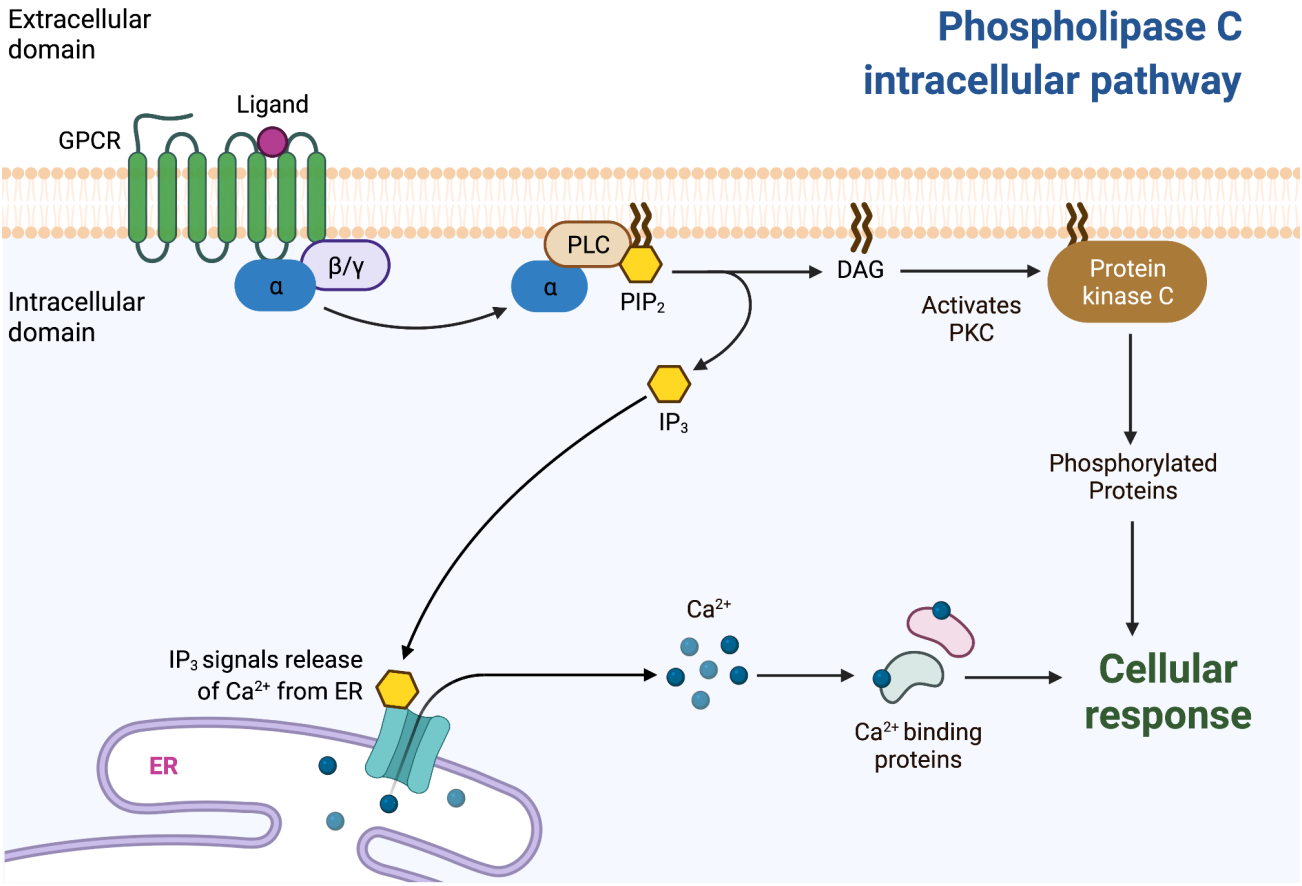

Figure 5: A simplified overview of the Phospholipase C Signal Transduction. Figure taking inspiration from Silverthorn´s Human physiology 4th edition (65). Adapted from "Activation of Protein Kinase C (PKC)", by BioRender.com (2022). Retrieved from https://app.biorender.com/biorender-templates

IP_3 and DAG have objectives as second messengers in the signaling pathway. While both molecules promote the gene expression and secretion of gonadotropins, their routes for achieving this is different from one another. IP_3 ends up binding to IP_3 receptors on the endoplasmic reticulum which leads to the release of Ca^{2+} intracellular. This together with DAG stimulate Protein kinase C (PKC) activation. PKC is a central enzyme in regulating specific proteins which bring forth the synthesis of gonadotropins(61, 63, 66). PKC will prompt the activation of extracellular signal-regulated kinases (ERK). ERKs together with Mitogen activated protein kinases (MAPK) makes up the ERK/MAPK pathway. This leads to differentiation and proliferation of gonadotropic cells (67).

2.4 Pathophysiology of GnRH and GnRH-R

GnRH together with GnRH-R are major factors when it comes to the pathophysiology regarding the reproductive system in females. The presence of GnRH-Rs on human cells located in the ovary and endometrium are undeniable and have been researched(68). Behind the GnRH/GnRH-R interaction there is a hypothalamic neural network which controls both the pulsatile secretion of GnRH and its synthesis. This neural network undergoes neuronal migration from medial olfactory placode to the hypothalamus, which happens in the timespan between conception and birth(69, 70). A defect in the migration of neurons can cause abnormal activity or, in worst cases, missing GnRH activity. This in turn, leads to hypogonadism which affect reproduction negatively (71).

GnRH-Rs have also been proven to be expressed on cancer cells. Types of cancer which GnRH-R is involved in are endometrial-, breast-, ovarian-, and prostate-cancer (72). A suggested function of GnRH-R on tumors is that it is a part of an autocrine or paracrine system. This means GnRH-R is stimulated either through the tumor cell it is expressed on or by nearby tumor cells. GnRH-R and its role in the autocrine system for tumors have been confirmed to control cell proliferation(72, 73).

GnRH-R expressed on tumor cells have different signaling pathways than non-cancer related GnRH-R (4). GnRH-R expressed on prostate cancer cells are coupled with the G_i protein, another family of G-proteins, therefore it also has another signaling cascade (4). After the

GnRH-R is activated and has recruited the Gα-subunit, G_i protein functions by lowering intracellular cyclic adenosine monophosphate (cAMP). This is done when the α-subunit inhibits the cAMP dependent pathway of protein kinase A. However, this leads to the activation of specific MAPK kinases, phosphatidylinositol-3-kinase and phosphotyrosine phosphatase (4).

2.4.1 Glioblastoma

Glioblastoma, also known as glioblastoma multiforme (GBM) is an overly aggressive type of cancer which can appear within the brain (74). In the U.S, it has been reported that patients with GBM have a 5-year survival rate of 5,1% and a 1-year survival rate of 37,2% (75). The cancer is defined as a malignant brain neoplasia, meaning it is highly uncontrollable and results in invasive growth in nearby brain tissue (76). GBM arise in glial cells in the central nervous system, glial cells are central for supplying nutrition along with oxygen for neurons located in the brain (77). While the complete pathophysiology of GBM is not fully understood, literature have reported expression of GnRH-R in GBM and its possible role as a regulator of metastasis and cell-growth of cancer (72). GnRH agonists have also been confirmed to have an antiproliferative effect on cancer cells (73).

2.5 Pharmaceuticals acting on GnRH-R

GnRH agonists and GNRH antagonists are the two types of drugs acting on GnRH-R. Agonists activates a biologic response similar to the endogenous GnRH binding to GnRH-R. Antagonists obstructs GnRH-R, effectively blocking the natural biologic response. GnRH antagonists will compete against GnRH when administered (78). Some known GnRH-agonists are Goserelin (Zoladex ®) and Leuprorelin (Eligard ®). These marketed drugs can be seen along with GnRH in Figure 6. While peptides make up the GnRH agonists, GnRH antagonists can either be peptides or non-peptides, which are small molecules.

Goserelin Leuprorelin Gonadotropin-releasing hormone

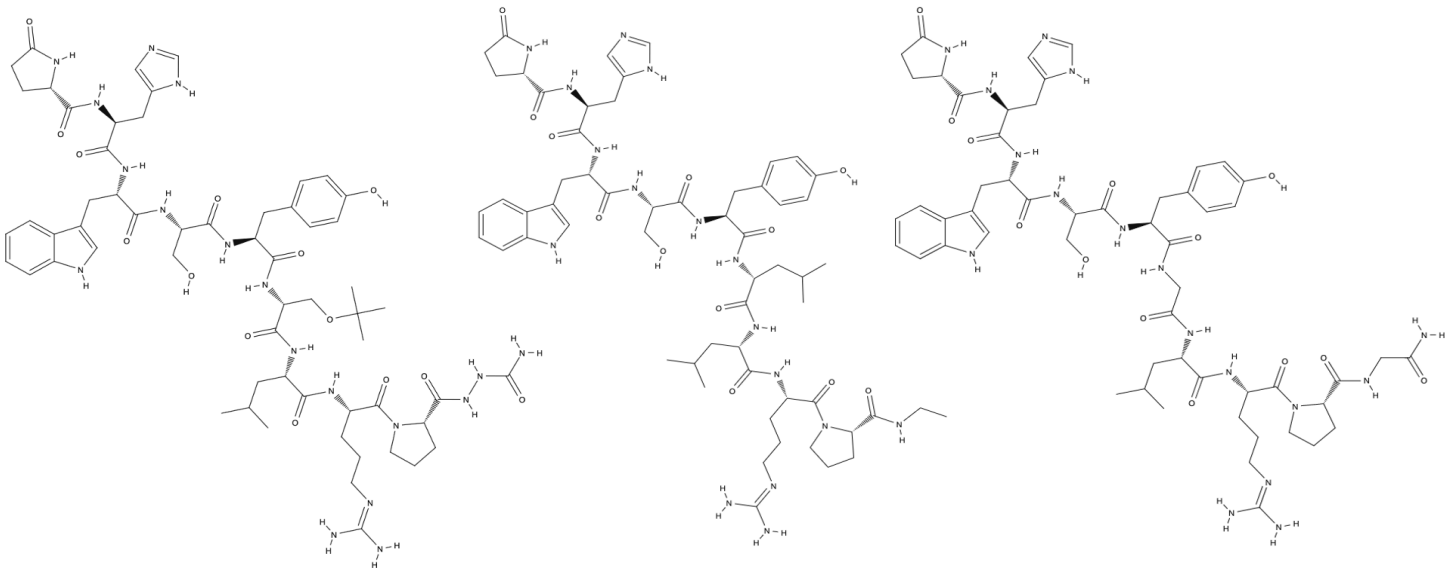

Figure 6: Structural formula image of the marketed drugs Goserelin (Zoladex ®) and Leuprorelin (Eligard ®), two GnRH analogues along with GnRH.

Agonists are also considered GnRH-analogues (79). Meaning the molecular structures are related and based on GnRH. In Figure 6 it is especially evident for Goserelin and Leuprorelin which have a modified sixth residue and a modified C-terminal compared to its endogenous counterpart GnRH. GnRH-analogues have been modified to bind to GnRH-R with higher affinity, having a dissociation constant of 1 nano molar, while also being more resistant to enzymes. Being more resistant to enzymes prevents rapid degradation when administered, therefore increasing the half-life (79). Position 6 in the peptide chain is often switched out with another d-amino acid to increase enzymatic stability or a hydrophobic group which proves to increase affinity for GnRH-R. Administrating GnRH analogues on a regular basis result in desensitization as well as reduced expression of GnRH-R (79).

GnRH antagonists exist either as GnRH analogues or small molecules (80). Over the last years the development of small molecules have been prioritized over peptide-like antagonists. The reason lies with peptides usually being prone to environmental degradation and having a shorter half-life overall (5). Examples of small molecule GnRH antagonists are Elagolix and Relugolix which can be seen in GFigure 7 (5, 81). Compared to GnRH agonist analogues, GnRH antagonists which are also GnRH analogues have further residue position modifications, which

are usually modifications at residue position one (pGlu)1, two (His2), three (Trp3) as well as eight (Arg8) (82). Small molecule GnRH antagonists like Elagolix and Relugolix are based on uracil derivates, with the uracil pharmacophore is widely used as a starting template for developing small molecule antagonists (80). GnRH antagonists binds reversible to GnRH-R and act to immediately suppress both LH and FSH without desensitizing GnRH-R (80).

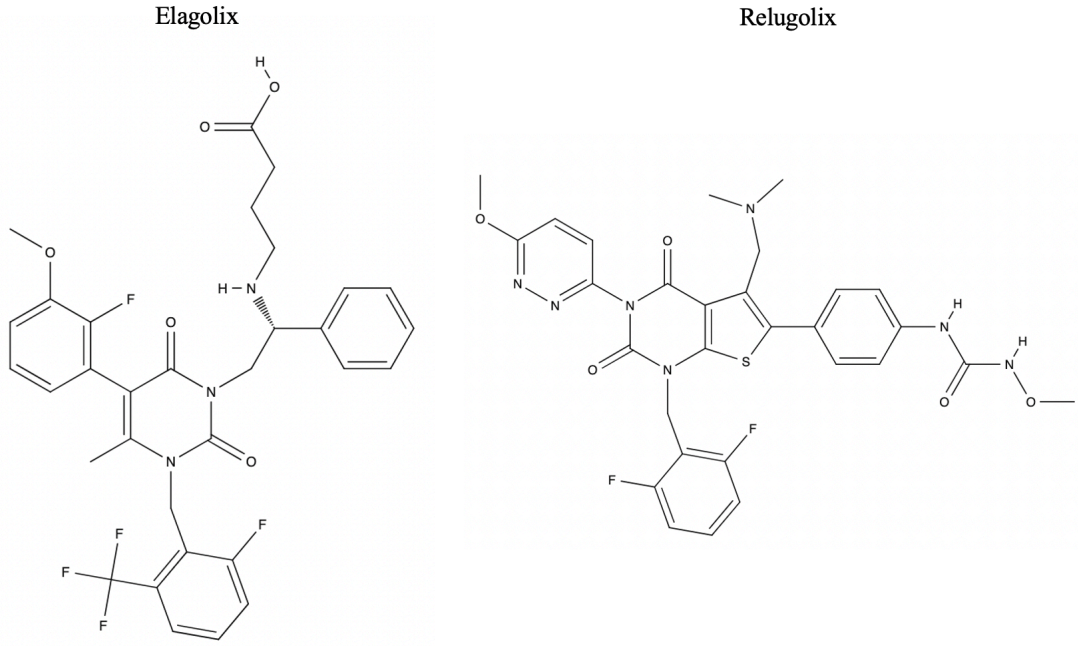

GFigure 7: The GnRH antagonists Elagolix and Relugolix.

2.6 Computational approaches to drug design

Development in technology has led to molecular modeling being an efficient approach in drug discovery and design (83). Essentially, molecular modeling is to simply replicate the role of a molecule or molecular system through either molecular mechanics, quantum mechanics or both (83). To be able to do molecular modeling a 3D model of the molecule or molecular system is needed, therefore suitable hardware and proper software is needed to visualize it (84).

3D models used for molecular modeling are acquired through published structures in databases e.g., PDB (85). Two modern approaches to structure determination are X-ray crystallography and cryo-electron microscopy (EM). X-ray crystallography uses X-rays on a protein crystal to

assess its 3D structure (85). Cryo-EM use electron rays through a microscopy on a frozen sample of proteins (86).

As molecules are not in fixed positions, conformational analyses are needed as molecules can attain different conformations considering the environment they occupy (84). Examples on two approaches are Monte Carlo methods and molecular dynamics (MD) (84). Monte Carlo is a random search method where newly obtained conformations are a result of random iterations on the structure e.g., torsion angles(84). MD simply explained are time based motions of a molecule or molecules (84).

The mechanics behind molecular modeling can be split into two distinct categories which form the basis of the computational approach to chemistry: molecular mechanics and quantum mechanics. Molecular mechanics do not include electrons. However, it assesses classical physics and its relation to molecules (nuclei and bonds), forcefields and torsions. Quantum mechanics do include electrons and assess the relationship between nuclei and electrons using quantum physics. Both methods and their application depend on the molecule and the given task. Quantum mechanics are applied when calculating orbital energies for molecules and electrostatic potentials. Molecular mechanics is used to study molecular motions such as MD and when identifying stable conformations of a molecule (87). Quantum mechanics are used for smaller molecules and its use requires hefty computational power considering the focus on electron distribution (87), therefore molecular mechanics has been used to acquire the results for this thesis, since its use can be applied to systems which contains larger molecules, such as proteins.

2.6.1 Force fields

Force fields, simply explained, are the calculation of torsional energy, bending of angles, bond stretching and interactions (non-bonded) along with polarizability using classical mechanics found in physics (87). Force fields in general are applied in conventional MD and ´force field´ as a term is used interchangeably with molecular mechanics. When force fields are applied, electrons are disregarded. Electrons are disregarded as a result of the Born-Oppenheimer approximation. This approximation views the movements of nuclei and the movements of

electrons as two separate movements. The Born-Oppenheimer approximation is implemented when working with computational methods where force fields are applied (88).

Early force fields and force fields used today are based on the work by the pioneers Norman Allinger, Shneior Lifson, and Harold Scheraga, all renowned scientists in the field of organic macromolecules. The well-known force field models CHARMM, AMBER and OPLS were developed during the 1980s. During the early developments of these force fields both CHARMM and AMBER were mainly used and tested on gas-phase simulations. While AMBER includes partial charges, CHARMM apply neutral charges. OPLS differs from CHARMM and AMBER by trying to implement liquid state properties connected to thermodynamics. Although all three models used a "united atoms" approach, meaning hydrogen bound to carbons were treated as ´one´, they have since moved from this and all three are still being updated and implemented in computational methods to this day(88).

2.6.2 Molecular docking

The main objective with computational molecular docking is to visualize and get a better understanding of the ligand binding mode as well as how two 3D structures interact with one another. Docking results in three-dimensional intramolecular complexes, usually called poses, consisting of two molecules: the ligand and the receptor. This means it is an efficient tool for exploring the binding mode for agonists. Different types of docking exist and are used on the basis of the objective for the docking simulation (89). In general, there is rigid docking (where both ligand and receptor is treated as rigid structures), flexible ligand docking (receptor is rigid, ligand is flexible), and flexible docking (both ligand and receptor are flexible) (89). A docking pose is also accompanied by a score. This score is used to evaluate a ligand´s pose relatively to one another. The score has basis in the free-energy related to the receptor-ligand complex. While different equations exist, an additive equation was proposed by Ajay and Murcko in 1995, it is regarded as a complete and general equation for the docking score and measured in kcal/mol:

$$\Delta G_{bind} = \Delta G_{solvent} + \Delta G_{conf} + \Delta G_{int} + \Delta G_{rot} + \Delta G_{\frac{t}{r}} + \Delta G_{vib}$$

solvent is related to the solvent effect, *conf* is related to conformational changes, *int* is related to free energy arising from interactions, *rot* represents loss of energy related to freezing

rotations, *t/r* is the loss of free energy connected to translation and rotation and *vib* is related to energy connected to the different modes of vibration. A more negative score is related to a strong binding between the ligand and the receptor. (83).

Induced fit docking (IFD) differs from rigid docking by accepting a flexible binding pocket for the ligand. The flexible site is a result of a conformational change which is induced by the ligand chosen for the docking. IFD usually result in negative change in enthalpy, loss of internal energy, which compensates for the newly interactions formed between ligand and receptor during the docking phase (90). IFD is available as a tool in Maestro and essentially combines the rigid receptor docking and the protein structure prediction with refinement. As tool, IFD is used especially for cases where the receptor undergoes movements because of the ligand, as it regards both conformational side-chain changes and small backbone relaxations of the protein (91).

2.6.3 Homology modeling

Homology modeling is to build a molecular 3D structure from an amino acid sequence using published 3D structures (termed templates) which are related (92, 93). The term homology is connected to the word ´corresponding´, and the term itself is rooted in the biologic consensus of shared ancestry. Throughout evolution, some specific characteristics have remained similar as a result of ancestry (94).From a molecular modeling standpoint, it can be correlated to how a target and a template once had a common ancestor.

Homology modeling is usually performed to acquire quaternary structures for sequences which do not have published 3D structures (93). At the beginning of the process relevant templates are selected or searched for based on the amino acid target sequence (93). Choosing a template of interest is an important step where the amino acid sequence is used as a basis to identify existing, published, three-dimensional structures in valid databases (93). It solely depends on the target sequence, as for some sequences there are a few well-known templates (93). However, some target sequences need a thorough template search as a result of a broader spectrum of templates to choose from (93).

After a template is chosen an alignment of the amino acid sequence and the chosen template is performed. The model building is done after the alignment. A model with sidechains, loops and backbone is built on the basis of the alignment. The last step is a model evaluation. A model evaluation can be superimposing the homology model with a native structure if possible, then analyzing the root mean square deviation (RMSD) value Cα carbons, which make up the backbone of the protein (95).

In addition to the template search, the sequence alignment is a crucial step as well, with grave errors in the sequence alignment resulting in an inferior model. The model evaluation is a validation and assessment of the result. If the model does not comply with the demands of the researcher, the full process can be repeated with a different template as well as another approach to the model building (92). Forrest et. al. have assessed that for membrane proteins, a template sequence identity of 30% indicates an applicable homology model (96). This is a good reference point for building e.g., GPCRs which are situated in the cell membrane.

2.6.4 Molecular dynamics simulations

First developed in the 1970s, MD-simulation is a computational method focusing on motions of molecules and atoms over a given time course. Simulations are based on physics, more specific Newton´s laws of motion, and approximations of forces between bonded and non-bonded atoms. A system containing a solvent model, boundary conditions including ion placement is needed before conducting a MD-simulation. A system used for MD is consists of the molecules of interest usually placed in a water model, a membrane, or both, this is then encased in a boundary box(97). Forces are then being calculated for each atom. The motion of each atom is based on these calculations. Finally, the motions are done over the specific time period chosen (98). MD-simulations is usually done on proteins alone or in complex with ligands/ other proteins to study the conformational change under set conditions such as temperature and pressure (98).

2.7 Aim of the study

It has been researched that GnRH agonists decrease proliferation on certain breast- and ovarian cancer cells, in addition to glioblastoma cells (73). The decapeptide GnRH provide the basis for many GnRH agonist analogues (99). While specific interactions between GnRH and GnRH-R have been reported and published in literature (44, 46), computational studies on both the receptor and ligand could prove valuable to see if the interactions lead to the conformational change and an active structure of GnRH-R. The aim of this research was to explore the activation mechanism of GnRH-R in addition to discover how an active model of GnRH-R in complex with its endogenous ligand, GnRH, would be like. The purpose of this study was also to investigate the peptide interactions GnRH made with its receptor through computational methods such as docking and MD. The reason for studying this is because both GnRH and GnRH-R have a central role in both hormonal diseases and specific cancers such as GBM.

3 Methods

3.1 Software packages used

The graphical user interface Maestro by Schrödinger® was used to visualize glide ligand docking and IFD poses, homology models, MD-simulations trajectories and post-MD analyses. The following Schrödinger programs were used: Glide® (Schrödinger, LLC, New York, NY, 2021) was used for the ligand docking, Induced Fit Docking Protocol®(Glide, Schrödinger, LLC, New York, NY, 2021; Prime, Schrödinger, LLC, New York, NY, 2021) was used for IFD, Prime®(Schrödinger, LLC, New York, NY, 2021) was used for the homology modeling, MD-simulations and its analyses were performed in Desmond® (D. E. Shaw Research, New York, NY, 2021. Maestro-Desmond Interoperability Tools, Schrödinger, New York, NY, 2021) . The Maestro version used was Maestro version 12.9.123, MMshare version 5.5.123, release 2021-3. The platform which Maestro was used on was Linux x86_64 which was on a computer in a molecular modeling pc-lab. SWISS-MODEL, a homology modeling web server, was used for template searching for the homology modeling. Superpositions with RMSD values including specific figures was completed and made in PyMol, a molecular visualization system by Schrödinger®. The PyMol version used was version 2.5.2. The platform PyMol was used on was macOS Monterey version 12.3.1 which was on a personal computer.

3.2 Glide ligand docking

Glide ligand docking is a docking tool which is found in the computer application Maestro by Schrödinger®. Glide finds the top docking poses based on a "funnel" method (100). Initially a specific receptor grid and relevant ligands are needed. A receptor grid defines the available space the ligand can occupy in the receptor structure. It is box-shaped with three different coordinates defining it (x, y, z) and measured in Ångstrøm (Å). The search for an optimal pose is narrowed down through initial scoring and rough positioning inside the receptor grid. An energy optimization is done using an Optimized Potentials for Liquid Simulations (OPLS) all atom force field. this is followed by Monte Carlo sampling. Monte Carlo sampling is repeated random sampling based on the probability distribution. Finally, the docked pose is chosen through an energy function based on force field and empirical terms(100). Along with a docking

score, Glide ligand docking also results with a glide ligand score. A glide ligand score does not include Epik state penalties, which is essentially empirical pKa prediction for molecules (101).

To explore the binding mode of GnRH (PDB: 1YY1) in GnRH-R (PDB: 7BR3) docking jobs were executed with focus on known information about the binding pocket and interactions. To begin with the GnRH-R structure was imported to Maestro through the PDB accession code: 7BR3, the published crystal structure of GnRH-R.

The protein was then pre-processed through the Protein Preparation Wizard. The role of protein preparation is necessary considering some structures from PDB are incomplete, contain molecular clashes or contain co-factors in form of molecules which are unwanted for the docking job coming up. Therefore, a protein preparation makes the protein complete and suitable for docking. In the Protein Preparation Wizard´s ´import and process´ tab the default settings were chosen: ´assign bond orders´, ´use CCD database´, ´add hydrogens´, ´create zero-order bonds to metals´, ´create disulfide bonds´. ´Fill in missing side chains using Prime´ and ´fill in missing loops using Prime´ were implemented as well. for ´Generate het states using Epik´ where the pH was set to 7,4+/- 0,3 to reflect the pH in vivo. Furthermore, in the ´review and modify´ tab, every non-covalently bound residue except Elagolix was removed, the covalently bound Pyrococcus enzyme was deleted as well. To complete the pre-processing, a refinement in the ´refine´ tab was done. Default settings for the Hydrogen bond (H-bond) assignment were applied: ´sample water orientations´, ´use PROPKA pH: 7.4´. Waters were removed: ´beyond hets 3.0 Å´. A restrained minimization was done: ´converge heavy atoms to RMSD: 0.30 Å.

Elagolix was used to localize the binding pocket, and then used as the center of the grid. After locating the grid Elagolix was removed to leave the binding pocket open and free for the docking of the ligand. Then the grid was generated using standard settings in the grid generation tab, it was also made to be ´suitable for peptide docking´, a setting in the grid generation tab which basically pre-chooses the precision to standard precision (SP)- Peptide. When it came to rotatable groups for the receptor, all rotations were allowed. Initial grid-size was set at 20 Å, which was a default setting.

The 1YY1 PDB file contains 21 conformers and out of these the first entry was chosen for the different docking jobs. The first entry of 1YY1 underwent the ligand preparation in LigPrep. The following settings were used in LigPrep: force field was set to OPLS4, generate possible states at target pH: 7,4+/- 0,3, desalt, generate tautomers, retain specified chiralities. A set of 50 (and later 100) stereoisomers were generated for the first entry of PDB: 1YY1 as two differ.

For the ligand docking, the receptor grid was uploaded as a file along with the ligands from the ligand preparation. For the docking job, default settings were used: ´sample nitrogen inversions´, ´sample ring conformations´, ´bias sampling of torsions for: all predefined functional groups´. The precision was set to Standard precision (SP)-Peptide with the ligand sampling set to flexible which was a part of the standard settings. No specific constraints settings were set, and the output was set to 5 poses per ligand. A post-docking minimization was also set. After some docking attempts which died, the enclosing box size was adjusted and the site was chosen to be 36 Å in size, which is the maximum possible grid size in Maestro. The glide ligand docking result was evaluated on the basis of published interactions between GnRH and GnRH-R by Tzoupis et. al (46). The orientation of the peptide in the ligand binding pocket was also evaluated. If the whole ligand was observed outside the ligand binding pocket, it was disregarded.

The results from the glide ligand docking of the crystal structure did not acquire poses with receptor-ligand interactions which were suggested by Tzoupis et. al. (46) and Flanagan et. al. (44) in their respective literature. The reason could be that a peptide agonist was too large to be docked into a receptor which had been crystallized with a small molecule antagonist in its binding pocket.

3.3 Induced fit docking

IFD was done on the basis of making the receptor more flexible to accept the ligand, considering GnRH being a decapeptide, a much larger ligand than Elagolix. For the IFD, the 50 stereoisomers from the ligand preparation of the glide ligand docking were implemented as a file. Standard protocol was chosen for the IFD, meaning a maximum of 20 poses per ligand were retained. For the box center, centroid of workspace ligand was picked, which was Elagolix. For the box size, dock ligands with length ≤ 36 Å was chosen. No constraints were defined, and standard settings across the following tabs: ligands, glide docking, prime refinement, glide redocking were implemented. For the jobs tab, the number of Glide and Prime CPU was set to 12, which was the maximum number of cores.

The IFD of the X-ray crystal structure did provide poses with one or more receptor-ligand interactions which were suggested by Tzoupis et. al. (46) and Flanagan et. al. (44) in their respective literature. However, with parts of the decapeptide still sticking out of the ligand-binding pocket and some interactions still not present, a homology model was generated to acquire an active conformation of GnRH-R.

3.4 Homology modeling

Homology modeling was done in order to obtain a GnRH-R structure with a more accessible ligand binding pocket than the crystal structure, so that the ligand could make the known interactions with the receptor residues. It was also done to acquire GnRH-R in an active state, considering the crystal structure was bound to Elagolix, an antagonist. The homology modeling was done in three steps: template selection, alignment, and then modelling. Another 3D structure of GnRH-R was needed to further explore the binding site of an active receptor. This was because the crystal structure 7BR3 was an inactive structure which was bound to a non-peptide antagonist. For the template selection, the homology modeling web server SWISS-MODEL was used to search for templates. To search for templates through SWISS-MODEL, the target sequence was needed. The target sequence used had UniProt accession number: P30968 (GNRHR_HUMAN).

After inserting the target sequence and running the template search, a list of templates is generated. A few select templates were chosen based on templates being class A GPCRs with ligands which were an agonist and a peptide. The templates considered were the human cholecystokinin receptor (PDB: 7MBX, 7EZH, 7F8X) and human orexin receptor 2 (PDB: 7L1U). The templates then went through a pairwise alignment with the target GnRH-R amino acid sequence in Maestro:

Table 1: The templates (PDB) evaluated and how they were acquired (method), along with resolution in Ångstrøm, sequence identity in %, the G-protein type they are coupled with, and their peptide-ligand.

PDB:	Method:	Resolution(Å):	Seq-ID (%):	G-protein	Ligand
7MBX	Cryo-EM	1,95	19	G_s	Cholecystokinin-8
7EZH	Cryo-EM	3,20	18	G_i	Cholecystokinin-8
7F8X	X-ray	3,00	20	-	NN9056 (Cholecystokinin analogue)
7L1U	Cryo-EM	3,20	17	G_{sqi}	Orexin

For modeling the ´Build Homology Model´ window in the Multiple Sequence Viewer/Editor (Maestro) was used to build a homology model after the following steps: The target sequence

found on UniProt was imported as a FASTA-file. Then one of the templates was chosen as the template structure. An alignment was run. Ligands and cofactors were not included. And the model setting was set to ´knowledge-based´ in maestro. ´Knowledge-based´ means the computational modeling process screens databases of published structures to close gaps as well as construct certain insertions where needed. To be able to compare the newly built homology model PyMol was used. This was done by importing the prepared crystal structure (7BR3) and the homology models of interest, then using the alignment tool in the ´Multiple Sequence Viewer/Editor´. The pairwise sequence alignment for GnRH-R and cholecystokinin receptor A (7EZH) can be seen in Appendix under Figure A1. In the end the homology model with 7EZH as template was chosen for further dockings and simulations.

The reason for choosing PDB: 7EZH as the template, was because the homology model generated, resulted in three docking poses which had two of the receptor-ligand interactions found in literature (44, 46) after docking GnRH using glide ligand docking. Besides the homology model using 7EZH as template, the homology model based on 7F8X produced only one pose with two interactions from literature (44, 46). None of the mentioned poses fully occupied the binding pocket. For the glide ligand docking of the homology models, the settings mentioned in **3.2 Glide ligand docking** were used, except for locating the binding pocket, where ´centroid of residues´ was chosen and the following residues defining the ligand binding pocket were picked: Asn212, Asp98, Lys121, Tyr290, Asp302, and Asn102. This was because Elagolix was not present to identify the binding pocket.

Since the homology model using 7EZH as template only acquired poses with two of the receptor-ligand interactions found in literature (44, 46) an IFD was executed to see if there was possible to acquire more interactions from the same literature, as well as to see if the ligand could fully occupy the binding pocket without ligand amino acids sticking out. Settings mentioned in **3.3 Induced fit docking** was used for the IFD, however for locating the binding pocket, ´centroid of residues´ was chosen and the following residues defining the ligand binding pocket were picked: Asn212, Asp98, Lys121, Tyr290, Asp302, and Asn102. After evaluating the poses after IFD, the pose with the docking score -13,448 kcal/mol was chosen for MD-simulations, on the basis of it making more than two interactions which have been published in literature (44, 46).

A multiple sequence alignment (MSA) for GnRH-R, cholecystokinin A receptor, and Orexin receptor 2 was executed in gpcrdb.org (43, 102), a web repository for GPCRs which can be used for visualization as well as alignment. This was compared with the pairwise alignment done in maestro where 7EZH and GnRH-R were involved (Appendix Figure A1). While the pairwise alignment did not align correctly for specific parts of the protein compared to the MSA done in gpcrdb.org, the following parts matched in terms of alignment and secondary structure: TM2, ECL1, TM3, ICL2, TM4, TM6, ECL3, and TM7. Other parts such as TM1, ICL1, ECL2, TM5, ICL3 did not align properly with whole sequences being shifted. It is to be noted that the TM helices are more important considering TM helices having conserved parts. Even though other structures of cholecystokinin receptors had better resolution and sequence identity, 7EZH was chosen on the basis of resulting in more poses where the ligand made interactions found in literature.

3.5 Molecular dynamics method

In total, three different MD-simulations were done:

1) Crystal structure of GnRH-R where IFD was used to dock GnRH (1YY1), the pose used made two ligand receptor interactions found in literature (44, 46). Docking score: -21,692 kcal/mol.
2) Homology model of GnRH-R where IFD was used to dock GnRH (1YY1), the pose made three ligand receptor interactions found in literature(44, 46). Docking score: -13,448 kcal/mol.
3) Homology model without ligand.

3.5.1 System building and molecular dynamics settings

To run a MD-simulation, a system needed to be built in the ´System Builder´. Default settings were used: ´box shape: orthorhombic´, ´box size calculation method: buffer´, ´distances(å): a:10.0, b: 10.0, c: 10.0´, ´angles (°): α: 90.0 β: 90.0 γ: 90.0´, ´no custom charges set´, ´ion placement: neutralize by adding 0 Na^+ ions´, ´force field: OPLS4´. The membrane model used was palmitoyl-oleoyl-phosphatidylcholine 300K (POPC), and transmembrane atoms were placed automatically. The solvent model was set to simple point charge (SPC). The system was then loaded from workspace to the MD setup. The simulation time was set to 1000 ns. The recording interval, trajectory, which was in picoseconds were set to 500 ps with the energy: 1,2 kcal/mol. Approximate number of frames was set to 1000. Ensemble class was automatically set to NPγT, temperature was set to 300 K, which meant the system was heated to 26,85 degrees Celsius, pressure bar: 1,01325, surface tension (bar*Å): 0,0. The model was set to relax model system before simulation.

After the simulation was finished a Simulation Interaction Diagram (SID) was set up and exported as a pdf file. SID is an analysis on the receptor and ligand, their movements and interactions during the MD-simulation are assessed. a Simulation Quality Analysis (SQA) was also done. SQA is a separate analysis which analyzes the quality of the simulation, this means averages of potential energy, total energy, temperature, pressure, and volume is displayed. SQA can also make plots of these values over time. The same procedure and analyses were done for the homology model without the ligand.

4 Results

The results consist of glide ligand docking of GnRH into the published GnRH crystal structure (7BR3), the homology modeling of GnRH-R based on a GPCR template (cholecystokinin receptor), IFD of GnRH into the homology model, and IFD of GnRH into the published crystal structure PDB: 7BR3. A total of three MD-simulations were also done: a MD-simulation of the homology model, a MD-simulation of the IFD pose of the homology model and ligand, and a MD-simulation of the IFD pose for the crystal structure and ligand. Post-MD analysis were also made. Specific structures were also superimposed in PyMol, which also resulted in a RMSD value.

4.1 Glide ligand docking of the X-ray crystal structure

The glide ligand docking of GnRH into the crystal structure resulted in a total of 379 different docking poses. The lowest energy pose had a docking score of -16,446 kcal/mol. In general, the lowest energy poses displayed the ligand with the N-terminus residues (pGlu1, His2 and Trp3) outside the ligand-binding pocket which can be seen in Figure 8. The ligand seems to have entered through the available space by the helices TM1, TM6 and TM7. However, the ligand seems to be far away from residue Asn212, which is supposed to form interactions with pGlu1(46). The protein residues Asp98 and Asp302 which are connected respectively to receptor activation and ligand binding did make interactions, however, these interactions were not the receptor-ligand interactions reported in literature by Tzoupis et. al. (46). Protein residue Asp98 made an interaction with the nitrogen in the peptide bond between Gly6 and Leu7. There was also a H-bond between protein residue Asp302 and GnRH residue pGlu1. The proper interactions would have been protein residue Asp98 and ligand residue His2, along with Asp302 and Arg8. The ligand not fitting into the binding pocket became the basis for IFD.

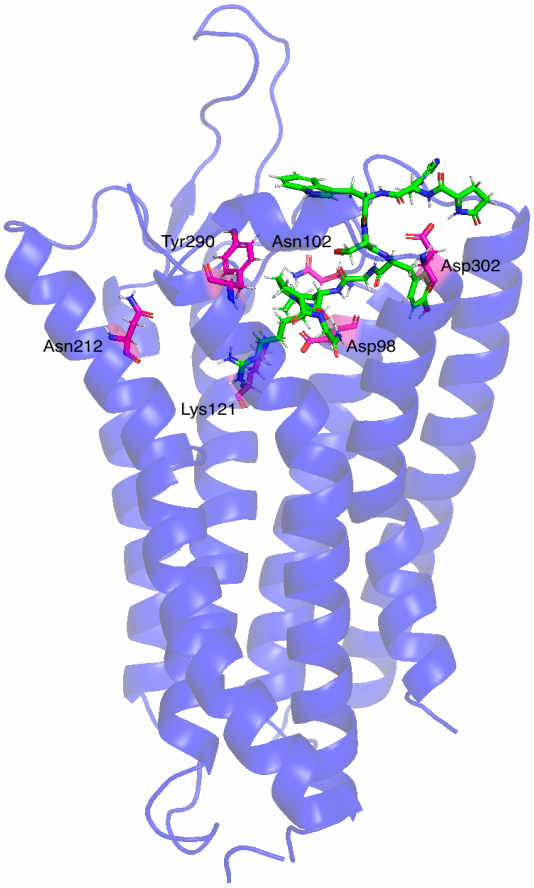

Figure 8: The X-ray crystal structure of GnRH-R in blue, and the docked GnRH in green. Magenta colored residues are labeled and have been highlighted to better visualize the binding pocket.

4.2 Induced fit docking of the X-ray crystal structure

The IFD of the crystal structure resulted in poses which had lower energy than the poses from the Glide ligand docking. The pose displayed in Figure 9 was a pose which made interactions with more than one residue in the binding pocket. The pose had a docking score of -21,692 kcal/mol. The full ligand interaction diagram (LID) can be seen in Appendix under Figure A2. The ligands N-terminus residues pGlu1, His2, Trp3, Ser4 seem to be located in the TM bundle, however C-terminus residues Arg8, Pro9, Gly10 are outside of the binding pocket. The ligand appears to have been docked into the available space by the helices TM1, TM6, TM7, and is close to ECL3 in terms of its placement. On the basis of the ligand still "poking" out of the binding-pocket, a homology model was made with the goal of obtaining more ligand receptor interactions.

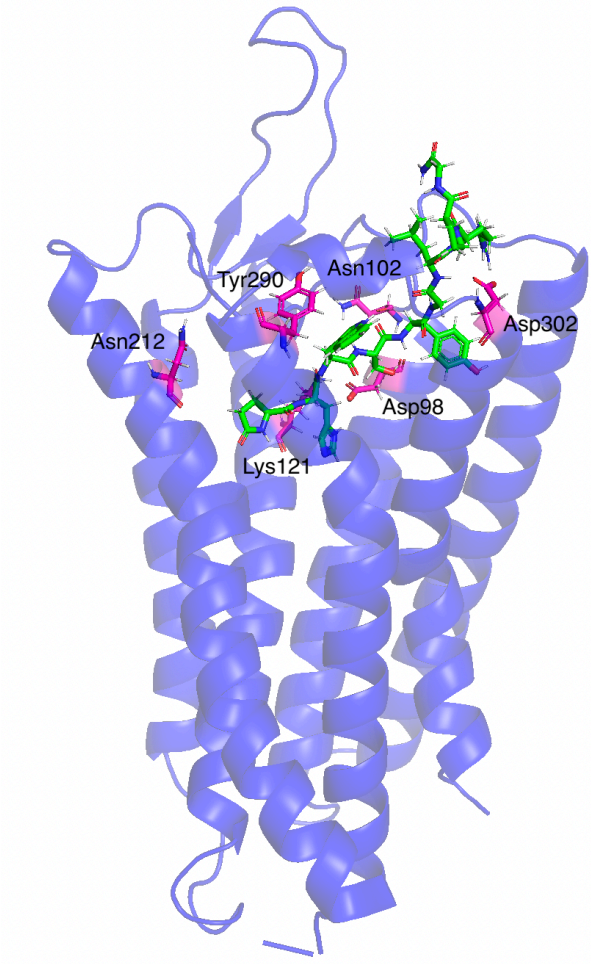

Figure 9: The IFD pose with a docking score of -21,692 kcal/mol. The X-ray crystal of GnRH-R have been colored blue while the ligand GnRH have been colored green. Magenta colored residues are labeled and have been highlighted to better visualize the binding pocket.

4.3 The GnRH-R homology model

7EZH was chosen as the template for the homology model of GnRH-R. The template description read as follows: chain D, Cholecystokinin receptor type A (homo sapiens). The GnRH-R sequence and Cholecystokinin receptor had an alignment identity of 18% after a pairwise sequence alignment was done in the ´Multiple Sequence viewer/editor´ as seen in Appendix Figure A1. Appendix Figure A1 also displays a similarity of 36% and shows the secondary structure alignment where salmon-colored bars represent TM helices and blue-colored arrow represent strands. Superimposing the homology model with the crystal structure in PyMol resulted in a RMSD of 5,576 Å indicating a conformational backbone change since RMSD values describe the average deviation of superimposed atoms. The reason the homology model based on 7EZH was chosen was because it resulted in more ligand poses with interactions found in literature compared to the other homology models when doing a glide ligand docking. In total, three ligand docking poses had a H-bond between the receptor residue Asp98 and ligand residue His2 including an interaction at the C-terminus, which was either a salt bridge and H-bond between receptor residue Asp302 and ligand residue Arg8 or a H-bond between receptor residue Asn102 and Gly10. When superimposing the homology model and the crystal structure, there are present differences which implies an active homology structure has been generated. The ´outward movement´ of TM6 and the ´inward movement´ of TM7 can be observed in Figure 10.

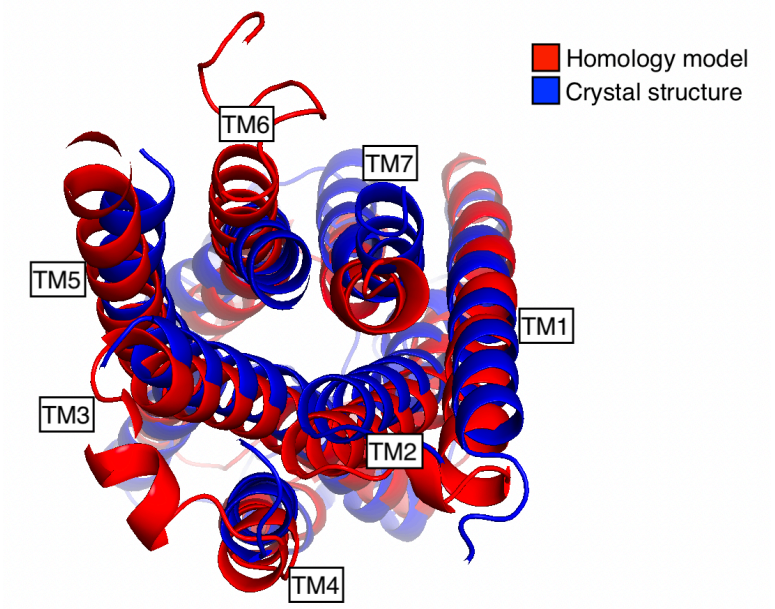

Figure 10: The crystal structure of the receptor and the homology model aligned and viewed from the cytoplasmic side.

4.3.1 Induced fit docking of the homology model

The IFD of the homology model resulted in different poses of the peptide in the receptor, where some of these poses also made interactions with residues present in the binding site. One of the poses, which can be seen in Figure 11, had -13,448 kcal/mol in docking score. The full LID can be seen in Appendix under Figure A3. This pose had the best docking score compared with the ligand-protein interactions it made and was later used for the MD-simulation. Similar to the IFD of the X-ray crystal structure, the ligands N-terminus residues pGlu1, His2, Trp3, Ser4 seem to be located in the TM bundle. C-terminus residues Arg8, Pro9, Gly10 is outside of the binding pocket. As for the orientation, the ligand is closer to TM5 and ECL2 than it is to TM1.

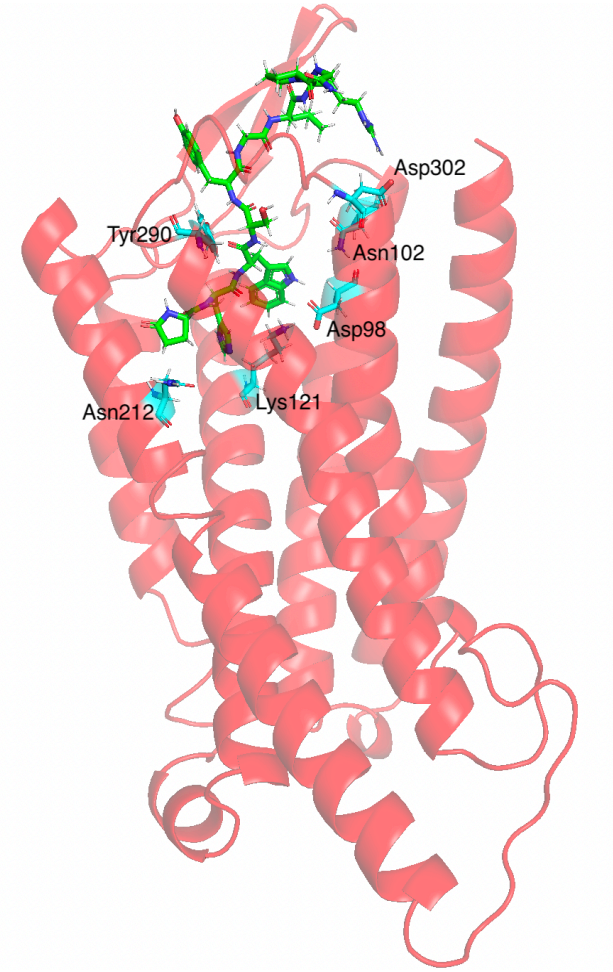

Figure 11: The IFD pose with a docking score of -13,448 kcal/mol. The X-ray crystal of GnRH-R have been colored red while the ligand GnRH have been colored green. Magenta colored residues are labeled and have been highlighted to better visualize the binding pocket.

4.4 The induced fit docking pose of the crystal structure and homology model

The protein residues Asp98, Lys121, Tyr283 and Asp302 have been reported in literature to be important for binding of GnRH (44, 46). The mentioned amino acids have been displayed in Figure 12 together with the ligand GnRH. As seen in Figure 12, the orientation of the mentioned receptor residues is different in the homology model than the orientation in the crystal structure. One observable difference is the distance between the protein residue Asp302 and the ligand residue Arg8. Another specific difference is the orientation of Trp3, as for the ligand in the homology model, Trp3 is much closer to protein residues Asp98 and Lys121 in the homology model. The only similarity is how the N-terminus residues pGlu1, His2 and Trp3 are closer the binding pocket residues than the C-terminal which is pointing out of the pocket for both.

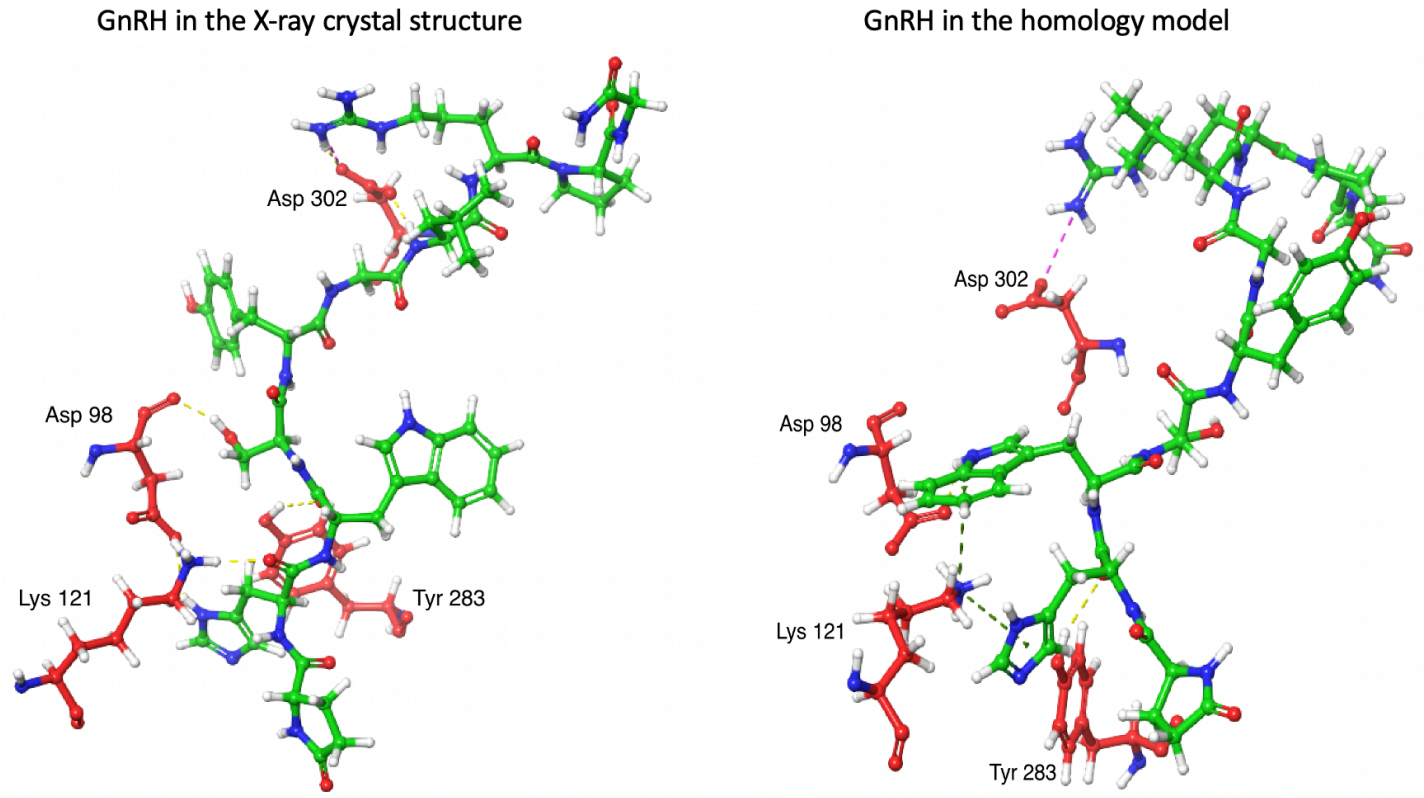

Figure 12: The ligand poses after IFD for GnRH in the crystal structure (left) and the homology model (right). GnRH has been colored green, while residues found in literature have been colored red. The rest of the receptor has been hidden.

4.5 Molecular dynamics results

4.5.1 System

The biological system was set up using the standard settings and resulted in the receptor being placed in the membrane which had water molecules on both sides of the membrane. This can be seen in Figure 13 where the homology model without the ligand is in a system. All the MD-simulations used a system with a SPC water model and a POPC membrane model. The receptor was automatically placed in the membrane based on the Orientations of Proteins in Membrane (OPM) database.

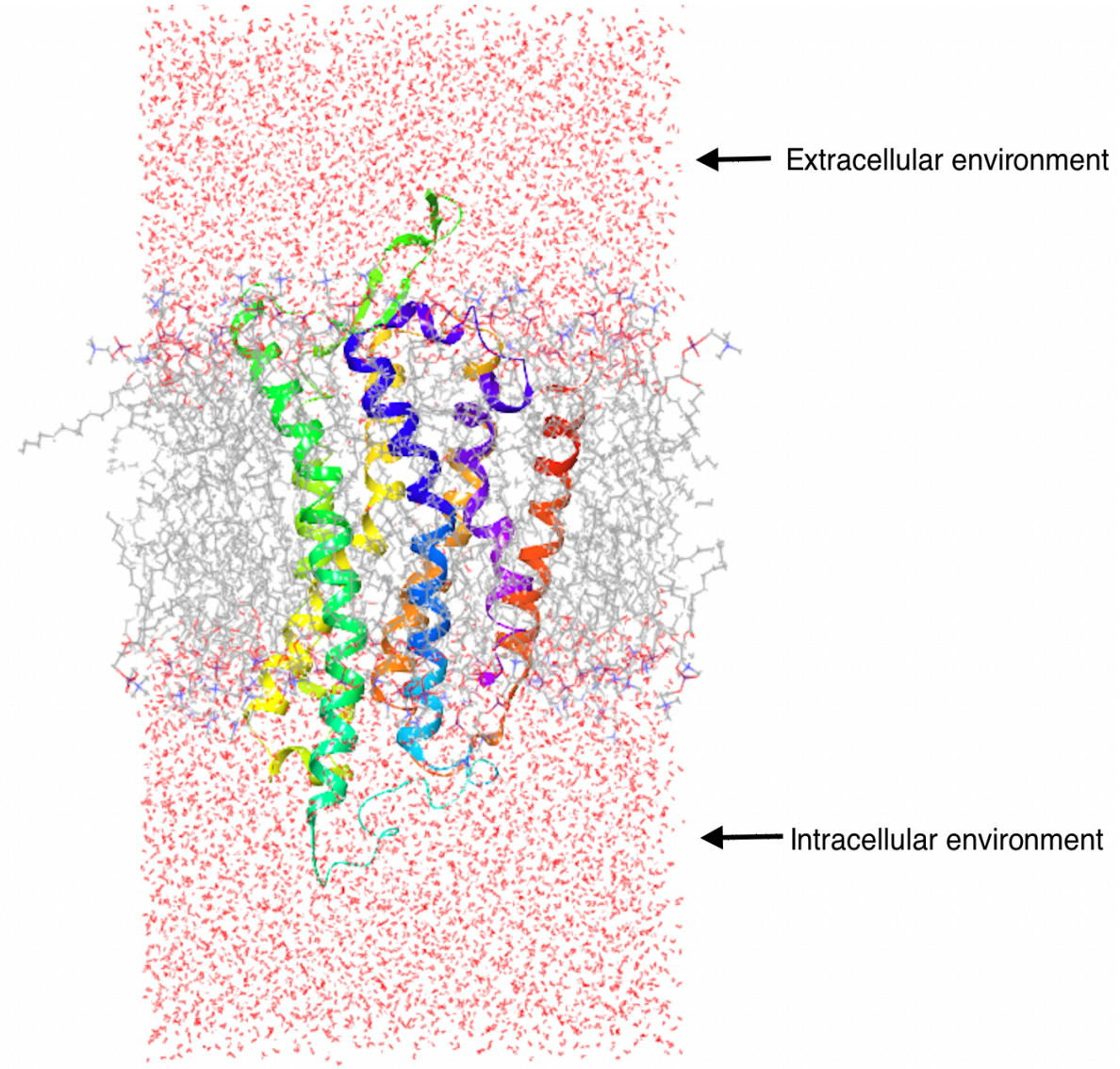

Figure 13: The system built for the MD of the homology model without the ligand. Text indications have been added to visualize the orientation of the proteins binding pocket.

4.5.2 Protein RMSD plots

The Simulation Interactions Diagram (SID) is a post-MD analysis report which visualizes and plots protein and ligand properties and relations throughout the MD-simulation. The Protein RMSD plot which is a part of SID is used to determine stability and to assess if the MD-simulation is stable. The three protein RMSD plots for the three MD-simulations can be seen in Figure 14. For the X-ray crystal structure, which was in complex with the ligand GnRH, the protein backbone (Cα) stabilized around 3Å at 1000 ns. The protein backbone (Cα) stabilized around 4,8-5,6 Å at 1000 ns for the homology model with ligand. For the homology model without ligand the protein RMSD value stabilized around 5.6-6.4 Å. It was assessed that these simulations were acceptable for further analysis considering the RMSD value never fluctuated past 3 Å or had massive fluctuations.

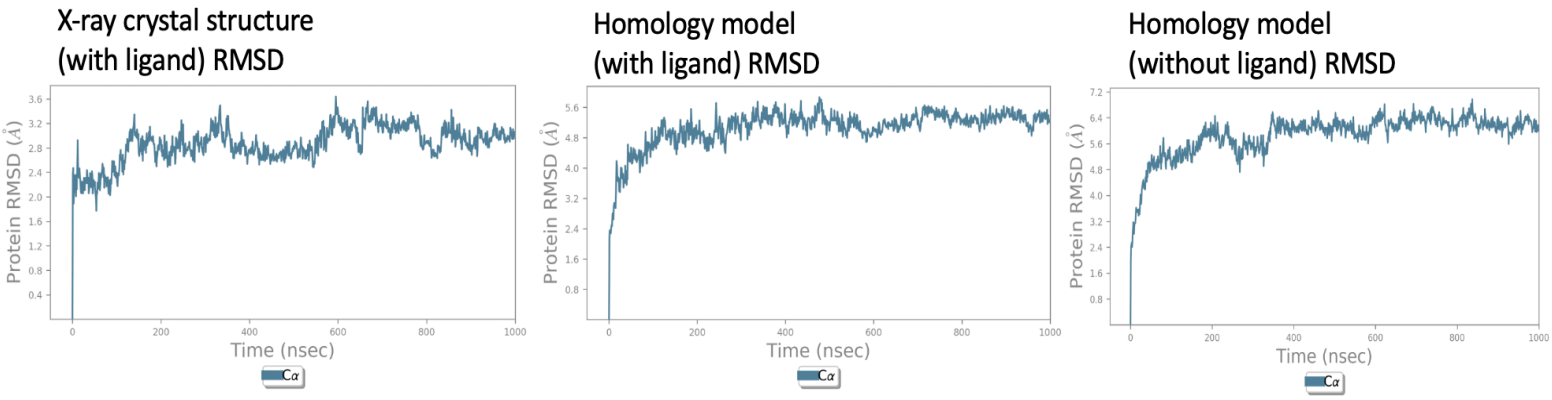

Figure 14: The three protein RMSD plot displayed. RMSD value in Ångstrøm is read along the y-axis while time in nanoseconds is read along the x-axis.

4.5.3 The X-ray crystal structure of GnRH and ligand

A MD-simulation was done for the IFD pose with the docking score -21,692 kcal/mol. A structure was done in PyMol. The structure for the last frame of the MD-simulation was aligned with the IFD pose before MD. It was apparent that no great conformational change had happened to the receptor (RMSD= 1,910 Å), this is displayed in Figure 15. Figure 15 shows the backbone for both structures having retained almost the same conformation as before the MD. The ligand which is also displayed in the Figure 15 have had its side chains change conformation, but the backbone of the ligand appears to be the same except for C-terminus residues Arg8, Pro9, Gly10 which show greater movements. The LID for frame 1 (0 ns) and frame 1001 (1000 ns) can be seen in Appendix under Figure A4 and A5 respectively.

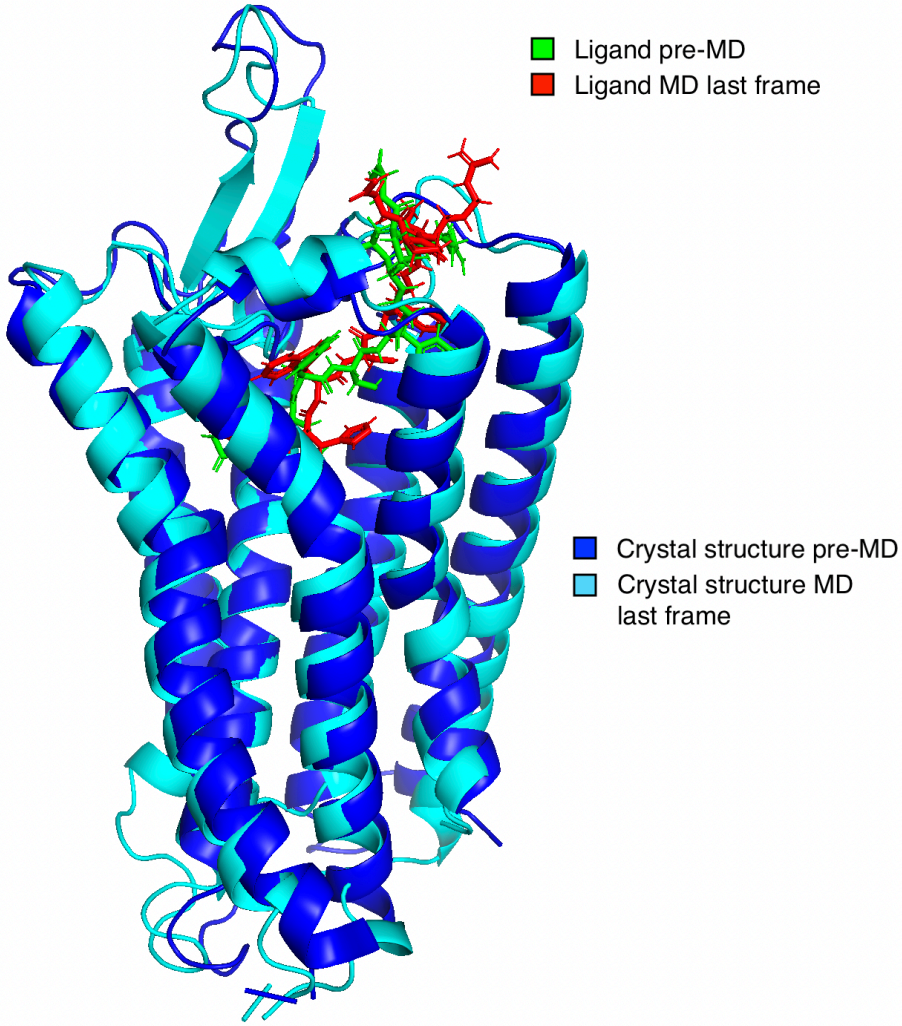

Figure 15: The alignment of the crystal structure after IFD and the crystal structure at the end of the MD. The ligand GnRH is colored differently than the receptor and have been labeled.

Figure 16 shows the helices of the aligned structures from the cytoplasmic side. There is no distinctive movement of any of the TM-helices in the figure, meaning that while the ligand has obtained another conformation after the MD, the X-ray crystal structure remains inactive just like its structure pre-MD.

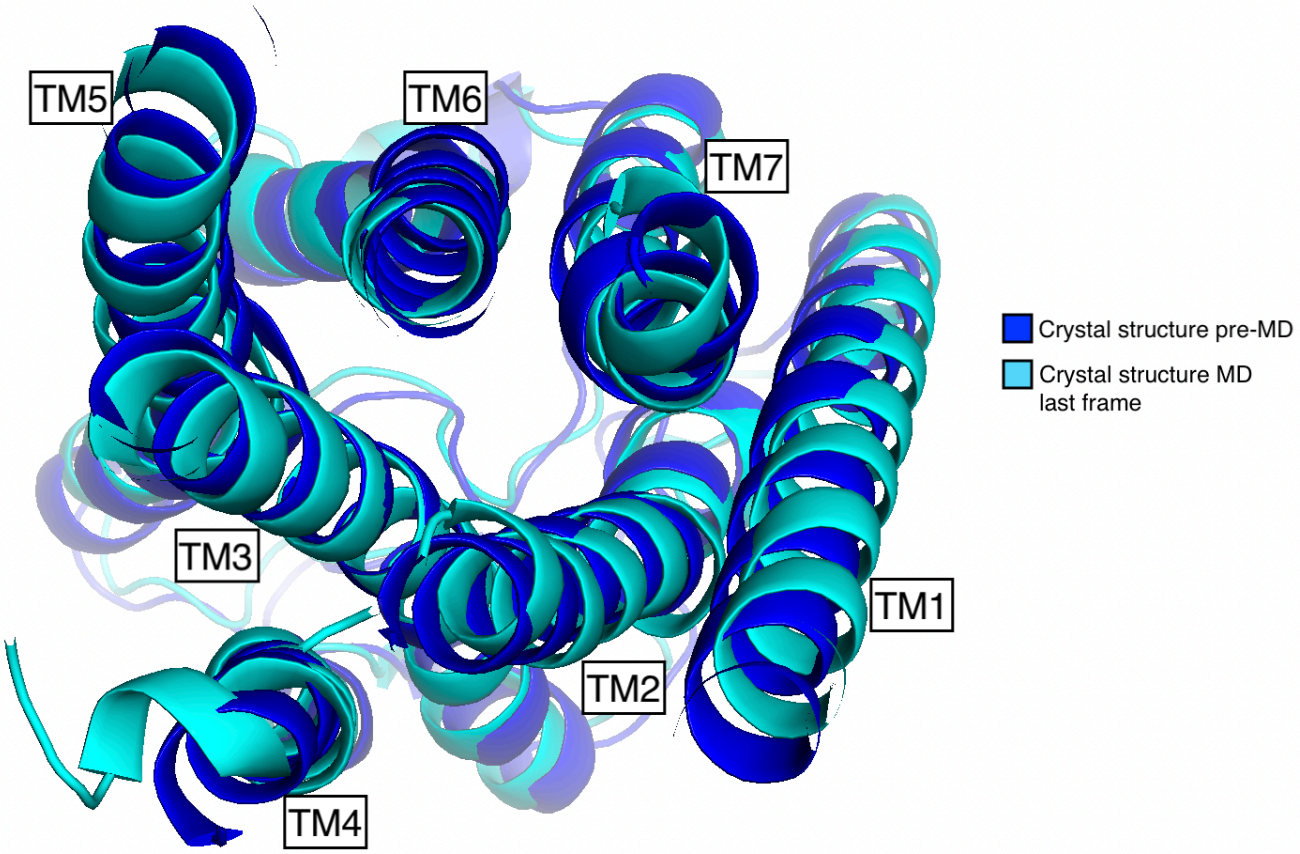

Figure 16: The alignment of the crystal structure´s IFD pose, and the last frame of the MD-simulation done on the same IFD pose (1000 ns). Helices have been labeled.

4.5.4 The homology model and ligand

The IFD pose of the homology receptor-ligand complex with the score: -13,448 kcal/mol was chosen for the MD, then the structure was aligned with the homology model and ligand structure at last frame (1000 ns). The alignment (RMSD= 4,213 Å) of the 3D-structures, both receptor and ligand are shown in Figure 17. The ligand which has been colored blue for the ligand in the IFD pose and yellow for the ligand at the end of MD, have changed drastically compared to the ligand in the crystal structure. C-terminus residues Arg8, Pro9 and Gly10 have changed their orientation and is pointing in a different direction than initially, this goes to show how the ligand in the homology model is more exposed to the environment outside the ligand binding pocket with the Arg8 residue now pointing towards TM5 while it was initially pointing towards TM1. The LID for frame 0 and frame 1001 can be seen in Appendix under Figure A6 and A7 respectively.

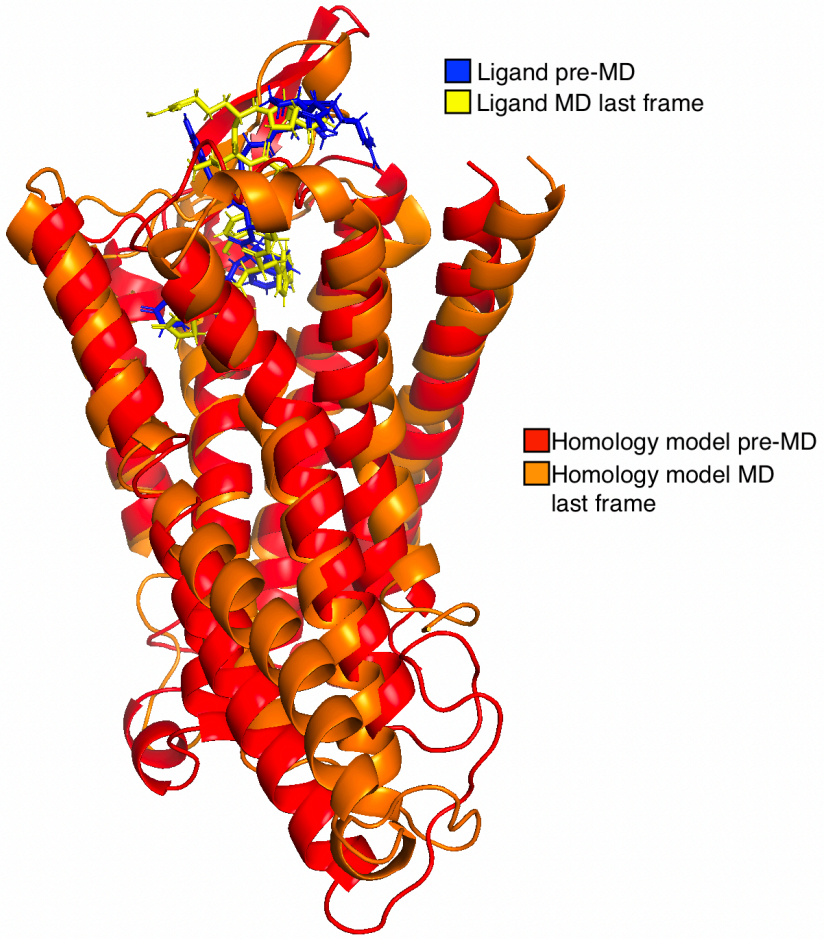

Figure 17: The alignment of the homology model after IFD and the homology model at the end of the MD. The ligand GnRH is colored differently than the receptor and have been labeled along with the receptor.

Figure 18 displays the same alignment from the cytoplasmic side, better visualizing the movement of certain helices after the MD. For instance, TM5 has moved outward from the TM-bundle compared to before MD. TM3 has moved slightly inward to the TM-bundle. TM4 remains unchanged. TM7 have moved a little outward on the cytoplasmic side, TM6 has rotated to TM5, there is no noticeable change with TM1.

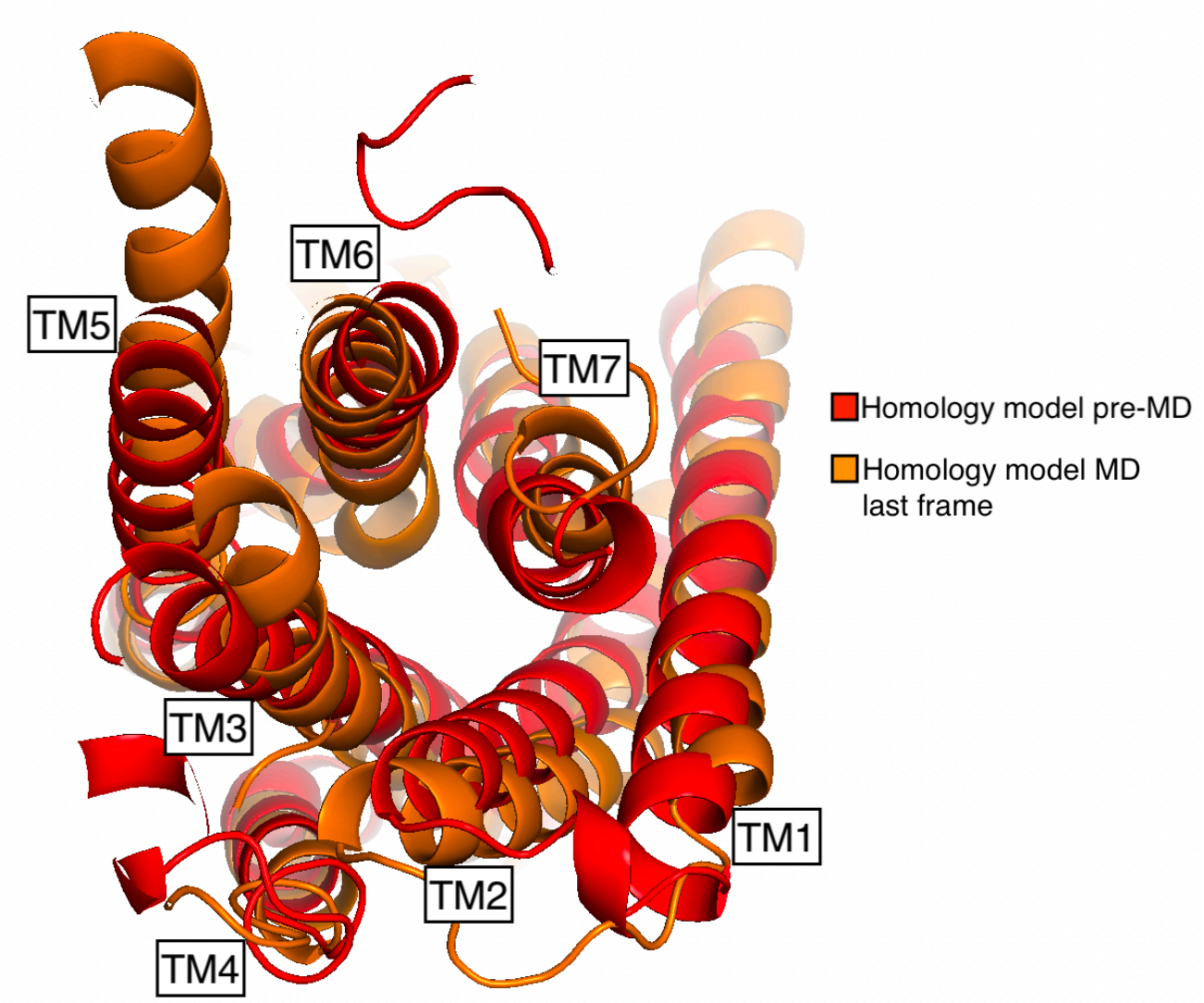

Figure 18: The alignment of the homology model structure´s IFD pose, and the last frame of the MD-simulation done on the same IFD pose (1000 ns). Helices have been labeled.

The last frame of the homology model was also aligned with the crystal structure PDB:7BR3 (RMSD= 6,233 Å), and the viewpoint from the cytoplasmic side is visible in Figure 19. Observable changes are TM5 outward movement from the TM-bundle, TM6 outward movement from the TM-bundle, TM7 slight inward movement to the TM bundle, TM2 outward movement from the TM-bundle. TM1, TM3 and TM4 have rotated in some capacity, however there is no noticeable movements.

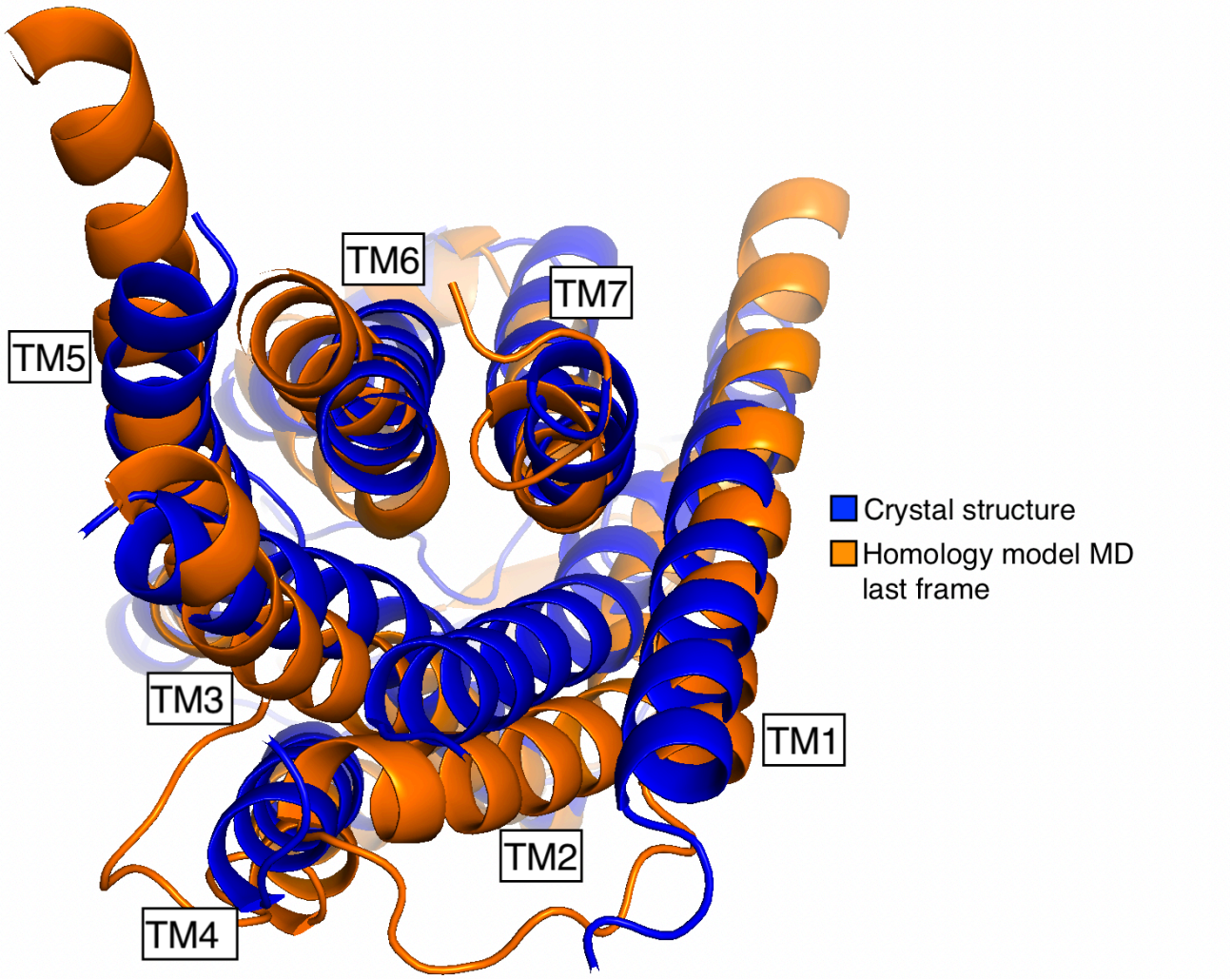

Figure 19: The alignment of the X-ray crystal structure, and the last frame of the MD-simulation on the homology model IFD pose (1000 ns). Helices have been labeled.

4.5.5 The homology model without the ligand

the homology model without ligand, also termed apo-structure, underwent an MD-simulation as well and was superimposed with the last frame of the very same MD-simulation (RMSD= 4, 926 Å). Figure 20 shows that major conformational changes are observable for the helices near the intracellular part after MD. Loops have moved as well, but that is to be expected because of their flexible nature.

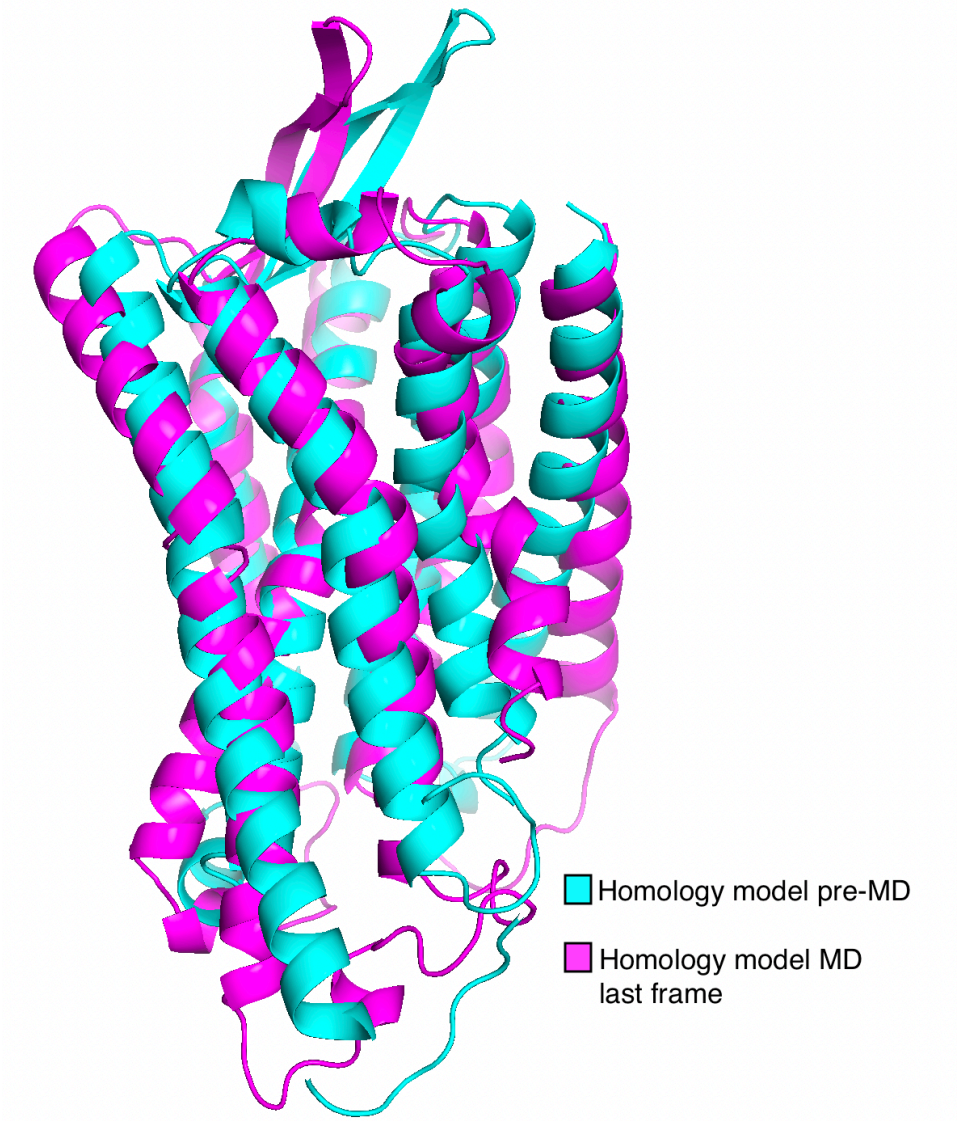

Figure 20: The homology model after IFD and the homology model at the end of the MD, superimposed.

Figure 21 displays the TM-helices in Figure 18 from the cytoplasmic side. The TM movements are visible in the figure with TM5 moving slightly outwards from the TM-bundle, TM 6 moving outwards from the TM-bundle, TM7 moving inward to the TM-bundle, TM3 and TM 1 moving outward. As for TM2 and TM4, it seems like no big movement has happened.

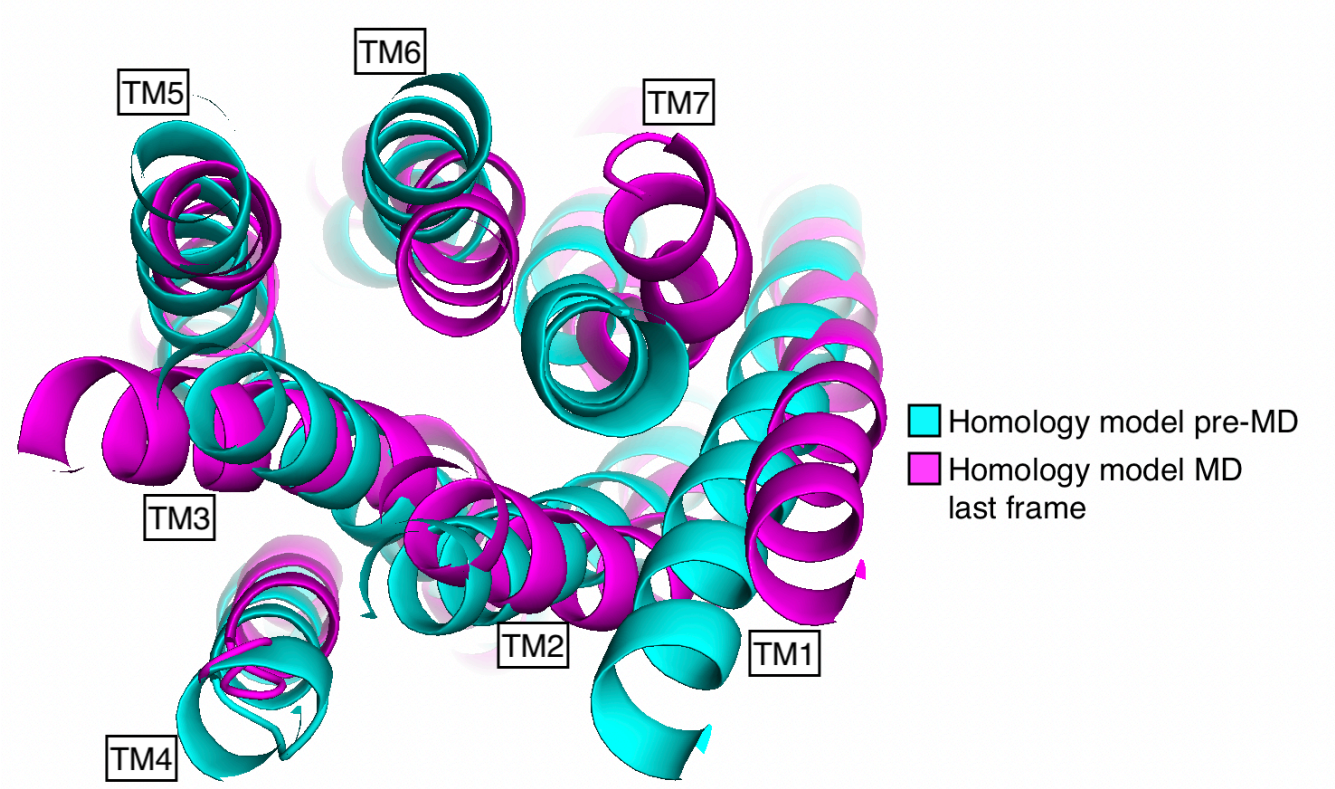

Figure 21: the apo structure, and the last frame of the MD-simulation on the same apo structure, superimposed. Helices have been labeled.

Figure 22 displays the crystal structure (PDB: 7BR3) superimposed with the last frame of the MD for the homology model (RMSD= 5,073 Å) viewed from the cytoplasmic side. This was done to observe if the homology model had returned to an inactive state on the cytoplasmic side. As seen in Figure 22, TM6 and TM7 have moved, however when compared to Figure 21, these movements are small, with TM6 moving slightly inward and TM7 rotating slightly outwards from the TM-bundle. TM5 seems to not have had any observable changes, as for TM3 it has moved slightly outward from the TM-bundle compared to the crystal structure. TM1 have moved outward from the TM-bundle compared to the crystal structure. TM2 seems to move inward at the end of the helix but is not directly overlapping with TM2 in the crystal structure. TM4 seems to overlap for both the homology model and crystal structure.

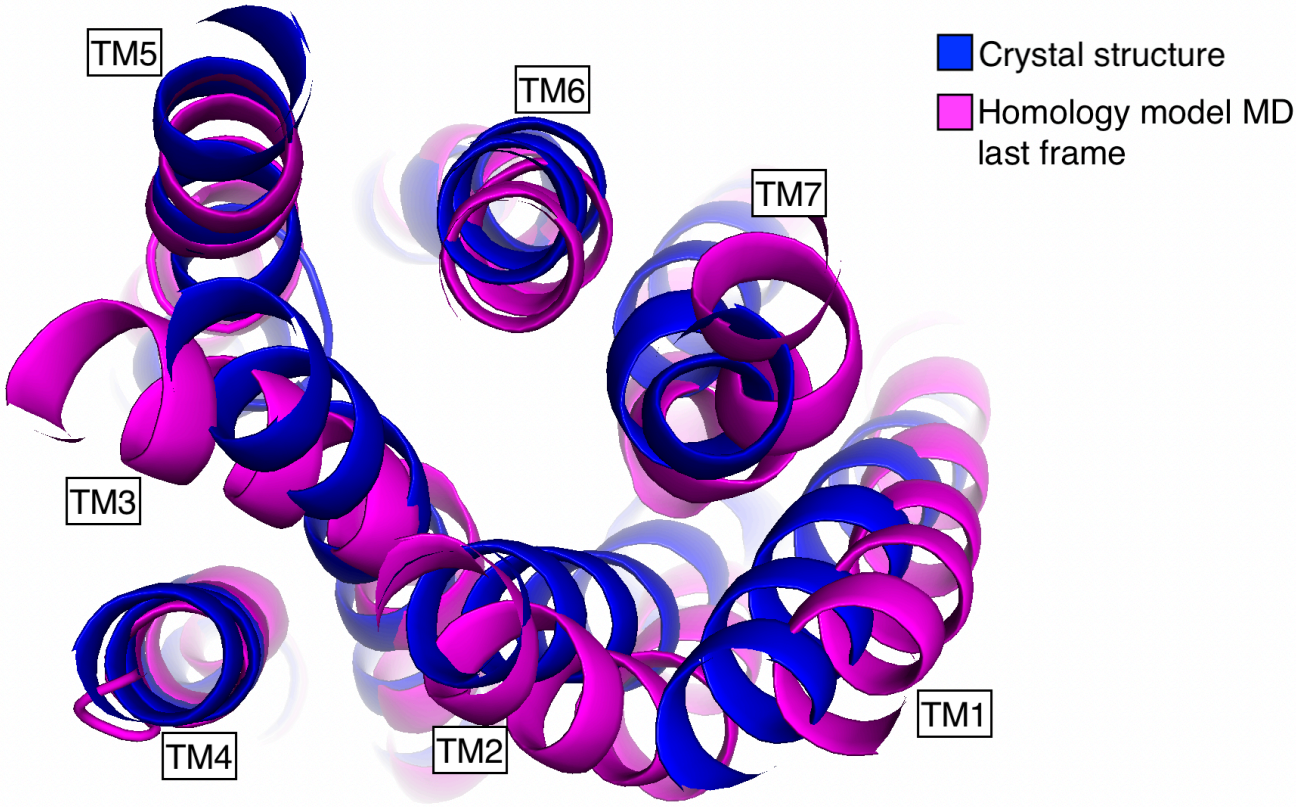

Figure 22: The X-ray crystal structure and the last frame of the MD-simulation on the homology model (1000 ns), superimposed. Helices have been labeled.

4.5.6 Conformational changes to the ligand after molecular dynamics

Figure 23 shows the movements of the ligand in both the homology receptor and the crystal structure. For the ligand in the homology receptor the residues near the C-terminus, namely Arg8, Pro9 and Gly10 seem to change drastically under the simulation compared to the ligand in the crystal structure. For the ligand in the crystal structure, the backbone of the initial pose seems to be unchanged. There also seems to be changes in the residues near the N-terminus for the ligand in the homology model, but those are minor compared to the drastic movement of the C-terminus residues.

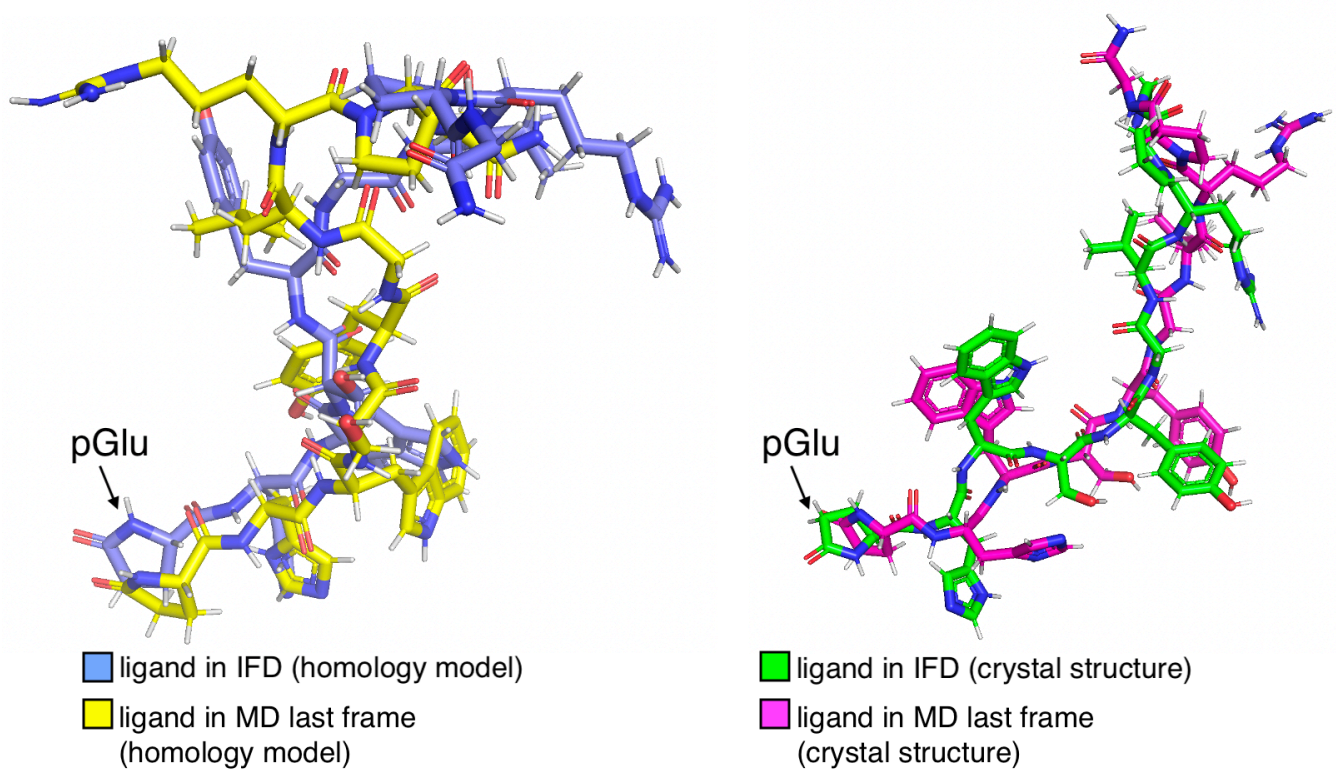

Figure 23: GnRH shown without the receptor in the homology model (left) and crystal structure (right) respectively. The last frame of MD has been superimposed with the output pose after IFD. pGlu1, the first residue of the decapeptide has been labeled to better visualize the ligand.

4.5.7 Movements of the GnRH-R during MD

Protein root mean square fluctuation (RMSF) plots were acquired through SID. RMSF is a time-averaged value which represents the fluctuation of the square deviation of a certain set of residues, in this case it is measured for the protein residues over the 1000 ns time course. Figure 24 displays three RMSF plots based on the three MD-simulations done. Both plots for the homology model show spikes with RMSF values up to 6-8 Å, while the X-ray crystal structure plot show spikes with RMSF values of 4,8-5,4 Å. Both RMSF plots done on the homology model, with and without ligand, show a broad spike near residue Cys200 which is the beginning of TM5. The crystal structure also has a spike around 200, but it is more distinct and seem to be for residues near Phe225 specifically. Another broad spike is around Met100 for the homology model with and without ligand, this is not seen for the crystal structure. Residues near Met100 are nearby ECL1 which connects TM2 and TM3.

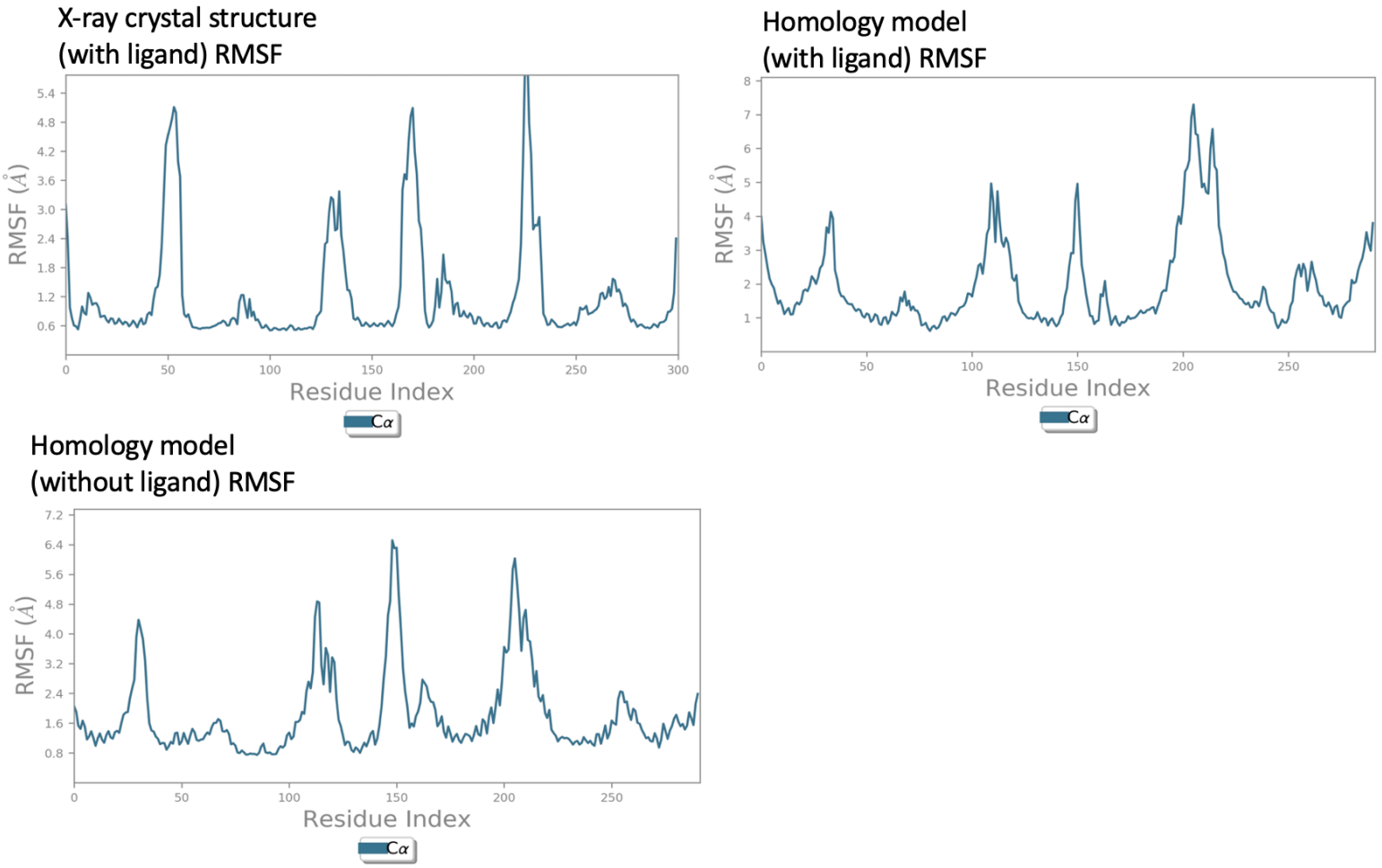

Figure 24: The three protein RMSF plots. Protein residues can be seen along the x-axis, while RMSF value in Ångstrøm can be seen along the y-axis.

4.5.8 Protein ligand interactions for the X-ray crystal structure and GnRH

Information on how the ligand and the crystal structure of GnRH-R interacts throughout the MD-simulation is present in Figure 25 and Figure 26. The protein ligand histogram in Figure 25 shows protein residues making contacts with the ligand. The interactions fraction represents the percentage of the simulation time where the interaction is being maintained, this meaning a value of 0,5 suggests 50% of the simulation time the specific interaction is maintained. However, there are some values over 1,0 these values signifies that the protein residue can make more than one type of contact to the ligand. In the protein ligand histogram specific residues stand out. These are Asn27, Asp98, Tyr283, Asn298, Asp302 and Asn305. Out of these residues Asp98 and Asp302 are found in literature, as well as Tyr283 (44, 46). In the crystal structure, the majority of the interactions Asp98 makes consists of H-bonds. As for Asp302 it makes both water bridges and H-bonds. Tyr283 seem to make mainly hydrophobic interactions, followed by water bridges and a few H-bonds.

Figure 26 shows a detailed schematic of the ligand GnRH and the interactions which occurred during the simulation. Interactions occurring more than 30% of the simulation time has been chosen and displayed. In the schematic Asp98 have a H-bond with His2 99% of the simulation time and a H-bond with Ser4 62% of the simulation time. Lys121 and Asp302 makes certain H-bonds with the peptide bonds in the decapeptide. Tyr283 has pi-stacking with Trp3 41% of the simulation time.

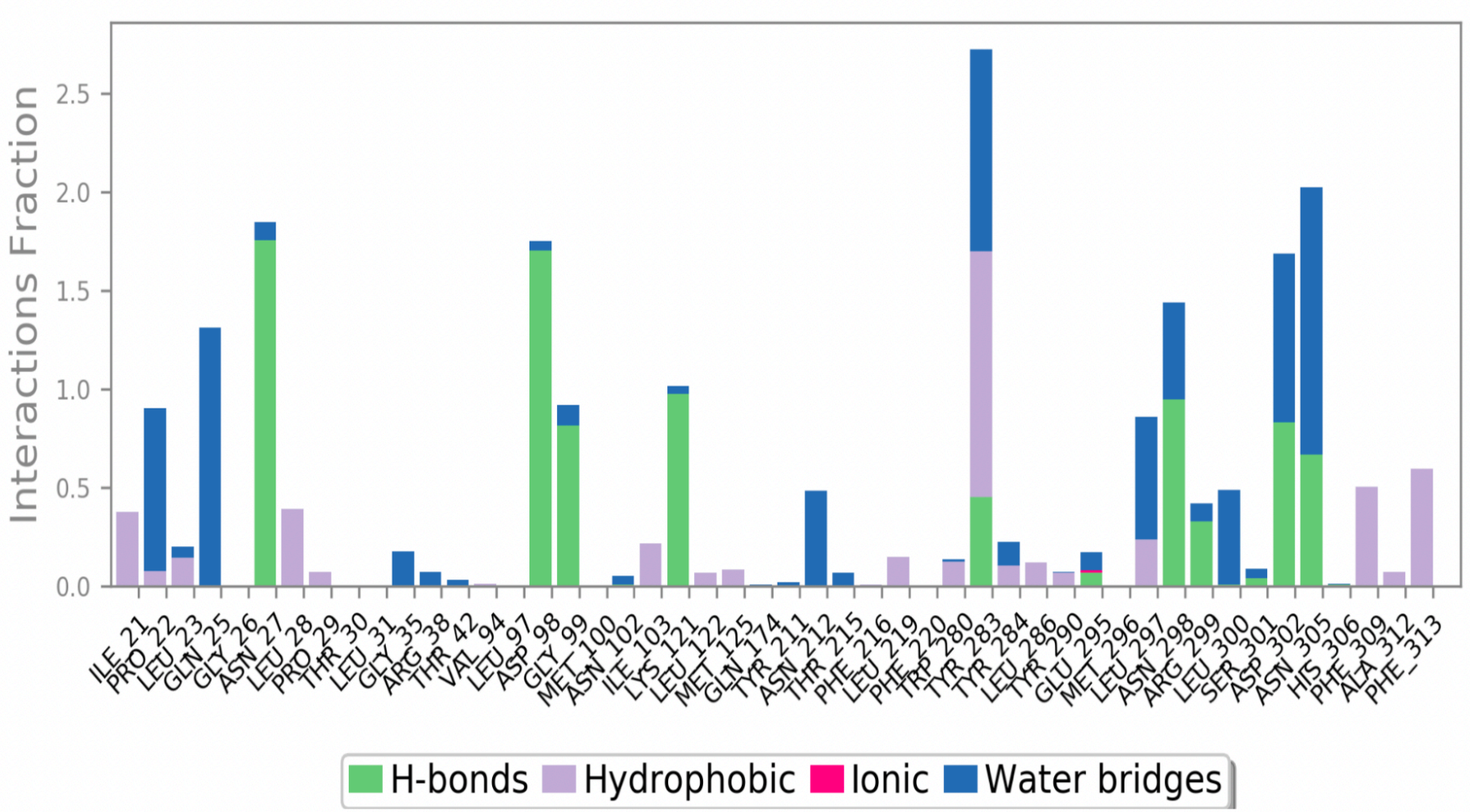

Figure 25: Protein ligand histogram for the crystal structure. The Y-axis show interaction fraction based on the simulation time. The X-axis show protein residues interacting with the ligand.

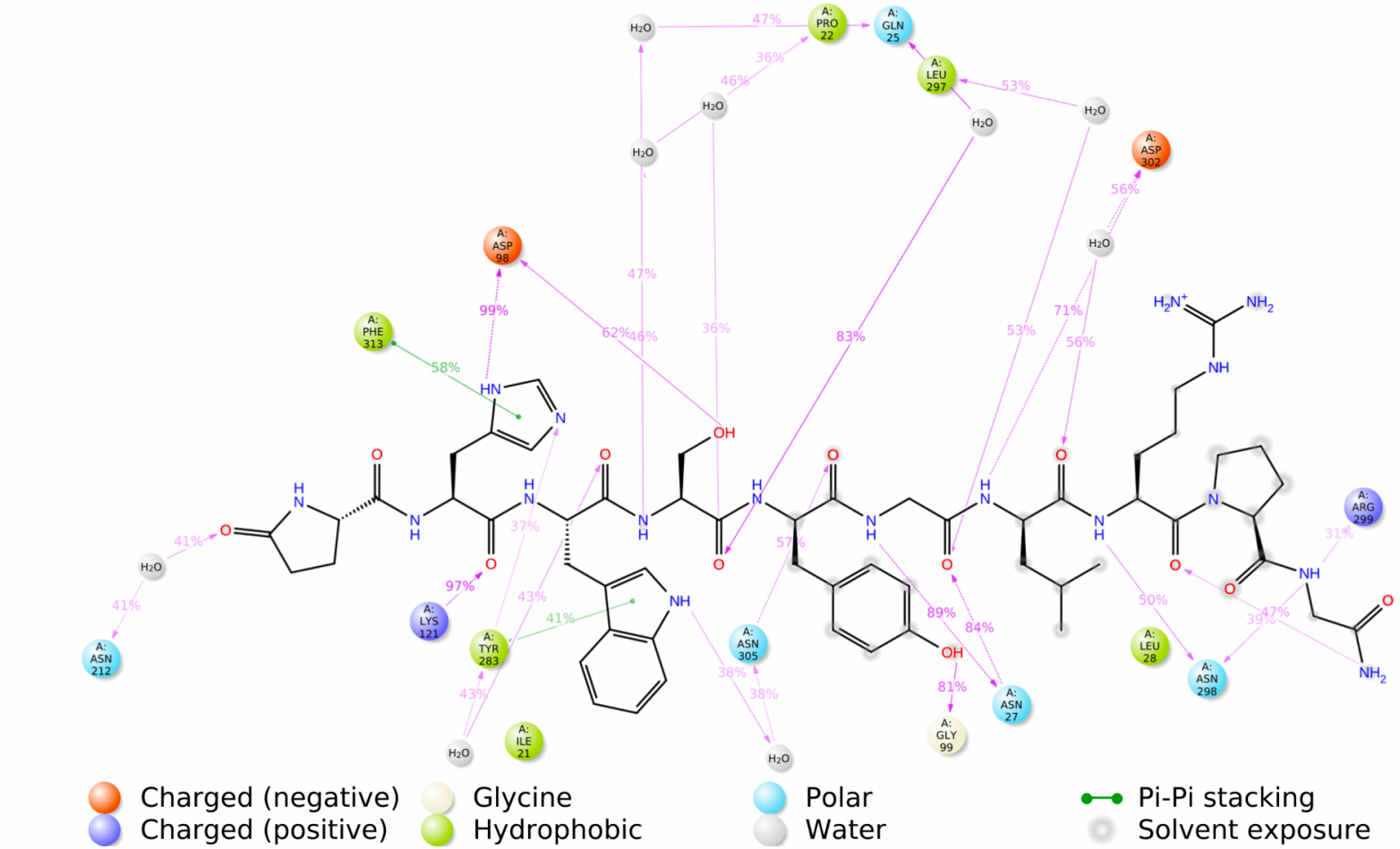

Figure 26: Schematic of detailed ligand atom interactions with the crystal structure residues. Interactions that occur more than 30% of the simulation time in the selected trajectory (0 through 1000 ns) are shown

4.5.9 Protein ligand interactions for the homology model and GnRH

A protein-ligand contacts histogram is being displayed in Figure 27 for the ligand GnRH in the homology model. The top residues responsible for interactions are Asp98, Ser194, Gln208, Tyr290, Asn298, Asp302 and Asn305. When comparing Figure 27 to the histogram in Figure 25, Asp98 is making hydrophobic interactions in the homology model compared to H-bonds and some water bridges in the crystal structure. As for Asp302, in the homology model it appears Asp302 mainly mediates water bridges, while in the crystal structure both water bridges and H-bonds are interactions occurring.

The ligand-protein contacts schematic sets the ligand in focus along with the interactions it has made with the homology model residues in Figure 28. Tyr283 made a H-bond with pGlu 31% of the simulation time. Asp98 had a water mediated bridge to Trp3. As for Asp302, in the homology model it only made water mediated bridges with the peptide bond. In the crystal structure it made a water mediated bridge and a H-bond with peptide bonds, however these peptide bonds were not the same in the homology model.

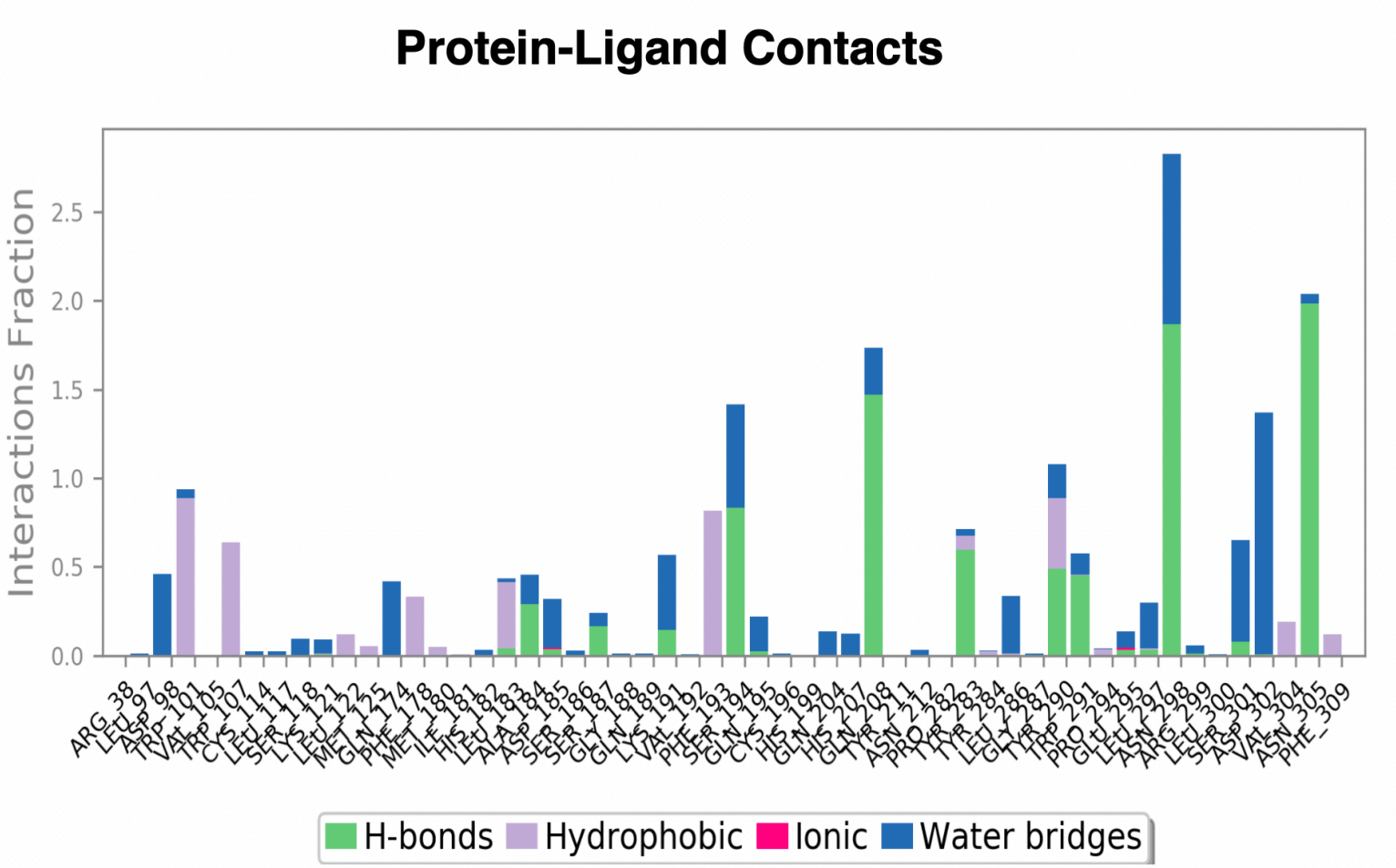

Figure 27: Protein ligand histogram for the homology model. The Y-axis show interaction fraction based on the simulation time. The X-axis show protein residues interacting with the ligand.

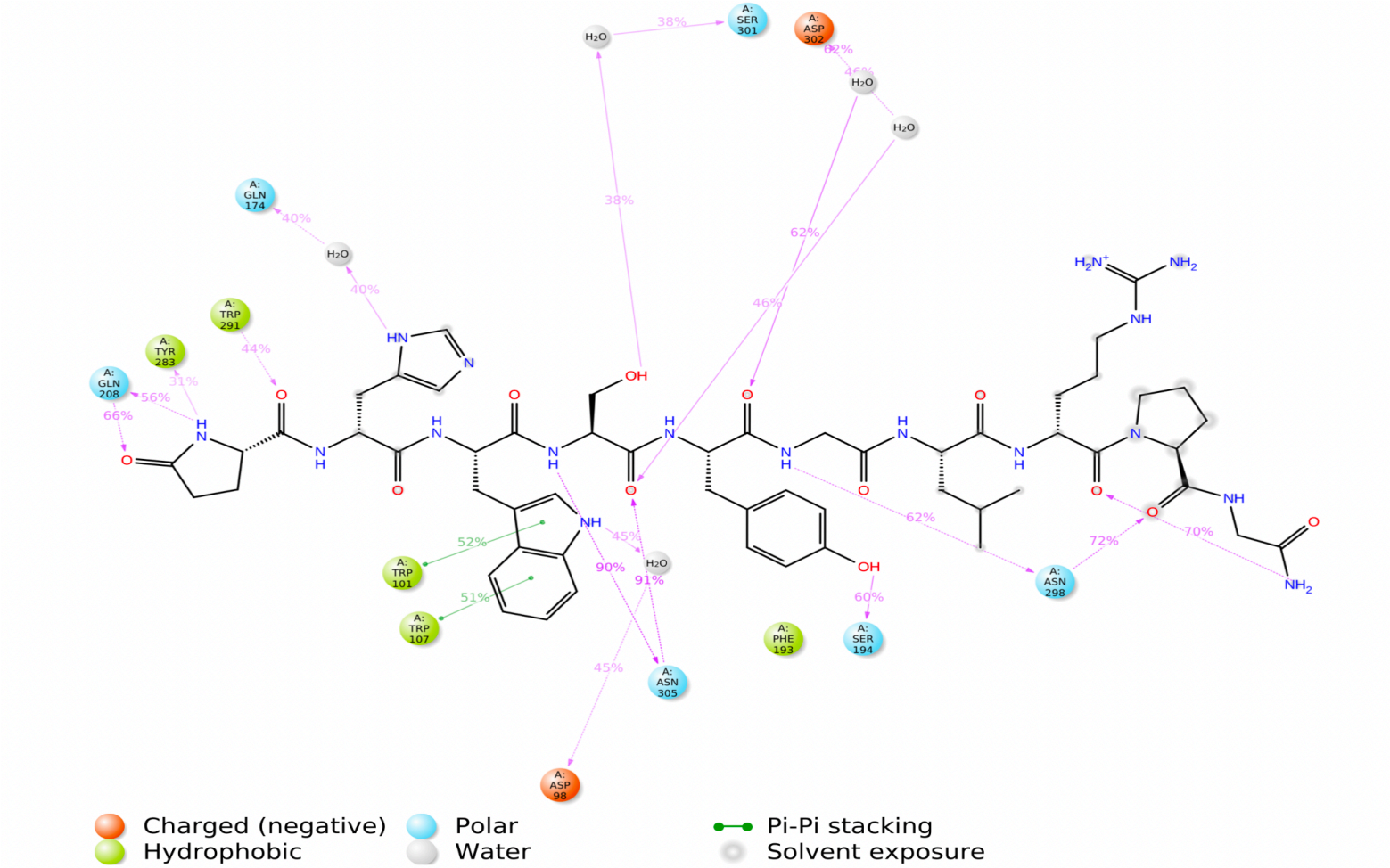

Figure 28: Schematic of detailed ligand atom interactions with the homology model residues. Interactions that occur more than 30% of the simulation time in the selected trajectory (0 through 1000 ns) are shown

4.5.10 Simulation Quality Analysis

The Simulation Quality Analysis (SQA) assesses properties regarding the quality of the MD-simulation. In Table 2 the averages of different properties have been displayed along with the standard deviation. The block length for averaging was set to 1000 ps, which is equivalent to 1ns. There are subtle differences in both the average total energy and average potential energy with the homology receptor alone having the lowest and the crystal structure and ligand having the highest. For the average volume the receptor alone has the largest average volume and the crystal structure with ligand having the smallest average volume. The quantities from the SQA plotted over time can be found in the Appendix under Figure A8, A9 and A10. The block length for averaging was 1000 ps (= 1ns)

Table 2: Simulation quality analysis of the three MD-simulations running for 1000 ns. Values in parentheses are standard deviation.

Energy file	Average total energy (kcal/mol)	Average potential energy (kcal/mol)	Average temperature (K)	Average pressure (Bar)	Average volume ($Å^3$)
GnRH-R (homology model only)	-73119,597 (55,500)	-101109,857 (55,354)	297,996 (0,055)	0,793 (6,289)	426870,277 (198,045)
GnRH-R (homology model + ligand)	-71696,950 (54,214)	-98770,011 (53,845)	298,023 (0,053)	1,254 (6,308)	413095,147 (206,620)
GnRH-R (crystal structure + ligand)	-70220,892 (45,605)	-96041,372 (45,484)	298,054 (0,055)	0,956 (6,315)	394888,588 (206, 620)

5 Discussion

5.1 Main findings

The main findings of this study can be separated into the docking results and the results from the MD-simulations.

5.1.1 The docking of GnRH into GnRH-R

For the initial glide ligand docking of the X-ray crystal structure (7BR3), the top scoring pose and other top poses, displayed GnRH with the three amino acids belonging to the N-terminus sticking out of the binding pocket. The three amino acids at the N-terminus: pGlu1, His2 and Trp3 have been assessed to be important for receptor activation (44). Furthermore, pGlu1 from the peptide made an interaction with the receptor residue Asp302 in the top-scoring pose in the results for the glide ligand docking. In literature however, Arg8 in GnRH (which is located by the C-terminus) and Asp302 in GnRH-R form an interaction important for ligand binding affinity (46). Thus, Glide ligand docking of the crystal structure did not result in ligand-receptor poses with any of the published ligand-receptor interactions by Tzoupis et. al. (46).

GnRH was later docked into the crystal structure and the generated homology model using IFD. IFD into both structures produced poses with some interactions found in literature (46) and a mutagenesis study(44). IFD of the crystal structure resulted in a pose where the ligand formed known interactions such as an interaction between peptide residue His2 and protein residue Asp98 which was important for receptor activation, and peptide residue Arg8 had an interaction with Asp302 which was important for ligand binding. Tyr283 had an interaction with a carbonyl oxygen in the peptide bond between Trp3 and Ser4.

For the IFD of the ligand into the homology model, Trp3 in the peptide made interactions with the protein residues Asp98 and Lys121. His2 in the peptide made interaction with Lys121 in the receptor as well and Arg8 in the peptide made interaction with Asp302 in the receptor. Tyr283 in GnRH-R also made interaction with the ligand, through the carbonyl oxygen in the

peptide bond between His2 and Trp3. With this, IFD resulted in the ligand conformationally able to adjust to the binding pocket and making specific published interactions. The ligand residues near the N-terminus were inside the binding pocket after the IFD. An interesting find throughout the different docking jobs was that there was never once a significant back-bone bend or a β-hairpin conformation. The back-bone bend of GnRH was expected regarding Gly6 being the sixth residue and having a hydrogen as its sidechain, therefore allowing bends (103). This could also indicate that the binding pocket of both the crystal structure and homology model were constricted.

5.1.2 Comparing and analyzing the MD-simulations

There were conformational changes to the ligand when comparing the last frame of the MD-simulations to the ligand pose before the MD-simulation. Observable conformational changes were residues near the C-terminus and specific ligand receptor interactions. At the end of the MD, the ligand in the homology model was not able to maintain the interactions it had made in the IFD pose. The ligand in the crystal structure however, maintained the H-bond between His2 and Asp98 throughout the simulation and at the end of it. When comparing the last frame of the MD-simulation with the IFD ligand poses for both homology model and crystal structure, the ligand in the homology model underwent greater back-bone movements compared to the ligand in the crystal structure, which maintained its backbone structure except for side chain movements. One of the reasons for this is that the ligand in the homology model did not penetrate the ligand binding pocket as much as the ligand in the crystal structure.

For the MD-simulation, the crystal structure did not show any significant movement when comparing the receptor after IFD and the last frame of the MD- simulation done on the receptor-ligand complex. Conformationally, the 3D structure of the homology model with the ligand is different from the crystal structure. For the homology receptor ligand complex after the MD, TM1 is pointing “outwards” from the binding pocket. TM5 in the complex is shown bend midway in helix as well and pointing outwards from the TM-bundle. For the intracellular part, the helices have moved when comparing the last frame of the homology model ligand complex with the crystal structure. TM6 showed outward movement and TM7 showed inward movement.

5.1.3 SID and SQA

SID and SQA were done for the three different MD-simulations and resulted in analysis reports which were distinctive. The protein RMSD plot for the homology receptor only showed a stabilization around 5-7 Å. This result was considerably higher than the protein-ligand RMSD for the homology receptor ligand complex which stabilized around 4,8-5,6 Å and the crystal structure with the ligand which stabilized around 2,8-3,2 Å. As for the protein RMSF plots, they showed loop movements at the spikes of the plot.

When comparing the bar charts of the protein ligand contacts diagram there are specific protein residues which they have in common. These residues are Asp98, Tyr283 and Asp302. Despite showing up in the bar chart, they are quite different in terms of what type of interaction. Asp98 and Asp302 are mainly mediated through water bridges in the homology model but maintain their H-bond in the crystal structure. For Tyr283, the homology model shows it makes H-bond, but the crystal structure shows it makes H-bond, hydrophobic interaction, and water bridges. For the ligand-protein contacts diagram, the most noticeable discovery was Asp98. Asp98 ended up making a contact with Trp3 through a water bridge in the homology model, but it made a direct contact with His2 in the crystal structure.

The SQA along with the SQA plot further strengthen the differences between the three MD-simulations. For the total energy and potential energy, the homology receptor had the lowest values, with the homology model-ligand complex coming second, and the crystal structure with ligand coming third. The average volume of the simulations is also in the same order, with the homology model without ligand being the largest in size and the crystal structure with ligand being the smallest.

5.2 Limitations regarding method and approach

Both glide ligand docking and IFD were done multiple times on the crystal structure. However, the use of glide ligand docking did not result in poses which were connected to the activation of the receptor when analyzing the receptor-ligand interactions. As a time-consuming aspect, it would have been more efficient to directly begin with IFD despite having an active or inactive structure. This is also supported with GPCRs commonly being flexible structures and their conformational change upon ligand binding (34).

When setting up the homology model a pairwise sequence alignment for the template was done. However, in retrospect, a proper MSA should have been done. A thorough MSA would have given a better overview of the sequences together, as well as map the conserved parts of the protein. Another advantage MSA offer is decreasing the probability of random mistakes (104). There should have been a more comprehensive MSA with more templates which should have been analyzed thoroughly. Because of time restrictions, this was never carried out. The homology model was chosen on the basis of the poses which made interactions found in literature after glide ligand docking since this was the focus of the docking jobs connected to the crystal structure. It could have been that other poses revealed new important interactions about the ligand binding mode, however this could not have been assessed considering the limited time for carrying out the docking jobs.

MD has a great limitation which is connected to the usage of molecular mechanics which disregards electron density and movement of electrons (87). This meaning the MD is a rough outline of movements but cannot fully replicate the in vivo ligand receptor binding. This is because MD is applying molecular mechanics, including force fields meaning the movements and inclusion of electrons in the system has been disregarded. The simulation time being 1000 ns for the different MD-simulations was a determining factor in getting the results, however a longer simulation could have produced different results. A study on the kinetics of GPCRs, estimated that the fastest activation time for specific class A GPCRs after binding a small agonist ranged between 40-100 milliseconds (105). Thus, the simulations would only represent a fraction if any greater conformational changes were to happen at a later timepoint.

5.3 Implications of findings

GnRH was not in a β-turn conformation before the glide ligand docking and the IFD, even though it has been proven important for making interactions with GnRH-R (106). One of the reasons could be that the ligand preparation resulted in specific conformations which did not form the β-turn. Yan et. al., the authors behind the X-ray crystal structure, also reported a 15 amino acids long N-terminus in the GnRH-R crystal structure which was forming a V-shape into the orthosteric binding pocket (5). This specific N-terminal could have prevented the ligand from fully docking into the crystal structure. However, for the homology model which did not have this peculiar N-terminal and a, the ligand never made the β-turn conformation and did not enter deep into the orthosteric binding pocket. The peptide ended up being outstretched, with the residues near the C-terminal showing more flexibility during MD as the residues near the N-terminus were penetrating the very core of the binding pocket.

In literature, the following interactions have been proposed: ligand residue pGlu1 with protein residue Asn212, His2 with Asp98 and/or Lys121, Tyr5 with Tyr290, Arg8 with Asp302, Gly10 with Asn102 (46). Other literature also put emphasis on the receptor binding pocket residues Tyr283 and Phe309 and how the three residues near the C-terminus of GnRH (pGlu1, His2, Trp3) are important for receptor activation and Arg8 being an important residue for high binding affinity (44). The salt-bridge between Arg8 in GnRH and Asp302 in GnRH-R is especially important for the β-turn conformation regarding high affinity, but the results show other conformations are also able to make that specific interaction. IFD of the ligand into both the homology model and the crystal structure displayed a salt bridge between Arg8 to Asp302, however the salt-bridge interaction between the residues was not maintained throughout MD. A reason for this could be that Arg8 was never inside the binding pocket, meaning increased flexibility of the peptide coupled along with water which affected the interaction. For the receptor activating interactions, Lys121 seemed to have a more prominent role for the ligand in the homology model by making interactions with both His2 and Trp3. However, when comparing this to a site-directed mutagenesis study (107) the interactions made in the IFD pose was a pi-cation interaction while the study resulted in H-bonds. In the crystal structure His2 and Asp98 were bound through a H-bond, but this never amounted to any specific conformational receptor changes, this may have been due to the inactive structure being docked.

As GnRH-R is a GPCR, MD-simulations done on other GPCRs can be compared to the MD-simulations done on GnRH-R. for GPCR structures in general, the transition to another conformation because of ligand binding is a crucial part of its ability to be able to activate the coupled G-protein along with downward cascades of signaling. Latorraca et. al. (2017) have made an overview of conformational movements of TM-helices in GPCRs and have concluded that the outward movement of TM6 and inward movement of TM7 are movements connected to active GPCR structures (34). While this was observed when comparing the last frame of MD with the homology model ligand complex with the crystal structure, it is not something which can be concluded, however, it is an interesting find and further comparisons need to be made to be able to confirm that these helical movements are important for an active GnRH-R coupling with a G-protein.

5.4 Thoughts on applied relevance and future

The results from the docking jobs and MD cannot be used as a conclusive answer to the exact binding mode of GnRH to GnRH-R and the conformational change of the GnRH-R. However, this work can serve as a supplementary for further studies and research regarding both GnRH and GnRH-R. Research on computational studies on the specific receptor is still limited, but hopefully the results acquired in this thesis can contribute to more knowledge on the GnRH-R and GnRH along with how to approach it using both docking and MD.

6 Reference list

1. Palczewski K, Kumasaka T, Hori T, Behnke CA, Motoshima H, Fox BA, et al. Crystal Structure of Rhodopsin: A G Protein-Coupled Receptor. Science. 2000;289(5480):739-45.
2. Congreve M, de Graaf C, Swain NA, Tate CG. Impact of GPCR structures on drug discovery. Cell. 2020;181(1):81-91.
3. Sriram K, Insel PA. G Protein-Coupled Receptors as Targets for Approved Drugs: How Many Targets and How Many Drugs? Mol Pharmacol. 2018;93(4):251-8.
4. Limonta P, Motta M, Moretti RM, Marzagalli M, Fontana F, Raimondi M, et al., editors. REPRODUCTIVE FUNCTION AND ANTITUMOR ACTIVITY: DIFFERENT ROLES FOR THE HYPOTHALAMIC HORMONE GnRH2020.
5. Yan W, Cheng L, Wang W, Wu C, Yang X, Du X, et al. Structure of the human gonadotropin-releasing hormone receptor GnRH1R reveals an unusual ligand binding mode. Nature Communications. 2020;11(1):5287.
6. Hiller-Sturmhöfel S, Bartke A. The endocrine system: an overview. Alcohol Health Res World. 1998;22(3):153-64.
7. Rosenbaum DM, Rasmussen SGF, Kobilka BK. The structure and function of G-protein-coupled receptors. Nature. 2009;459(7245):356-63.
8. Molina PE. Endocrine Physiology. United States of America: The McGraw-Hill Companies, Inc.; 2010. 303 p.
9. Molina PE. THE ENDOCRINE SYSTEM: PHYSIOLOGIC FUNCTIONS & COMPONENTS. In: Weitz M, Naglieri C, editors. Endocrine Physiology. 3rd ed. United States of America: The McGraw-Hill Companies, Inc. ; 2010. p. 1-3.
10. Molina PE. The Hypothalamus & Posterior Pituitary Gland. In: Weitz M, Naglieri C, editors. Endocrine Physiology. 3rd ed. United States of America: The McGraw-Hill Companies, Inc.; 2010. p. 27-47.
11. Molina PE. Anterior Pituitary Gland In: Weitz M, Naglieri C, editors. Endocrine Physiology. 3rd ed. United States of America: The McGraw-Hill Companies, Inc.; 2010

. p. 49-71.
12. Molina PE. Thyroid Gland. In: Weitz M, Naglieri C, editors. Endocrine Physiology. 3rd ed. United States of America: The McGraw-Hill Companies, Inc.; 2010. p. 75-99.
13. Molina PE. Endocrine Pancreas. In: Weitz M, Naglieri C, editors. Endocrine Physiology. 3rd ed. United States of America The McGraw-Hill Companies, Inc.; 2010. p. 165-86.
14. Molina PE. Adrenal Gland. In: Weitz M, Naglieri C, editors. Endocrine Physiology. 3rd ed. United States of America: The McGraw-Hill Companies, Inc.; 2010. p. 129-61.
15. Molina PE. Male Reproductive System. In: Weitz M, Naglieri C, editors. Endocrine Physiology. 3rd ed. United States of America: The McGraw-Hill Companies, Inc.; 2010. p. 189-209.
16. Molina PE. Female Reproductive System. In: Weitz M, Naglieri C, editors. Endocrine Physiology. 3rd ed. United States of America: The McGraw-Hill Companies, Inc.; 2010. p. 215-50.
17. Constanti A. Basic endocrinology for students of pharmacy and allied health sciences: CRC Press; 1998.
18. Molina PE. CONTROL OF HORMONE RELEASE. In: Weitz M, Naglieri C, editors. Endocrine Physiology. 3rd ed. United States of America: The McGraw-Hill Companies, Inc.; 2010. p. 14-9.

19. Saper CB, Lowell BB. The hypothalamus. Current Biology. 2014;24(23):R1111-R6.
20. Dampney R. The hypothalamus and autonomic regulation: an overview. Central regulation of autonomic functions. 2011:47-61.
21. Pop MG, Crivii C, Opincariu I. Anatomy and function of the hypothalamus. Hypothalamus in health and diseases: IntechOpen; 2018.
22. Amar AP, Weiss MH. Pituitary anatomy and physiology. Neurosurgery Clinics of North America. 2003;14(1):11-23.
23. Plant TM. 60 YEARS OF NEUROENDOCRINOLOGY: The hypothalamo-pituitary-gonadal axis. J Endocrinol. 2015;226(2):T41-T54.
24. Loveland JL, Giraldo-Deck LM, Lank DB, Goymann W, Gahr M, Küpper C. Functional differences in the hypothalamic-pituitary-gonadal axis are associated with alternative reproductive tactics based on an inversion polymorphism. Hormones and Behavior. 2021;127:104877.
25. Gonadotropins. LiverTox: Clinical and Research Information on Drug-Induced Liver Injury. Bethesda (MD): National Institute of Diabetes and Digestive and Kidney Diseases; 2012.
26. Dufau ML. Endocrine Regulation and Communicating Functions of the Leydig Cell. Annual Review of Physiology. 1988;50(1):483-508.
27. J S Richards a, Hedin L. Molecular Aspects of Hormone Action in Ovarian Follicular Development, Ovulation, and Luteinization. Annual Review of Physiology. 1988;50(1):441-63.
28. Molina PE. Endocrine Physiology, Third Edition: McGraw-Hill Education; 2009.
29. Harris GW. Neural Control of the Pituitary Gland.—I. British Medical Journal. 1951;2(4731):559.
30. Tuteja N. Signaling through G protein coupled receptors. Plant Signal Behav. 2009;4(10):942-7.
31. Chan HCS, Filipek S, Yuan S. The Principles of Ligand Specificity on beta-2-adrenergic receptor. Sci Rep. 2016;6:34736-.
32. Stevens RC, Cherezov V, Katritch V, Abagyan R, Kuhn P, Rosen H, et al. The GPCR Network: a large-scale collaboration to determine human GPCR structure and function. Nature Reviews Drug Discovery. 2013;12(1):25-34.
33. Cvicek V, Goddard WA, III, Abrol R. Structure-Based Sequence Alignment of the Transmembrane Domains of All Human GPCRs: Phylogenetic, Structural and Functional Implications. PLOS Computational Biology. 2016;12(3):e1004805.
34. Latorraca NR, Venkatakrishnan A, Dror RO. GPCR dynamics: structures in motion. Chemical reviews. 2017;117(1):139-55.
35. Basith S, Cui M, Macalino SJY, Park J, Clavio NAB, Kang S, et al. Exploring G Protein-Coupled Receptors (GPCRs) Ligand Space via Cheminformatics Approaches: Impact on Rational Drug Design. Frontiers in Pharmacology. 2018;9(128).
36. Vidhyasekaran P. G-Proteins as Molecular Switches in Signal Transduction. PAMP Signals in Plant Innate Immunity: Signal Perception and Transduction. Dordrecht: Springer Netherlands; 2014. p. 163-205.
37. Neves SR, Ram PT, Iyengar R. G Protein Pathways. Science. 2002;296(5573):1636-9.
38. Naor Z, Huhtaniemi I. Interactions of the GnRH receptor with heterotrimeric G proteins. Frontiers in Neuroendocrinology. 2013;34(2):88-94.
39. Schiöth HB, Fredriksson R. The GRAFS classification system of G-protein coupled receptors in comparative perspective. General and Comparative Endocrinology. 2005;142(1):94-101.

40. Venkatakrishnan A, Deupi X, Lebon G, Tate CG, Schertler GF, Babu MM. Molecular signatures of G-protein-coupled receptors. Nature. 2013;494(7436):185-94.
41. Hauser AS, Kooistra AJ, Munk C, Heydenreich FM, Veprintsev DB, Bouvier M, et al. GPCR activation mechanisms across classes and macro/microscales. Nature Structural & Molecular Biology. 2021;28(11):879-88.
42. Weis WI, Kobilka BK. The Molecular Basis of G Protein-Coupled Receptor Activation. Annual review of biochemistry. 2018;87:897-919.
43. Kooistra AJ, Mordalski S, Pándy-Szekeres G, Esguerra M, Mamyrbekov A, Munk C, et al. GPCRdb in 2021: integrating GPCR sequence, structure and function. Nucleic Acids Research. 2020;49(D1):D335-D43.
44. Flanagan CA, Manilall A. Gonadotropin-Releasing Hormone (GnRH) Receptor Structure and GnRH Binding. Frontiers in Endocrinology. 2017;8(274).
45. Toufaily C, Fortin J, Alonso CA, Lapointe E, Zhou X, Santiago-Andres Y, et al. Addition of a carboxy terminal tail to the normally tailless gonadotropin-releasing hormone receptor impairs fertility in female mice. Elife. 2021;10:e72937.
46. Tzoupis H, Nteli A, Androutsou ME, Tselios T. Gonadotropin-Releasing Hormone and GnRH Receptor: Structure, Function and Drug Development. Curr Med Chem. 2020;27(36):6136-58.
47. Kmiecik S, Jamroz M, Kolinski M. Structure prediction of the second extracellular loop in G-protein-coupled receptors. Biophysical journal. 2014;106(11):2408-16.
48. Noel SD, Kaiser UB. G protein-coupled receptors involved in GnRH regulation: Molecular insights from human disease. Molecular and Cellular Endocrinology. 2011;346(1):91-101.
49. Choi D. Evolutionary Viewpoint on GnRH (gonadotropin-releasing hormone) in Chordata - Amino Acid and Nucleic Acid Sequences. Dev Reprod. 2018;22(2):119-32.
50. Kumar A, Bachhawat AK. Pyroglutamic acid: throwing light on a lightly studied metabolite. Current Science. 2012;102(2):288-97.
51. Sealfon SC, Weinstein H, Millar RP. Molecular Mechanisms of Ligand Interaction with the Gonadotropin-Releasing Hormone Receptor. Endocrine Reviews. 1997;18(2):180-205.
52. Millar RP, Lu Z-L, Pawson AJ, Flanagan CA, Morgan K, Maudsley SR. Gonadotropin-Releasing Hormone Receptors. Endocrine Reviews. 2004;25(2):235-75.
53. Marques P, Skorupskaite K, George JT, Anderson RA. Physiology of GNRH and gonadotropin secretion. Endotext [Internet]. 2018.
54. Pincus SM, Padmanabhan V, Lemon W, Randolph J, Rees Midgley A. Follicle-stimulating hormone is secreted more irregularly than luteinizing hormone in both humans and sheep. J Clin Invest. 1998;101(6):1318-24.
55. Padmanabhan V, McFadden K, Mauger DT, Karsch FJ, Midgley AR, Jr. Neuroendocrine control of follicle-stimulating hormone (FSH) secretion. I. Direct evidence for separate episodic and basal components of FSH secretion. Endocrinology. 1997;138(1):424-32.
56. Bowen JM, Dahl GE, Evans NP, Thrun LA, Wang Y, Brown MB, et al. Importance of the Gonadotropin-Releasing Hormone (GnRH) Surge for Induction of the Preovulatory Luteinizing Hormone Surge of the Ewe: Dose-Response Relationship and Excess of GnRH*. Endocrinology. 1998;139(2):588-95.
57. Conte FA, Grumbach MM, Kaplan SL, Reiter EO. Correlation of luteinizing hormone-releasing factor-induced luteinizing hormone and follicle-stimulating hormone release from

infancy to 19 years with the changing pattern of gonadotropin secretion in agonadal patients: relation to the restraint of puberty. J Clin Endocrinol Metab. 1980;50(1):163-8.
58. Marshall JC, Dalkin AC, Haisenleder DJ, Griffin ML, Kelch RP. GnRH pulses--the regulators of human reproduction. Trans Am Clin Climatol Assoc. 1993;104:31-46.
59. Berga SL. Oxford Textbook of Endocrinology and Diabetes. Disorders of gonadotropin secretion: Oxford University Press; 2011.
60. Balasubramanian R, Crowley Jr WF. Isolated gonadotropin-releasing hormone (GnRH) deficiency. 2017.
61. Perrett RM, McArdle CA. Molecular mechanisms of gonadotropin-releasing hormone signaling: integrating cyclic nucleotides into the network. Frontiers in endocrinology. 2013;4:180-.
62. Zheng L, Stojilkovic SS, Hunyady L, Krsmanovic LZ, Catt KJ. Sequential activation of phospholipase-C and -D in agonist-stimulated gonadotrophs. Endocrinology. 1994;134(3):1446-54.
63. Putney JW, Tomita T. Phospholipase C signaling and calcium influx. Adv Biol Regul. 2012;52(1):152-64.
64. Litosch I. Novel Mechanisms for Feedback Regulation of Phospholipase C‐β Activity. IUBMB life. 2002;54(5):253-60.
65. Silverthorn DU. Communication, integration, and Homeostasis. In: Espinoza D, Nunes I, George-O´Brien N, German K, Earl W, Fortier E, editors. Human physiology: an integrated approach. 4 ed. San Fransisco, USA Pearson Benjamin Cummings; 2009

. p. 185.
66. Pincas H, Choi SG, Wang Q, Jia J, Turgeon JL, Sealfon SC. Outside the box signaling: Secreted factors modulate GnRH receptor-mediated gonadotropin regulation. Molecular and Cellular Endocrinology. 2014;385(1):56-61.
67. Kahnamouyi S, Nouri M, Farzadi L, Darabi M, Hosseini V, Mehdizadeh A. The role of mitogen-activated protein kinase-extracellular receptor kinase pathway in female fertility outcomes: a focus on pituitary gonadotropins regulation. Ther Adv Endocrinol Metab. 2018;9(7):209-15.
68. Maggi R, Cariboni AM, Marelli MM, Moretti RM, Andrè V, Marzagalli M, et al. GnRH and GnRH receptors in the pathophysiology of the human female reproductive system. Human Reproduction Update. 2016;22(3):358-81.
69. Quinton R, Hasan W, Grant W, Thrasivoulou C, Quiney RE, Besser GM, et al. Gonadotropin-Releasing Hormone Immunoreactivity in the Nasal Epithelia of Adults with Kallmann's Syndrome and Isolated Hypogonadotropic Hypogonadism and in the Early Midtrimester Human Fetus. The Journal of Clinical Endocrinology & Metabolism. 1997;82(1):309-14.
70. Schwarting GA, Wierman ME, Tobet SA. Gonadotropin-releasing hormone neuronal migration. Semin Reprod Med. 2007;25(5):305-12.
71. Forni PE, Wray S. GnRH, anosmia and hypogonadotropic hypogonadism – Where are we? Frontiers in Neuroendocrinology. 2015;36:165-77.
72. Gründker C, Emons G. The Role of Gonadotropin-Releasing Hormone in Cancer Cell Proliferation and Metastasis. Frontiers in endocrinology. 2017;8:187-.
73. Limonta P, Marelli MM, Mai S, Motta M, Martini L, Moretti RM. GnRH Receptors in Cancer: From Cell Biology to Novel Targeted Therapeutic Strategies. Endocrine Reviews. 2012;33(5):784-811.

74. Davis ME. Glioblastoma: Overview of Disease and Treatment. Clin J Oncol Nurs. 2016;20(5 Suppl):S2-S8.
75. Ostrom QT, Gittleman H, Fulop J, Liu M, Blanda R, Kromer C, et al. CBTRUS statistical report: primary brain and central nervous system tumors diagnosed in the United States in 2008-2012. Neuro-oncology. 2015;17(suppl_4):iv1-iv62.
76. Bahadur S, Sahu AK, Baghel P, Saha S. Current promising treatment strategy for glioblastoma multiform: A review. Oncol Rev. 2019;13(2):417-.
77. Zong H, Verhaak RGW, Canoll P. The cellular origin for malignant glioma and prospects for clinical advancements. Expert Rev Mol Diagn. 2012;12(4):383-94.
78. Khazeni S, Varamini P. Gonadotropin Releasing Hormone. Reference Module in Biomedical Sciences: Elsevier; 2018.
79. Ortmann O, Weiss JM, Diedrich K. Gonadotrophin-releasing hormone (GnRH) and GnRH agonists: mechanisms of action. Reprod Biomed Online. 2002;5 Suppl 1:1-7.
80. Tukun F-L, Olberg DE, Riss PJ, Haraldsen I, Kaass A, Klaveness J. Recent Development of Non-Peptide GnRH Antagonists. Molecules. 2017;22(12):2188.
81. Osuga Y, Seki Y, Tanimoto M, Kusumoto T, Kudou K, Terakawa N. Relugolix, an oral gonadotropin-releasing hormone receptor antagonist, reduces endometriosis-associated pain in a dose-response manner: a randomized, double-blind, placebo-controlled study. Fertil Steril. 2021;115(2):397-405.
82. Felberbaum RE, Ludwig M, Diedrich K. Clinical application of GnRH-antagonists. Molecular and Cellular Endocrinology. 2000;166(1):9-14.
83. Leach AR. The Use of Molecular Modelling and Chemoinformatics to Discover and Design New Molecules Molecular Modelling: Principles and Applications 2nd ed. Harlow, Essex: Pearson Education Limited 2001. p. 661-6.
84. Holtje HD, Sippl W, Rognan D, Folkers G. Small Molecules Molecular Modeling. 3rd ed. Weinheim, Germany: WILEY-VCH Verlag GmbH & Co.; 2008. p. 9-44.
85. Ilari A, Savino C. Protein structure determination by x-ray crystallography. Bioinformatics. 2008:63-87.
86. Martin TG, Bharat TAM, Joerger AC, Bai X-c, Praetorius F, Fersht AR, et al. Design of a molecular support for cryo-EM structure determination. Proceedings of the National Academy of Sciences. 2016;113(47):E7456-E63.
87. Patrick G. Computers in Medicinal Chemistry. An Introduction to Medicinal Chemistry 5th ed. Great Clarendon Street, Oxford: Oxford University Press; 2013. p. 337-9.
88. Monticelli L, Tieleman DP. Force Fields for Classical Molecular Dynamics. In: Monticelli L, Salonen E, editors. Biomolecular Simulations: Methods and Protocols. Totowa, NJ: Humana Press; 2013. p. 197-213.
89. Dar AM, Mir S. Molecular docking: approaches, types, applications and basic challenges. J Anal Bioanal Tech. 2017;8(2):1-3.
90. Du X, Li Y, Xia Y-L, Ai S-M, Liang J, Sang P, et al. Insights into Protein-Ligand Interactions: Mechanisms, Models, and Methods. Int J Mol Sci. 2016;17(2):144.
91. Sherman W, Beard HS, Farid R. Use of an Induced Fit Receptor Structure in Virtual Screening. Chemical Biology & Drug Design. 2006;67(1):83-4.
92. Jalily Hasani H, Barakat K. Homology Modeling: an Overview of Fundamentals and Tools. International Review on Modelling and Simulations (IREMOS). 2017;10:129.
93. Cavasotto CN, Phatak SS. Homology modeling in drug discovery: current trends and applications. Drug Discovery Today. 2009;14(13):676-83.
94. Mindell DP, Meyer A. Homology evolving. Trends in Ecology & Evolution. 2001;16(8):434-40.

95. Dalton JAR, Jackson RM. An evaluation of automated homology modelling methods at low target–template sequence similarity. Bioinformatics. 2007;23(15):1901-8.
96. Forrest LR, Tang CL, Honig B. On the Accuracy of Homology Modeling and Sequence Alignment Methods Applied to Membrane Proteins. Biophysical Journal. 2006;91(2):508-17.
97. Patrick G. Computers in Medicinal Chemistry. An Introduction to Medicinal Chemistry. 5th ed. Great Clarendon Street, Oxford: Oxford University Press 2013. p. 346-7.
98. Durrant JD, McCammon JA. Molecular dynamics simulations and drug discovery. BMC Biology. 2011;9(1):71.
99. Padula AM. GnRH analogues—agonists and antagonists. Animal Reproduction Science. 2005;88(1):115-26.
100. Friesner RA, Banks JL, Murphy RB, Halgren TA, Klicic JJ, Mainz DT, et al. Glide: A New Approach for Rapid, Accurate Docking and Scoring. 1. Method and Assessment of Docking Accuracy. Journal of Medicinal Chemistry. 2004;47(7):1739-49.
101. Shelley JC, Cholleti A, Frye LL, Greenwood JR, Timlin MR, Uchimaya M. Epik: a software program for pKaprediction and protonation state generation for drug-like molecules. Journal of Computer-Aided Molecular Design. 2007;21(12):681-91.
102. Pándy-Szekeres G, Esguerra M, Hauser AS, Caroli J, Munk C, Pilger S, et al. The G protein database, GproteinDb. Nucleic Acids Research. 2021;50(D1):D518-D25.
103. Millar RP, Newton CL. Current and future applications of GnRH, kisspeptin and neurokinin B analogues. Nature Reviews Endocrinology. 2013;9(8):451-66.
104. Ranwez V, Chantret N. Strengths and limits of multiple sequence alignment and filtering methods. No commercial publisher| Authors open access book; 2020.
105. Vilardaga J-P. Theme and variations on kinetics of GPCR activation/deactivation. J Recept Signal Transduct Res. 2010;30(5):304-12.
106. Lu Z-L, Coetsee M, White CD, Millar RP. Structural Determinants for Ligand-Receptor Conformational Selection in a Peptide G Protein-coupled Receptor*. Journal of Biological Chemistry. 2007;282(24):17921-9.
107. Zhou W, Rodic V, Kitanovic S, Flanagan CA, Chi L, Weinstein H, et al. A Locus of the Gonadotropin-releasing Hormone Receptor That Differentiates Agonist and Antagonist Binding Sites (∗). Journal of Biological Chemistry. 1995;270(32):18853-7.

7 Appendix

Figure A1

Figure A2

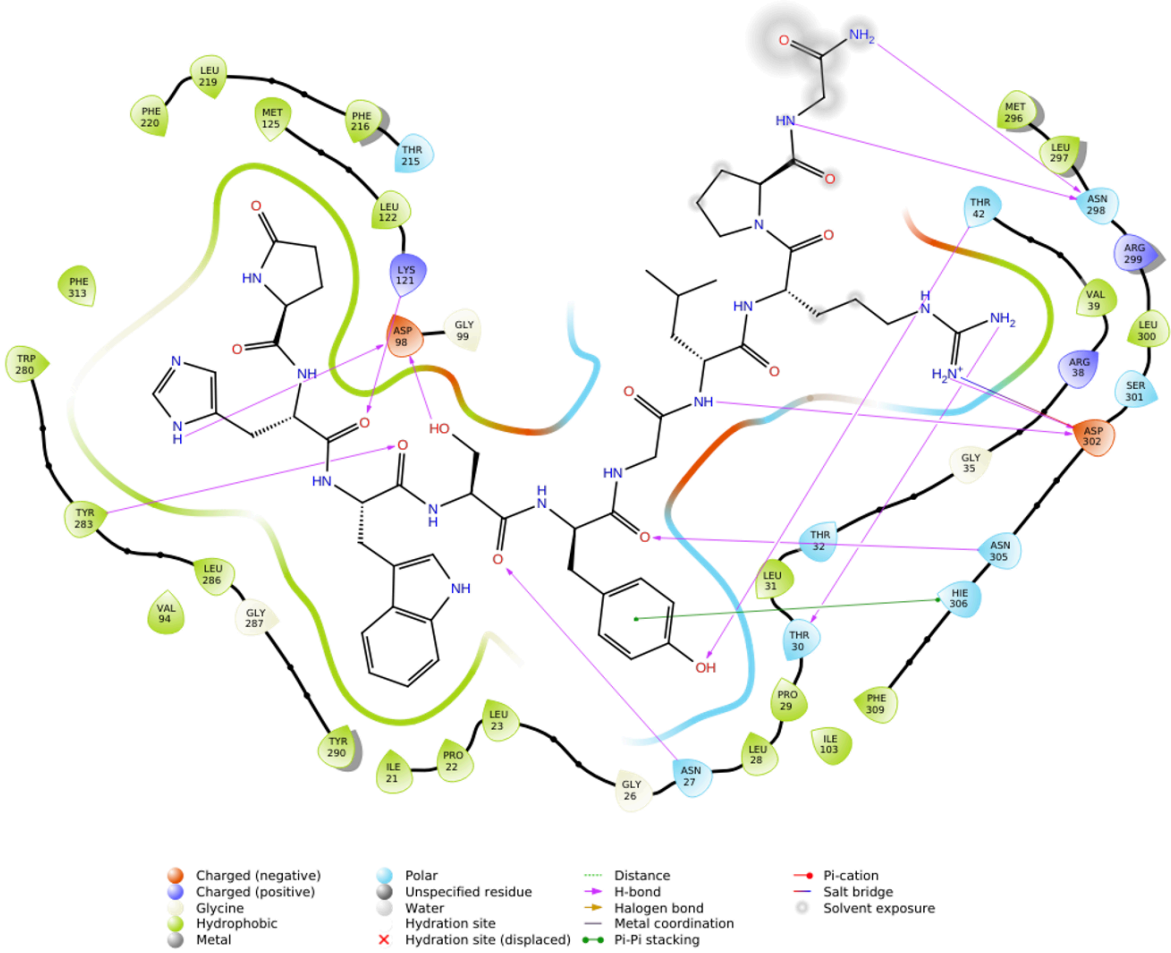
LEU 219
PHE 220
MET 125
PHE 216
THR 215
LEU 122
LYS 121
ASP 98
GLY 99
PHE 313
TRP 280
TYR 283
LEU 286
VAL 94
GLY 287
TYR 290
ILE 21
PRO 22
LEU 23
GLY 26
ASN 27
LEU 28
PRO 29
THR 30
LEU 31
THR 32
GLY 35
ASP 302
SER 301
ARG 38
VAL 39
LEU 300
ARG 299
ASN 298
LEU 297
MET 296
THR 42
ASN 305
HIE 306
PHE 309
ILE 103
Charged (negative)
Charged (positive)
Glycine
Hydrophobic
Metal
Polar
Unspecified residue
Water
Hydration site
Hydration site (displaced)
Distance
H-bond
Halogen bond
Metal coordination
Pi-Pi stacking
Pi-cation
Salt bridge
Solvent exposure

Figure A3

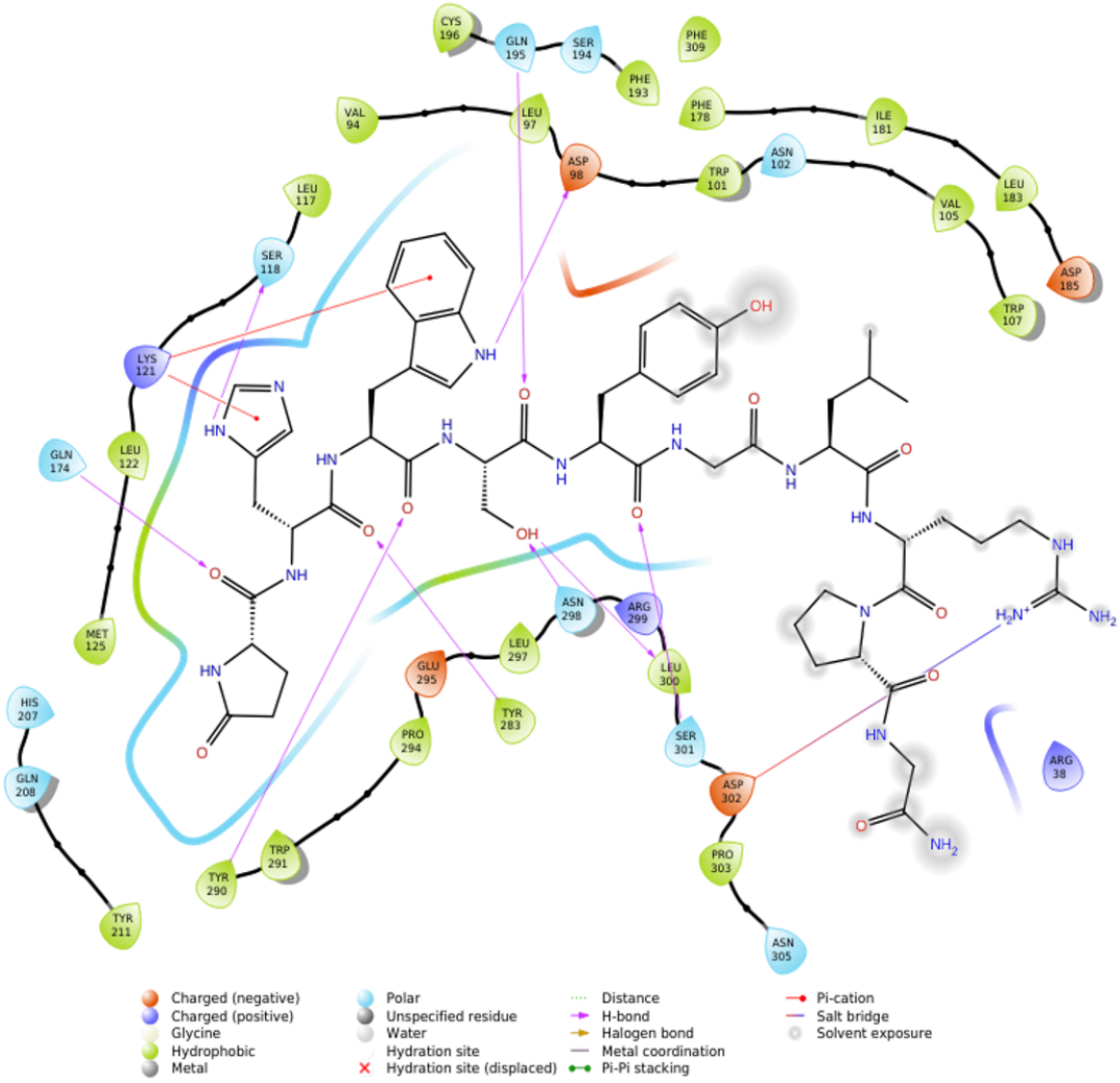
CYS 196
GLN 195
SER 194
PHE 193
PHE 309
PHE 178
ILE 181
LEU 183
ASP 185
TRP 107
VAL 105
ASN 102
TRP 101
ASP 98
LEU 97
VAL 94
LEU 117
SER 118
LYS 121
LEU 122
GLN 174
MET 125
HIS 207
GLN 208
TYR 211
TYR 290
TRP 291
PRO 294
GLU 295
LEU 297
ASN 298
ARG 299
LEU 300
SER 301
ASP 302
PRO 303
ASN 305
TYR 283
ARG 38
Charged (negative)
Charged (positive)
Glycine
Hydrophobic
Metal
Polar
Unspecified residue
Water
Hydration site
Hydration site (displaced)
Distance
H-bond
Halogen bond
Metal coordination
Pi-Pi stacking
Pi-cation
Salt bridge
Solvent exposure

Figure A4

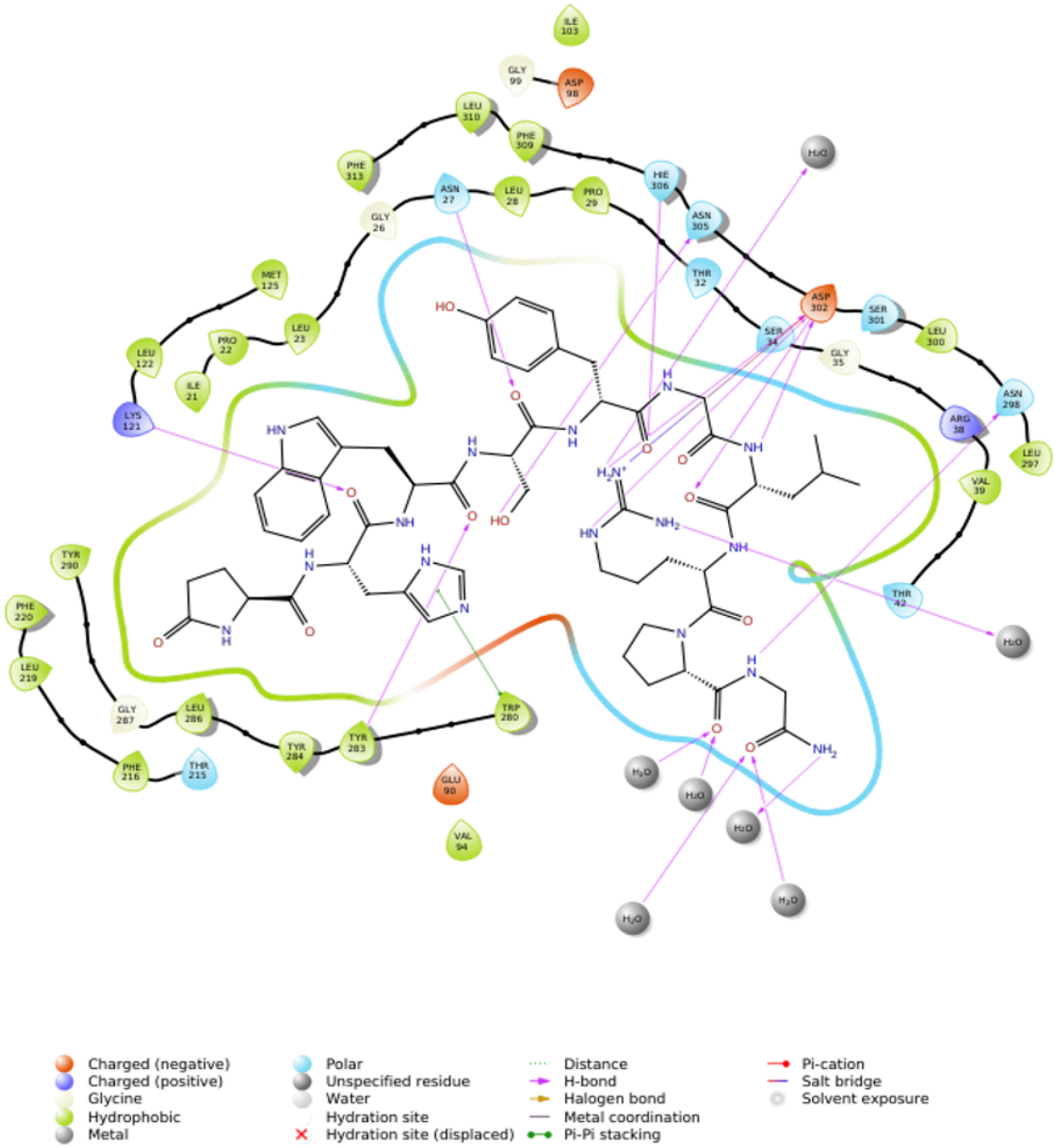
Charged (negative)
Charged (positive)
Glycine
Hydrophobic
Metal
Polar
Unspecified residue
Water
Hydration site
Hydration site (displaced)
Distance
H-bond
Halogen bond
Metal coordination
Pi-Pi stacking
Pi-cation
Salt bridge
Solvent exposure

Figure A5

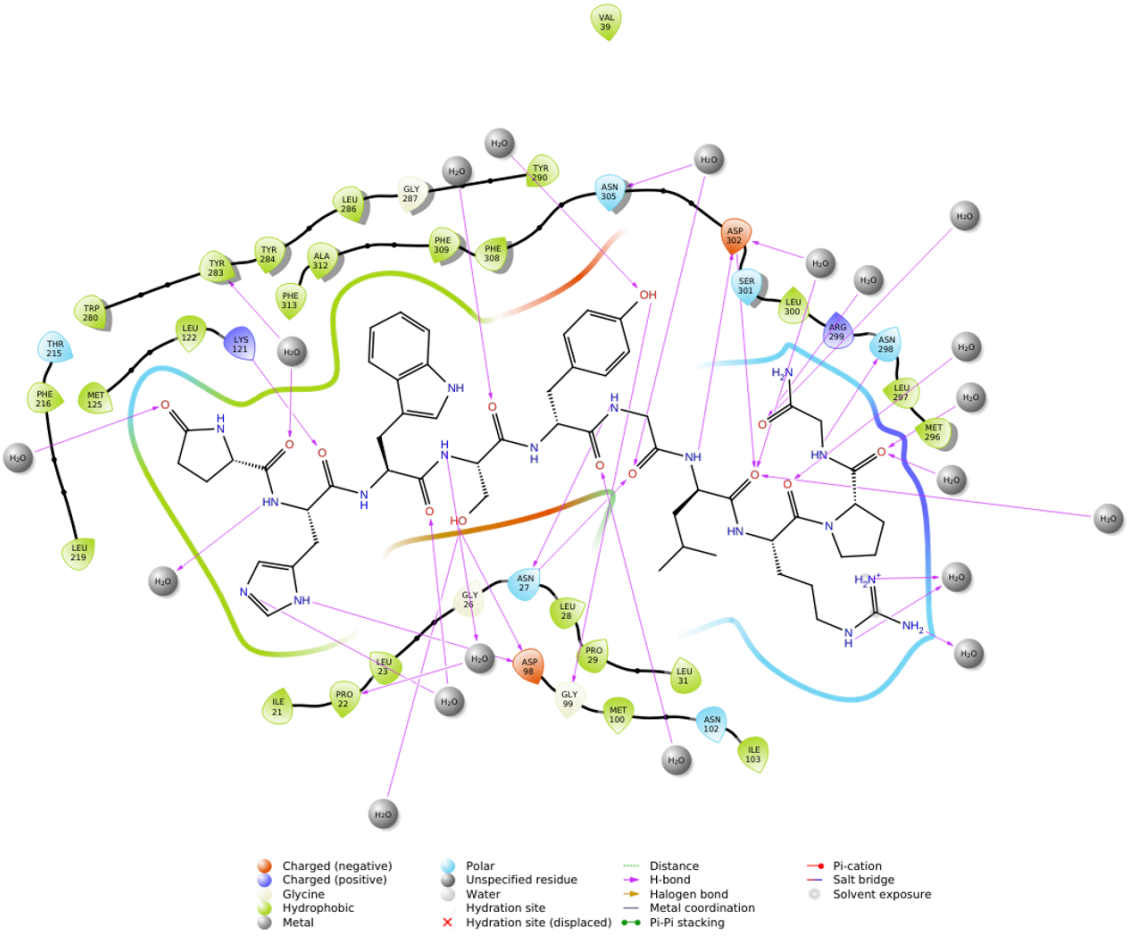
VAL 39
TYR 290
ASN 305
ASP 302
SER 301
LEU 300
ARG 299
ASN 298
LEU 297
MET 296
GLY 287
LEU 286
PHE 309
PHE 308
TYR 284
TYR 283
ALA 312
PHE 313
TRP 280
LEU 122
LYS 121
THR 215
PHE 216
MET 125
LEU 219
ASN 27
GLY 26
LEU 28
PRO 29
LEU 31
LEU 23
ASP 98
PRO 22
ILE 21
GLY 99
MET 100
ASN 102
ILE 103
Charged (negative)
Charged (positive)
Glycine
Hydrophobic
Metal
Polar
Unspecified residue
Water
Hydration site
Hydration site (displaced)
Distance
H-bond
Halogen bond
Metal coordination
Pi-Pi stacking
Pi-cation
Salt bridge
Solvent exposure

Figure A6

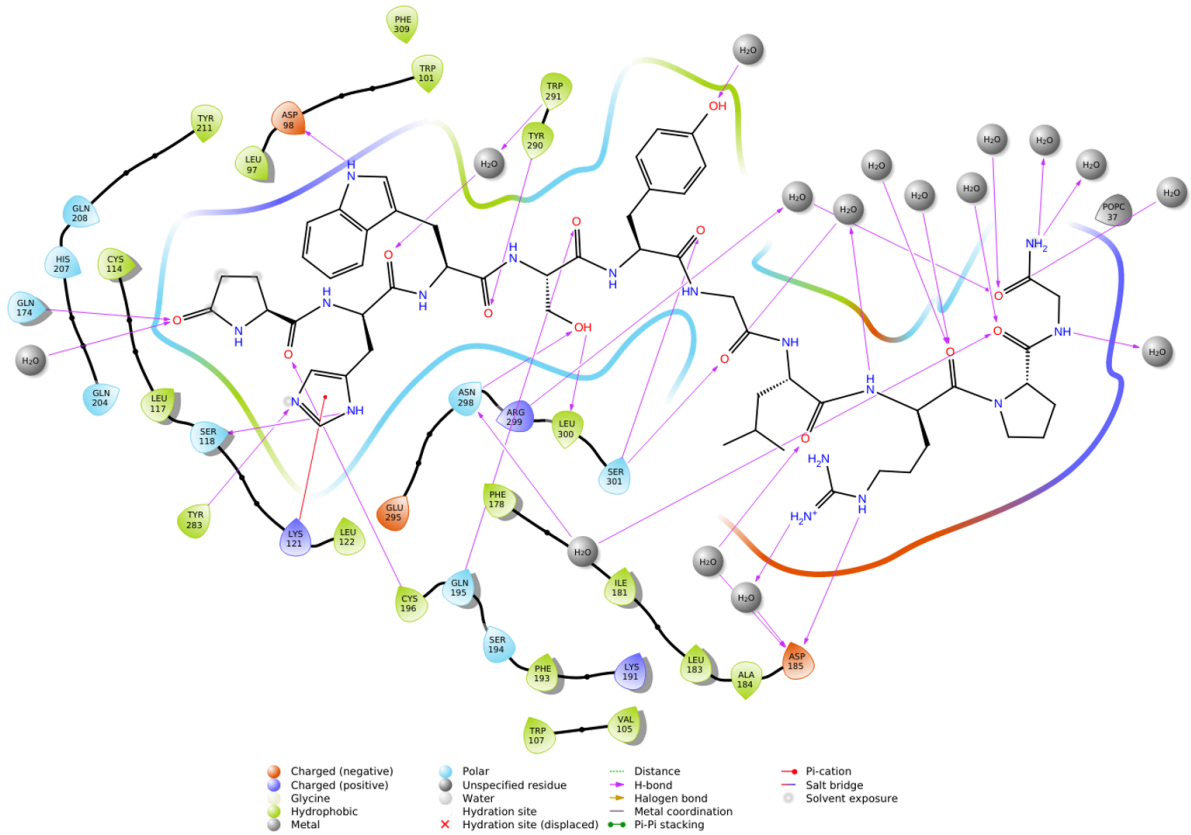
PHE 309
TRP 101
TYR 211
ASP 98
LEU 97
TRP 291
TYR 290
GLN 208
HIS 207
CYS 114
GLN 174
GLN 204
LEU 117
SER 118
TYR 283
LYS 121
LEU 122
ASN 298
ARG 299
LEU 300
SER 301
GLU 295
PHE 178
GLN 195
CYS 196
SER 194
PHE 193
LYS 191
ILE 181
LEU 183
ALA 184
ASP 185
TRP 107
VAL 105
POPC 37
Charged (negative)
Charged (positive)
Glycine
Hydrophobic
Metal
Polar
Unspecified residue
Water
Hydration site
Hydration site (displaced)
Distance
H-bond
Halogen bond
Metal coordination
Pi-Pi stacking
Pi-cation
Salt bridge
Solvent exposure

Figure A7

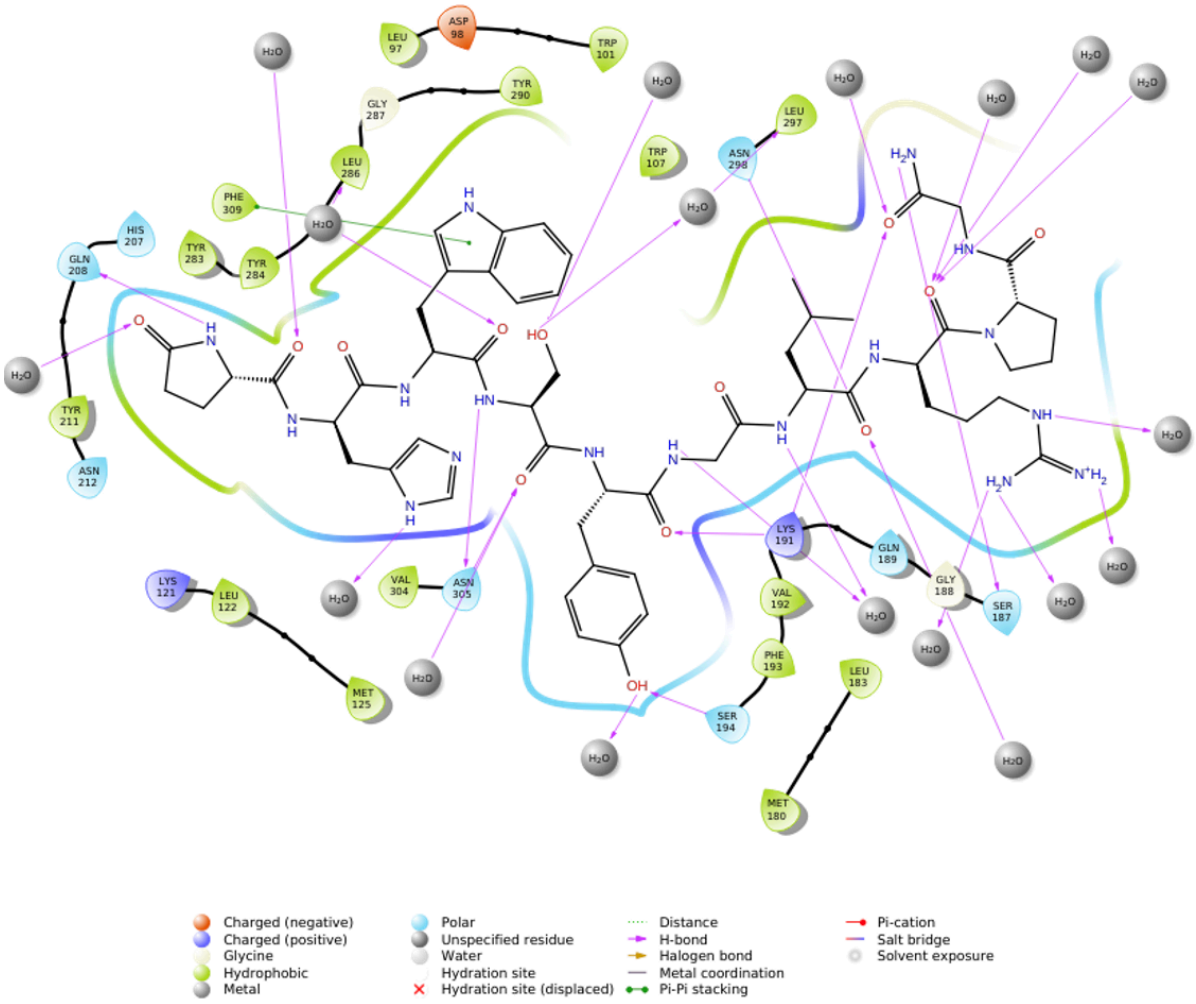
ASP 98
LEU 97
TRP 101
TYR 290
GLY 287
LEU 286
PHE 309
HIS 207
GLN 208
TYR 283
TYR 284
TYR 211
ASN 212
LYS 121
LEU 122
MET 125
VAL 304
ASN 305
TRP 107
ASN 298
LEU 297
LYS 191
GLN 189
GLY 188
SER 187
VAL 192
PHE 193
SER 194
LEU 183
MET 180
Charged (negative)
Charged (positive)
Glycine
Hydrophobic
Metal
Polar
Unspecified residue
Water
Hydration site
Hydration site (displaced)
Distance
H-bond
Halogen bond
Metal coordination
Pi-Pi stacking
Pi-cation
Salt bridge
Solvent exposure

Figure A8

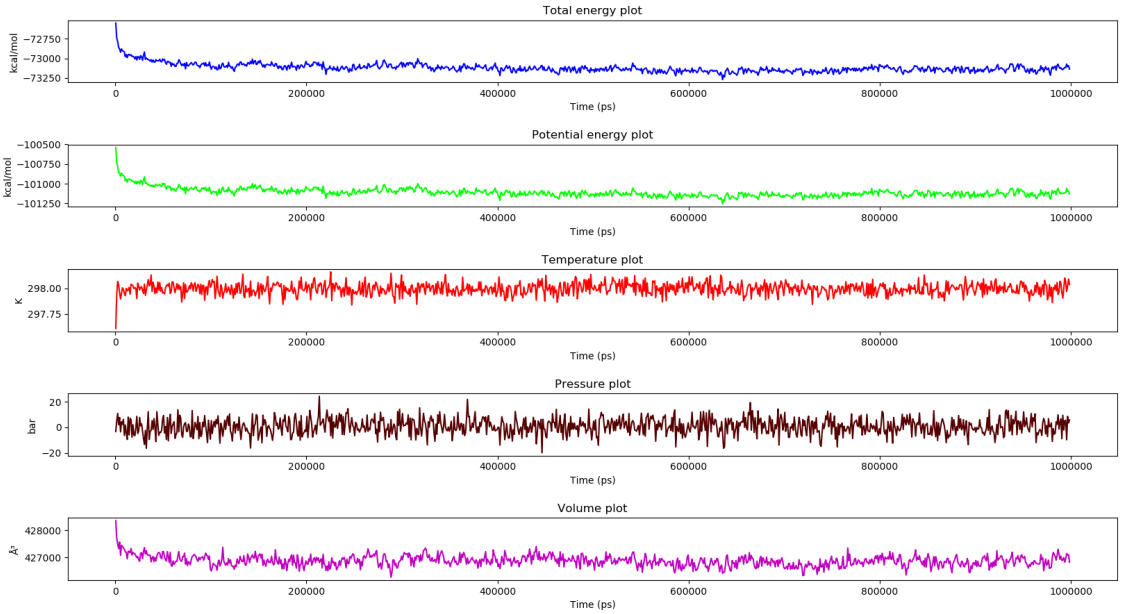

Figure A9

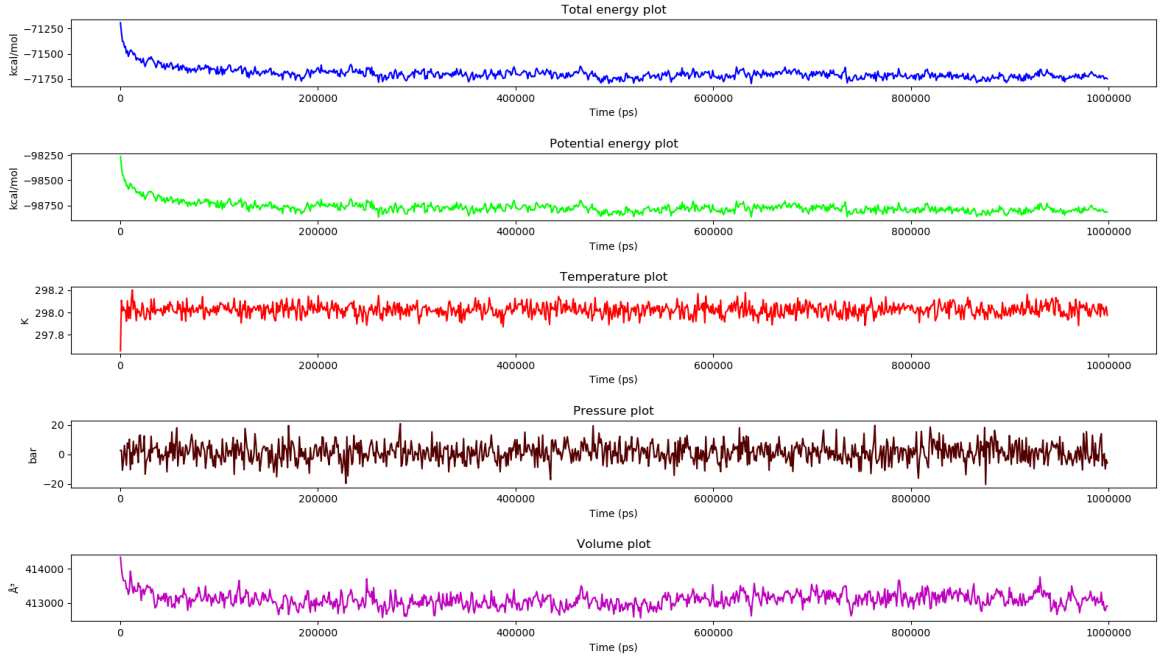

Figure A10

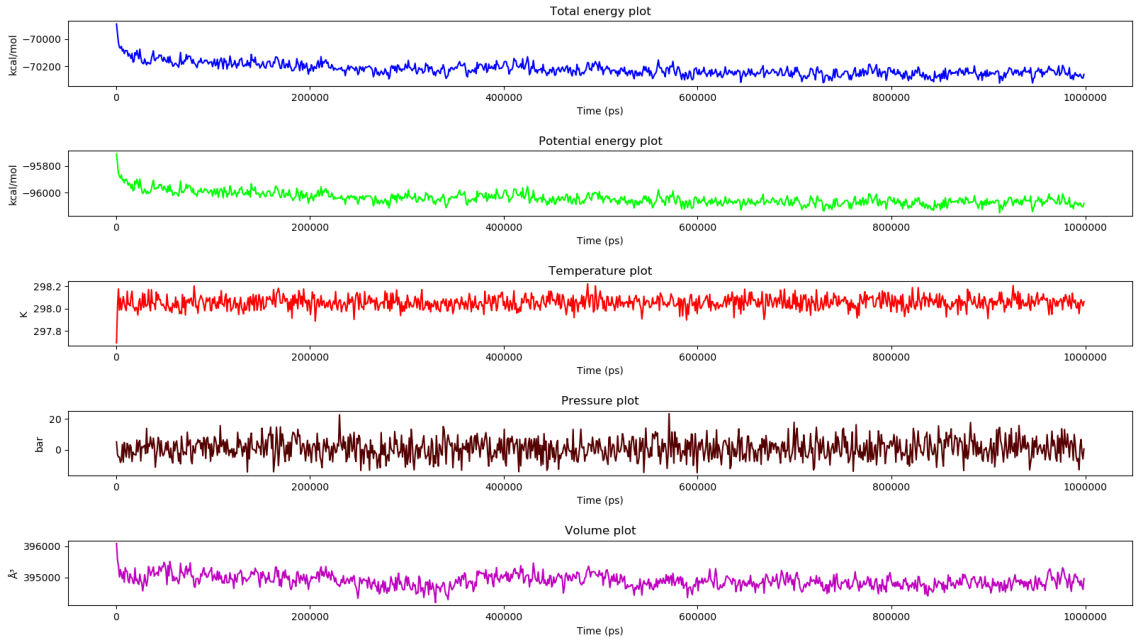
Total energy plot
kcal/mol
−70000
−70200
0
200000
400000
600000
800000
1000000
Time (ps)
Potential energy plot
kcal/mol
−95800
−96000
0
200000
400000
600000
800000
1000000
Time (ps)
Temperature plot
K
298.2
298.0
297.8
0
200000
400000
600000
800000
1000000
Time (ps)
Pressure plot
bar
20
0
0
200000
400000
600000
800000
1000000
Time (ps)
Volume plot
Å³
396000
395000
0
200000
400000
600000
800000
1000000
Time (ps)